1-1-1973

Crusting And Swelling Effects On Water Infiltration Into Soil

D. L. Nofziger

D. Swartzendruber

L. R. Ahuja

TECHNICAL REPORT 28

CRUSTING and SWELLING EFFECTS on WATER INFILTRATION into SOIL

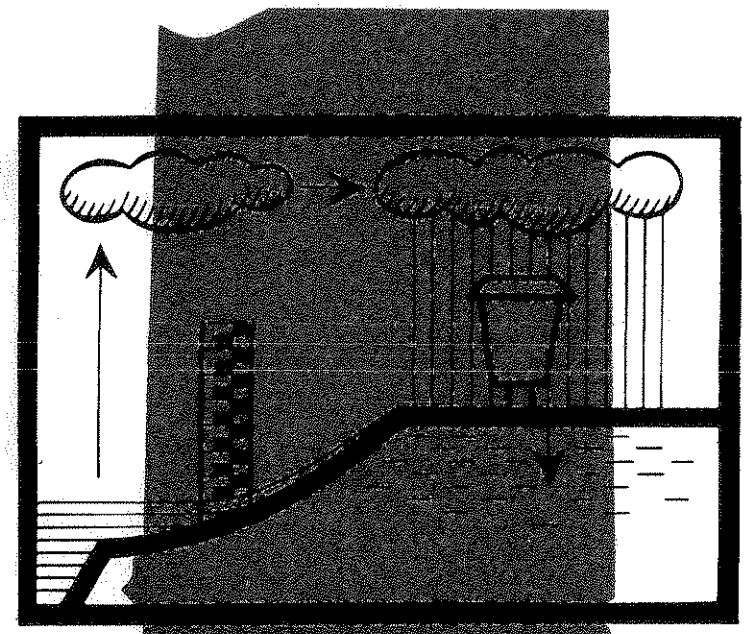

by
D. L. Nofziger
D. Swartzendruber
L. R. Ahuja

JANUARY 1973

PURDUE UNIVERSITY
WATER RESOURCES RESEARCH CENTER
LAFAYETTE, INDIANA

CRUSTING AND SWELLING EFFECTS ON WATER INFILTRATION INTO SOIL

by

D. L. Nofziger

D. Swartzendruber

L. R. Ahuja

A completion report of OWRR Project No. B-014-IND, "Dynamics of Water Infiltration into Soil as Governed by Surface Crusting and Sealing", Agreement No. 14-01-0001-1904. Period of Project: July, 1968 to September, 1972. Principal Investigator: D. Swartzendruber.

Purdue University

Department of Agronomy

West Lafayette, Indiana

The work upon which this report is based was supported in part by funds provided by the United States Department of the Interior, Office of Water Resources Research, as authorized by the Water Resources Research Act of 1964.

Technical Report No. 28

Purdue University Water Resources Research Center

West Lafayette, Indiana

January, 1973

FOREWORD

The project under which the reported study was performed was entitled "Dynamics of Water Infiltration into Soil as Governed by Surface Crusting and Sealing". Financial support was provided by the United States Department of the Interior as authorized by the Water Resources Research Act of 1964, and by the Agricultural Experiment Station, Purdue University. The project was administered by Dr. Dan Wiersma, Director of the Purdue University Water Resources Research Center, and Dr. Marvin W. Phillips, Head of the Department of Agronomy.

Project personnel consisted of Dr. Lajpat R. Ahuja, Postdoctoral Research Associate, who is now Assistant Soil Scientist, University of Hawaii, Honolulu; Dr. David L. Nofziger, then Graduate Research Assistant, who is now with the Institute for Agricultural Research, Ahmadu Bello University, Zaria, Nigeria; Dr. Munna L. Sharma, Postdoctoral Research Associate, who is now Research Scientist, Riverina Laboratory, Commonwealth Scientific and Industrial Research Organization, Deniliquin, N. S. W. Australia; and Dr. Dale Swartzendruber, Professor of Soils, who was Principal Investigator for the project.

TABLE OF CONTENTS

Page

LIST OF TABLES

LIST OF FIGURES

Figure

Figure

Page

ABSTRACT

One-dimensional, horizontal soil-water absorption through a thin zone of constant nonzero hydraulic resistance was examined theoretically and experimentally. Mathematically, this involved a numerical solution, as well as a similarity reduction of the problem for early to intermediate times. The flow equations were transformed by introducing a dimensionless parameter, which enabled the solution for any value of thin-zone resistance to be obtained from the solution for a given known thin-zone resistance. At the inlet boundary between the thin zone and the soil column, the soil-water content increased with time to approach the saturated value. The cumulative absorption of water by the soil column increased more than proportionally with the square root of time for early and intermediate times, and approached a square-root-of-time proportionality at large times. For both the soil-water content at the inlet boundary and the cumulative water absorption by the soil column, simple expressions arose from the similarity-reduction analysis, which was based on specific functional forms of the soil-water diffusivity and suction head. For early to intermediate times of flow, the similarity-reduction analysis described adequately the calculated numerical-solution flow data for Yolo soil, as well as the measurements obtained experimentally on Salkum silty clay loam.

Water movement into confined swelling and nonswelling porous media was studied by dual-energy gamma-ray attenuation. The dual-energy beam of gamma-rays was devised by placing a 280-mc source of Cs-137 behind a 389-mc source of Am-241. Lead collimators were mounted in front of each source and in front of the scintillation probe. The collimators were aligned so that gamma rays from both sources passed simultaneously through the same portion of soil and were detected in a single scintillation probe. The probe was connected in parallel to two amplifier-analyzers, and each analyzer was connected to a separate scaler. One amplifier-analyzer was operated in the integral mode to count pulses corresponding to photons from Cs-137 having energies greater than 0.55 Mev, and the other was operated in a differential mode to count pulses corresponding to photons from Am-241 having energies in the wide band of 0.035 to 0.085 Mev. The intensity in the Am-241 band due to Cs-137 was found empirically to be independent

of the material being measured (soil and/or water), and could be expressed as a cubic polynomial function of the Cs-137 intensity. This cubic polynomial was used to correct the measured intensity in the Am-241 band for the effect of Cs-137 and, thus, to determine the intensity due to Am-241 only. Overall measuring accuracy was on the order of ± 0.01 cc/cc in water content and ± 0.02 g/cc in bulk density, for counting periods of several minutes. These respective values changed to ± 0.04 cc/cc and ± 0.04 g/cc for counting periods of 5 sec.

The dual-energy gamma-ray attenuation apparatus was used to study water movement into several confined, air-dry porous media. For a highly swelling mixture of 50% bentonite and 50% silt, the bulk density near the inlet end of the column decreased very rapidly as water entered. The expansion of the wetted medium compressed the dry portion of the column. A plot of water saturation versus the reduced material coordinate was found to be essentially invariant, except for positions nearer than 1 cm to the inlet. For three so-called nonswelling soils, essentially no swelling was observed during wetting. Hence, previous measurements of water content by single-energy gamma-ray attenuation are valid for these soils. Although no swelling was observed, rigid media soil-water diffusivity theory failed to describe precisely the movement of water into these three soils.

CHAPTER 1.

INTRODUCTION AND OBJECTIVES

The role of the soil surface in affecting water infiltration into the soil profile has long been recognized as an important one. Particularly is this true if the soil surface is somehow bestowed with a lower permeability than the remainder of the profile. An obvious case in point is the development of a raindrop-induced crust on a bare soil. As an aid in better understanding and characterizing the infiltration effects of soil crusts, the project objectives originally set forth were:

1. To obtain a complete mathematical solution for the one-dimensional entry of water into unsaturated soil when a thin layer of low intrinsic permeability is located at the inlet surface of the soil; simplified approximations of the solution will also be sought.
2. To test the experimental validity of the mathematical solutions on idealized simulated crusted-sealed systems in which water is admitted through a low-permeability fritted-glass filter into an unsaturated soil or sand of higher intrinsic permeability than the filter.
3. To obtain experimental measurements of water infiltration into unsaturated soils containing a crust-seal produced by either natural or artificial rainfall, thus enabling comparison with both the mathematical solution and the behavior of the idealized simulated crusted-sealed system; quantitative characterization of the flow properties of the crust-seal will be sought.

Objectives 1 and 2 were carried through rather comprehensively for one-dimensional horizontal flow. A complete mathematical solution was carried out numerically with the computer, and a new approximate analysis (similarity reduction) was also developed with considerable success. Fairly extensive experimental observations were made for horizontal columns of a silt loam soil with various fritted-glass "crusts", using single-energy gamma-ray attenuation to measure the soil-water content. Correlation and conformity of the experimental data with the two mathematical approaches was very encouraging, and

suggests that further efforts of this nature, as applied to one-dimensional downward flow, should be of considerable interest and promise. The work dealing in detail with Objectives 1 and 2 is set out in Chapter 2 of the present report.

In approaching Objective 3, however, it was eventually decided that the existing methods of measurement would not provide information of the desired usefulness. Even single-energy gamma-ray attenuation would not be capable of following the development of a crust under wet conditions, since in principle the soil bulk density cannot be allowed to change. It was thus deemed advisable to attempt the development of the dual-energy gamma-ray attenuation principle as a nondestructive method of measuring both soil-water content and soil bulk density. This effort was carried through with exceptionally gratifying results, which are presented in detail in Chapter 3 of the present report. With instrumentation very similar to that used for single-energy gamma-ray attenuation, it was found that both water content and bulk density could be monitored with good precision and rapidity in both swelling and nonswelling soils. This opens the door to a whole new area of more realistic research in infiltration and soil-water flow; namely, the flow behavior in soils that exhibit swelling or other kinds of bulk density change.

CHAPTER 2.

HORIZONTAL INTAKE OF SOIL WATER THROUGH A THIN ZONE (CRUST) OF REDUCED PERMEABILITY

The condition of the soil surface is often considered to be a dominating factor in regulating the entry of water into a soil profile (Duley, 1939; Ellison, 1947). Crusting-sealing effects caused by raindrop impact have been observed (Duley, 1939; Mannering and Wiersma, 1970) to cause reductions in the rate of water infiltration into certain field soils by as much as 3 to 8 fold. Compared with the original uncrusted soil, relative reductions in the hydraulic conductivity of a soil crust have been reported as enormous in some instances (McIntyre, 1958) and much more modest in others (Tackett and Pearson, 1965). A least-permeable layer at the soil surface may exert a more marked reduction on water entry into an unsaturated soil (Horton, 1940; Hanks and Bowers, 1962; Hillel and Gardner, 1970) than on the flow through a saturated profile (Swartzendruber, 1960; Sor and Bertrand, 1962).

The approach of Green and Ampt (1911) has been extended by van Duin (1955) and Hillel and Gardner (1970) to enable approximate solution of the problems of water entry into layered and crusted soils. Edwards and Larson (1969) employed a numerical analysis to assess the infiltration-rate effects of a crust wherein the water-transmitting properties changed with time. In the present considerations, one-dimensional, horizontal soil-water absorption through a thin zone of constant hydraulic resistance is examined in two ways theoretically, and then compared with experimental measurements. The analysis and results here presented will also be of some applicability in the very early stages of vertical infiltration through a superficial crust before gravity can exert an appreciable effect.

THEORETICAL

The problem is formulated as one-dimensional, isothermal water absorption by a semi-infinite, horizontal, unsaturated uniform soil column when water is admitted through a saturated porous plate (thin zone) of constant hydraulic

resistance. Because of its analogy with a superficial crust in vertical infiltration, the porous plate shall hereinafter also be referred to as a crust. The governing equation is taken as that of Richards (1931) in the form (e.g., Swartzendruber, 1969)

$$\frac{\partial\theta}{\partial t} = \frac{\partial}{\partial x}\left[D(\theta)\frac{\partial\theta}{\partial x}\right] \tag{1}$$

subject to the initial condition

$$\theta = \theta_a, \; x > 0, \quad t = 0 \tag{2}$$

and the boundary condition

$$-D(\theta)\frac{\partial\theta}{\partial x} = \frac{\tau(\theta)}{r}, \quad x = 0, \quad t > 0 \tag{3}$$

where θ is the volumetric soil-water content, θ_a is the constant initial value, t is the time, x is the horizontal distance coordinate taken positive in the soil, $D(\theta)$ is the soil-water diffusivity function ($= -K(\theta)d\tau/d\theta$, where $K(\theta)$ is the unsaturated conductivity function), $\tau(\theta)$ is the soil-water suction-head function (in centimeters of water, taken positive in unsaturated soil), and $r = L_c/K_c$ is the unit-area hydraulic resistance of the porous plate of thickness L_c and hydraulic conductivity K_c. The porous plate (crust) is taken as already saturated prior to and at time $t = 0$, and the water pressure on the non-soil side of this plate (at $x = -L_c$) is essentially atmospheric for all $t \geq 0$. Equations (1) and (3) are based upon the continuity and Buckingham-Darcy equations (Swartzendruber, 1969).

By introducing the scaled variables

$$X = \gamma x, \quad T = \gamma^2 t, \quad R = \gamma r \tag{4}$$

where γ is a dimensionless parameter, Eqs. (1) through (3) become

$$\frac{\partial\theta}{\partial T} = \frac{\partial}{\partial X}\left[D(\theta)\frac{\partial\theta}{\partial X}\right] \tag{5}$$

subject to

$$\theta = \theta_a, \quad X > 0, \quad T = 0 \tag{6}$$

$$-D(\theta)\frac{\partial\theta}{\partial X} = \frac{\tau(\theta)}{R}, \quad X = 0, \quad T > 0 \tag{7}$$

The great advantage of this manner of expression is that the solution to the transformed problem of Eq. (5) subject to conditions (6) and (7) need to be obtained but once, for a given value of R. The solution of Eq. (1) subject to conditions (2) and (3) for any desired r then follows by appropriate back calculation using γ, R, X, and T.

Numerical Solution

Since the nonlinear problem of Eqs. (5), (6), and (7) has no known analytical solution, a numerical approach was undertaken first. Using the well-known central-difference scheme of Crank and Nicolson (1947), Eq. (5) was approximated by the finite-difference form

$$\frac{\theta_j^{n+1}-\theta_j^n}{\Delta T} = D(\theta_{j+1/2}^{n+1/2})\left[\theta_{j+1}^{n+1} - \theta_j^{n+1} + \theta_{j+1}^n - \theta_j^n\right]/2(\Delta X)^2$$

$$-D(\theta_{j-1/2}^{n+1/2})\left[\theta_j^{n+1} - \theta_{j-1}^{n+1} + \theta_j^n - \theta_{j-1}^n\right]/2(\Delta X)^2 \tag{8}$$

where

$$\theta_{j\pm1/2}^{n+1/2} = (\theta_{j\pm1}^{n+1} + \theta_j^{n+1} + \theta_{j\pm1}^n + \theta_j^n)/4,$$

The subscripts j = 1, 2, 3, . . . and the superscripts n = 0, 1, 2, . . . denote

successive grid lines along the X and T axes, respectively, while ΔX and ΔT are the respective mesh sizes. Boundary Eq. (7) was approximated by two methods, the first resulting from differentiation at X = 0 of a second-degree approximation for θ, namely

$$\left(\frac{\partial\theta}{\partial X}\right)^{n+1}_{0(X=0)} = \frac{-3\theta_0^{n+1} + 4\theta_1^{n+1} - \theta_2^{n+1}}{2\Delta X}$$

$$= \frac{-\tau(\theta_0^{n+1})}{RD(\theta_0^{n+1})} \qquad (9)$$

where the subscripts and superscripts again denote the distance and time steps, respectively. In the second method, due to J. von Neuman (Forsythe and Wasow, 1960), the line X = 0 is taken to be located between the first two mesh lines of X, thus introducing a set of θ values at the fictitious point $X = -\Delta X/2$. Boundary Eq. (7) is then approximated at the $(n + 1/2)$ time step by

$$\left(\frac{\partial\theta}{\partial X}\right)^{n+1/2}_{1/2(X=0)} = \frac{-\theta_0^{n+1/2} + \theta_1^{n+1/2}}{\Delta X}$$

$$= \frac{-\tau(\theta_{1/2}^{n+1/2})}{RD(\theta_{1/2}^{n+1/2})} \qquad (10)$$

Each of the approximations represented by Eqs. (9) and (10) has a formal error of order $(\Delta X)^2$.

Numerical solution of the nonlinear system of Eq. (8) subject to conditions (6) and (7), with the boundary equation of condition (7) being either Eq. (9) or (10), would commonly be approached by an iterative process, solving at each step the resulting linear system by a Gauss-elimination procedure. In place of the iterative process, however, a linearization technique has been suggested (Eddy, 1952) and described (Forsythe and Wasow, 1960), and used in a water

infiltration problem by Rubin and Steinhardt (1963). This involves the estimation of $\theta_{j\pm1/2}^{n+1/2}$ in Eqs. (8) and (10) and of θ_0^{n+1} in Eq. (9) by an extrapolation procedure. To obtain some guidance in choosing the best overall scheme, some preliminary experience was obtained by applying several of the foregoing numerical alternatives to the solution of the running-wave problem, which involves a nonlinear diffusion-type equation subjected to a nonlinear flux condition at X = 0, and that has a known solution in analytical form (Richtmeyer and Morton, 1967). In particular, it was desired to compare the iterative process with Eddy's linearization technique, and Eq. (9) with Eq. (10), where in all cases the Gauss-elimination procedure was the modified method of Richtmeyer and Morton (1967).

After a few early time steps in the running-wave problem, Eddy's linearization technique was found unstable near X = 0, thus suggesting that the technique may be sensitive to the form of the boundary equation at X = 0 and to the mesh sizes ΔX and ΔT. In contrast, the results from the iterative process were in good agreement with the analytical solution for both Eqs. (9) and (10), with Eq. (10) being very slightly better. An offsetting disadvantage, however, is that Eq. (10) is inflexible as regards changes in the ΔX mesh as solution proceeds. It is necessary to have a very fine mesh size (ΔX and ΔT) when θ at the boundary is changing rapidly, as happens at small values of T. Then, as time T increases, it is desirable in practice to increase both ΔX and ΔT progressively. Since Eq. (9) allows such change in ΔX, it was chosen in preference to Eq. (10).

Solution of Eq. (5) subject to conditions (6) and (7) was thus obtained by expressing Eq. (5) in the finite-difference form of Eq. (8), with the boundary equation of condition (7) in the form of Eq. (9), using the iterative process with the modified Gauss-elimination method (Richtmeyer and Morton, 1967). Experimental data for the so-called Yolo light clay soil of Moore (1939) were used to obtain functional forms of $\tau(\theta)$ and $K(\theta)$, while θ_a of condition (6) was taken as 0.04 cc/cc. The suction data were expressed as

$$\tau(\theta) = 0.5610\theta^{-4.8198} \text{ for } \theta_a \leq \theta \leq 0.455$$

$$\tau(\theta) = -1606.22 + 7434.45\theta - 8460.28\theta^2 \text{ for } \theta \geq 0.455$$

where $\theta = 0.455$ cc/cc is the "knot" at which both the function and the first derivative of the two above mathematical forms are made continuous. The unsaturated conductivity data were represented by $K(\theta) = 0.25490^{8.6567}$, so that the diffusivity function could be obtained from its definition $D(\theta) = -K(\theta)d\tau/d\theta$. These suction and conductivity relationships are compared with Moore's (1939) data by the logarithmic plots in Fig. 1, and indicate that the functional representations are reasonably good over the range of the data.

The numerical solution is illustrated graphically in Fig. 2 for a porous-plate (crust) hydraulic resistance of $R = \gamma r = 17{,}274$ min, which is 20 times the resistance of a 0.5-cm thick layer of water-saturated Yolo soil. The solid-line curves are of water content versus Boltzmann variable ($X/T^{1/2} = x/t^{1/2}$) at nine different fixed times. Several features of these curves are noteworthy. The water content at the inlet boundary ($X = 0$) increases with time, very rapidly in the beginning but very slowly later as the saturated value θ_s is approached asymptotically. The curves also move outward with time, seemingly in close association with the increasing θ at the inlet boundary. At large times, each curve changes but little from its immediate predecessor. Hence, the broken-line curve, determined for zero resistance of porous plate (crust) and for $\theta = \theta_s$ at the inlet boundary, would appear to mark a reasonable outer limit for the progression of solid-line curves as time increases without bound. Furthermore, the nature of the curves suggests that the cumulative amount of water absorbed by the soil column will increase more than proportionally with the square root of time during early and intermediate times, but will tend to be proportional to the square root of time at large times. Qualitatively, the numerical solution shown in Fig. 2 is similar to its constant-diffusivity counterpart given by Carslaw and Jaeger (1959) and Crank (1956).

To use Fig. 2 to determine the solution for any desired crust resistance r, one uses $R = 17{,}274 = \gamma r$ to establish the numerical value of γ. From this γ and the scaled time T for any curve, the use of the time equation of condition (4) yields $t = T/\gamma^2$, and, of course, the position equation $X = \gamma x$ is also available if needed.

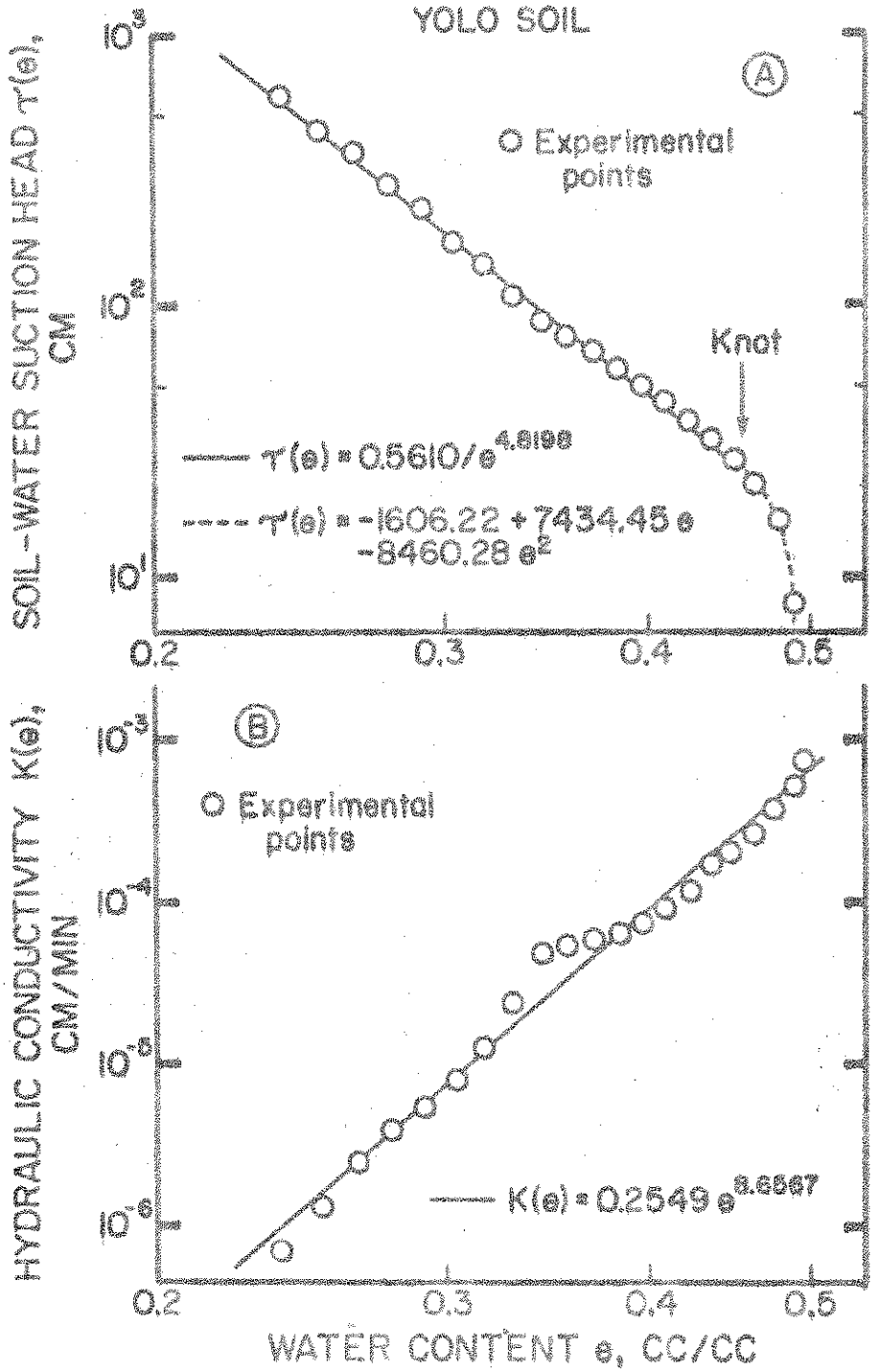

Figure 1 -- Experimental data for Yolo soil (Moore, 1939) as described by fitted functions; (A) for suction head versus water content, a two-form specification joined at the "knot" $\theta = 0.455$ cc/cc; (B) for hydraulic conductivity, a power function over the complete range in θ.

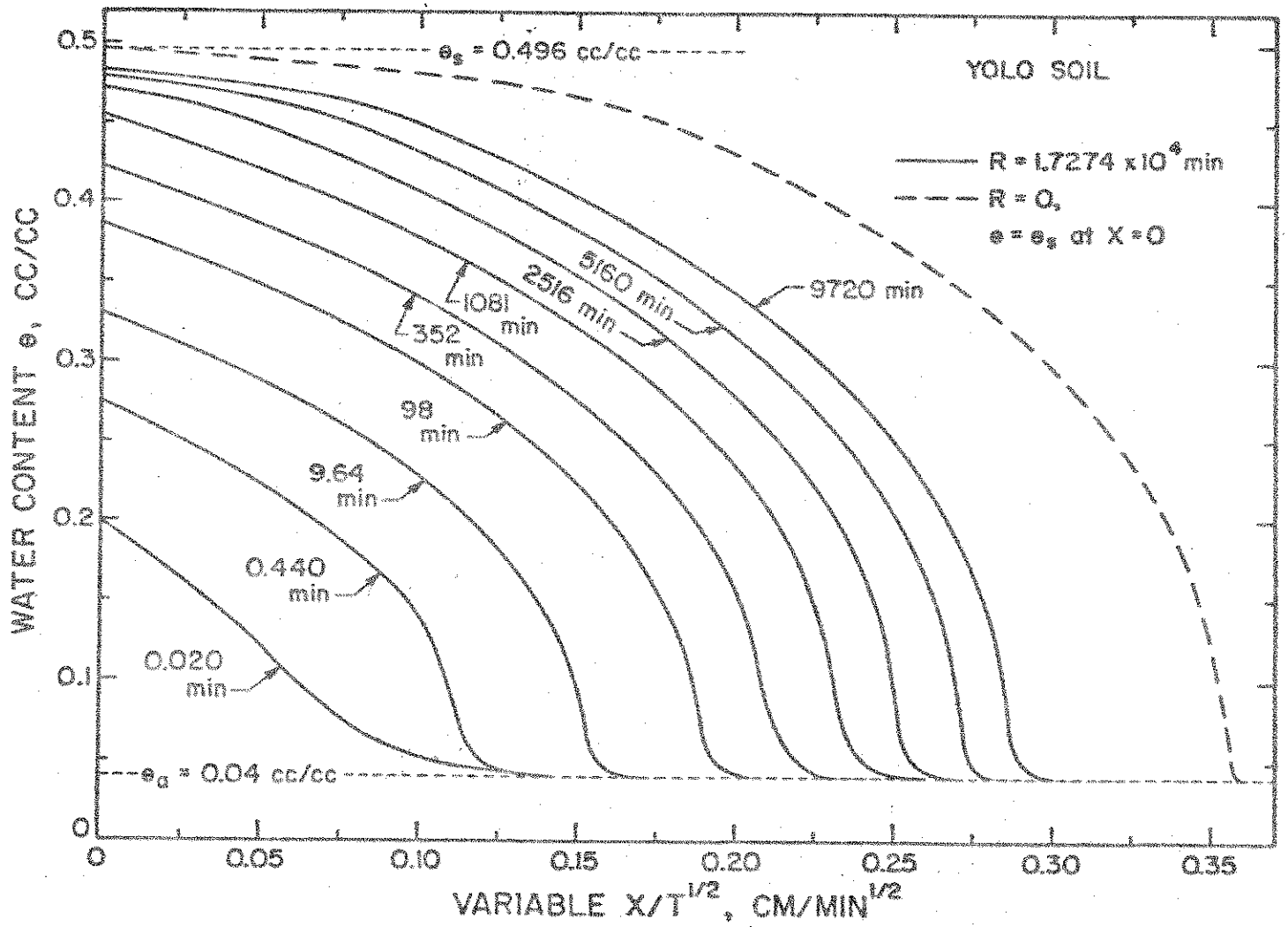

Figure 2 — Numerical solution for θ versus $X/T^{1/2}$ at different times during horizontal water entry into Yolo soil through a crust resistance of 17,274 min (solid-line curves), and for zero crust resistance (broken-line curve); θ_s is the water content at saturation.

Partial Analysis by Similarity Reduction

The technique of the so-called S-parameter group of transformations, described by Ames (1965), may be applied to the problem of Eq. (5) subject to conditions (6) and (7), provided that the diffusivity and suction functions can be expressed in forms compatible with the specification of appropriate similarity variables. Consider the forms

$$D(\theta) = A(\theta - \theta_a)^N \tag{11}$$

$$\tau(\theta) = B(\theta - \theta_a)^{-M} \tag{12}$$

where A, N, B, and M are positive constants. Using Eqs. (11) and (12) in the general definition of diffusivity, $D(\theta) = -K(\theta)d\tau/d\theta$, implies the unsaturated conductivity function as $K(\theta) = (A/BM)(\theta - \theta_a)^{N+M+1}$. This conductivity function and the suction function of Eq. (12) are similar to those of Brooks and Corey (1964), and will not be greatly different from those in Fig. 1 for $\theta < 0.455$, provided that θ_a is small enough to allow θ to be replaced by $\theta - \theta_a$ without serious error. Admittedly, the diffusivity function $A(\theta - \theta_a)^N$ is rather different in appearance from $b\theta^m(\theta_c - \theta)^{-p}$, which recently (Ahuja and Swartzendruber, 1972) has been found very satisfactory over the complete water-content range including the very wet. Quantitites b, m, θ_c, and p are constants, and θ_c is the saturated or near-saturated water content. It is mainly in the very wet region, however, that there is crucial need for the factor $(\theta_c - \theta)^{-p}$. Deleting it for intermediate and low water contents and replacing θ^m by $(\theta - \theta_a)^m$ would thus approximately reconcile even these two diffusivity forms.

Before proceeding further, however, actual tests of the functional dependence on $(\theta - \theta_a)$ are needed, and are shown as log-log plots in Fig. 3 for the suction and conductivity functions. For $\theta < 0.455$ [$\theta - \theta_a < 0.415$], Eq. (12) and $K(\theta) = (A/BM)(\theta - \theta_a)^{N+M+1}$ are good representations of the suction and conductivity data, respectively, but with coefficients and exponents somewhat changed from their similar counterparts in Fig. 1, as would be expected by the replacing of θ with $\theta - \theta_a$. While $\theta < 0.455$ clearly means that the extremely

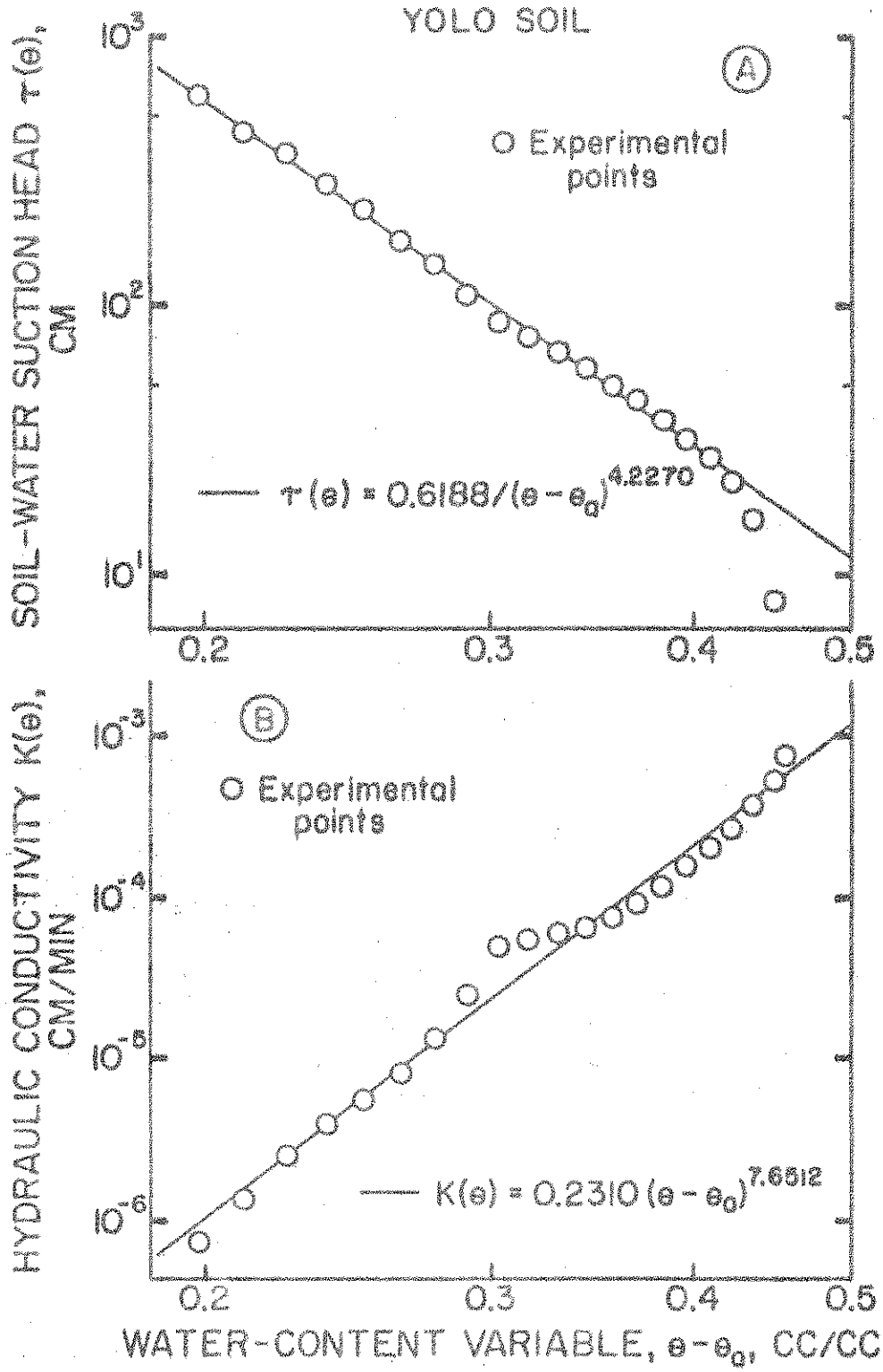

Figure 3 — Fitting of data for (A) suction head and (B) hydraulic conductivity of Yolo soil (Moore, 1939), as provided by the special functions used in the similarity-reduction analysis; $\theta_a = 0.04$ cc/cc.

wet region is excluded, it is seen from Fig. 2 that a substantial range of intermediate to low water contents is still included and of definite interest for solution of the problem.

Proceeding with the similarity reduction (see Ames, 1965), a variable η and a unique function $f(\eta)$ are postulated as

$$\eta = XT^{-\alpha} \tag{13}$$

$$f(\eta) = (\theta - \theta_a)T^{-\beta} \tag{14}$$

where α and β are positive real constants to be determined. Applying Eq. (11) along with these transformations [Eqs. (13) and (14)], and choosing

$$\beta = (2\alpha - 1)/N \tag{15}$$

to eliminate the explicit presence of T, enables Eq. (5) to be written

$$A(f^N f')' = \beta f - \alpha\eta f' \tag{16}$$

where the primes indicate ordinary derivatives with respect to η. Similarly, using Eqs. (11), (12), (13) and (14) in conditions (7), and now choosing

$$\alpha = \beta(N + M + 1) \tag{17}$$

to eliminate the explicit presence of T, enables condition (7) to be written

$$-Af^N f' = (B/R)f^{-M} \quad \text{at} \quad \eta = 0 \tag{18}$$

Finally, using Eqs. (13) and (14) in condition (6) yields

$$f = 0 \quad \text{at} \quad \eta = \infty \tag{19}$$

Hence, the problem of Eq. (5) subject to conditions (6) and (7) can indeed be

transformed to the ordinary problem in f and η, of Eq. (16) subject to conditions (18) and (19).

Rather than seeking to solve for $f(\eta)$ in the usual and complete sense, its existence and uniqueness will be accepted, its general nature will be noted, and it will be used to derive several overall relationships of interest. Note first that f is zero at $\eta = \infty$, by condition (19). Next, at $\eta = 0$, uniqueness requires f(0) to have a given constant value, and this value must be finite and greater than zero or else the water content $\theta(0, T)$ at the inlet boundary $X = 0$ cannot increase with time. Putting these conditions into Eqs. (13) and (14) yields the important relationship

$$\theta(0, T) - \theta_a = f(0)T^{\beta} \tag{20}$$

Furthermore, taking the partial derivative of Eq. (14) with respect to X yeilds

$$\frac{\partial \theta}{\partial X} = T^{\beta-\alpha} f'(\eta) \tag{21}$$

which shows $f'(\eta)$ to be negative since $\partial\theta/\partial X$ is intrinsically negative, except at large X where the water content has not yet changed from θ_a and $\partial\theta/\partial X$ is zero. Finally, because of uniqueness and the negative slope of $f(\eta)$

$$\int_0^{\infty} f(\eta)d\eta = \text{constant} = S_R \tag{22}$$

At a fixed time T, Eq. (22) becomes, with the aid of Eqs. (13) and (14)

$$T^{-(\beta+\alpha)} \int_0^{\infty} (\theta - \theta_a)dX = S_R \tag{23}$$

but the integral in Eq. (23) is the scaled cumulative quantity of water Q absorbed per unit cross sectional area during time T. Hence, Eq. (23) can be rearranged to give

$$Q = S_R T^{\beta+\alpha} \tag{24}$$

If $X = \gamma x$ is used to write $dX = \gamma dx$ in the integral of Eq. (23), the resulting integral of $(\theta - \theta_a)dx$ is the unscaled cumulative quantity of absorbed water q, so that the resulting $Q = \gamma q$ is similar to the scaling transformations (4).

Q can also be determined from the flux at the inlet boundary $X = 0$ by

$$Q = \int_0^T V_{X=0} dT = -\int_0^T [D(\theta)(\partial\theta/\partial X)]_{X=0} dT \tag{25}$$

where $V_{X=0}$ is the scaled flux at the inlet boundary expressible by either side of the boundary equation of condition (7). Using Eqs. (11), (13), (14), (15), (18), and (21) to evaluate the integrand in Eq. (25), the integration yields

$$Q = BT^{\alpha+\beta}/[(\alpha + \beta)Rf^M(0)] \tag{26}$$

Comparing Eqs. (24) and (26) shows that

$$S_R = B/[R(\alpha + \beta)f^M(0)] \tag{27}$$

which expresses the reciprocal dependence of S_R upon the hydraulic resistance R of the porous plate (crust). The f(0) of Eq. (20) can be obtained from Eq. (27) as

$$f(0) = [B/(RS_R[\alpha + \beta])]^{1/M} \tag{28}$$

To investigate the applicability of Eq. (24) for the numerical-solution results shown in Fig. 2, Q was computed from the area under each curve at its fixed value of T, and was then plotted against T on log-log scales in Fig. 4. The points from the numerical solution fall perfectly on the straight line of slope 0.671 up to T = 1000 min, but thereafter they fall very slightly below the line. Even up to T = 10,000 min, however, the agreement is very close.

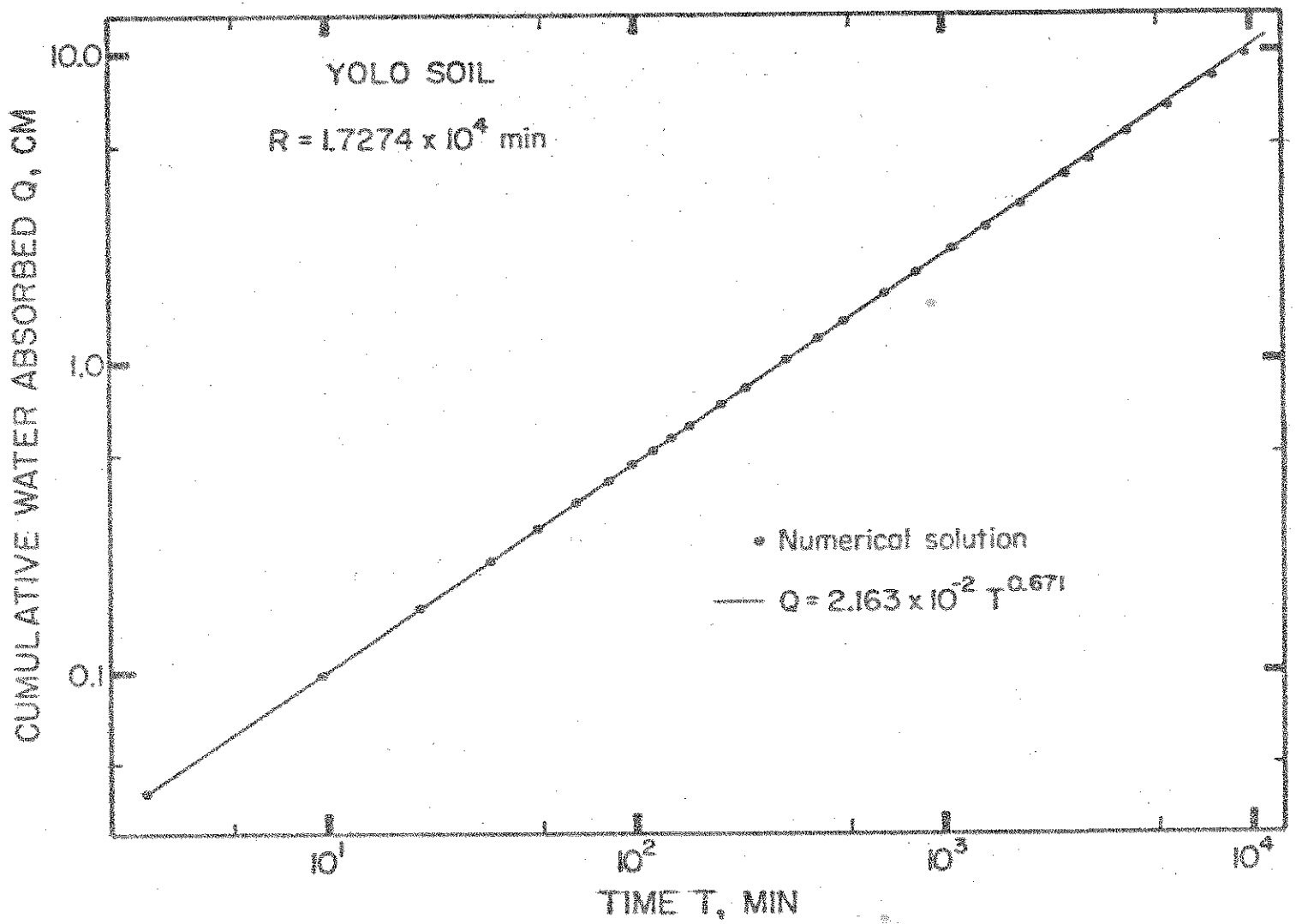

Figure 4 -- Cumulative water absorbed horizontally by Yolo soil as a function of time, as obtained from the numerical solution (Fig. 2). The applicability of Eq. (24) from similarity reduction is shown by the straight line drawn through the points for $0 < T < 1000$ min.

The T of 1000 min corresponds well with the inlet-boundary water content of 0.455 (at X = 0 in Fig. 2) beyond which the suction function of Eq. (12) would not be expected to hold (see also Fig. 3). If the values of N = 2.4242 and M = 4.2270 from Fig. 3 are used in Eqs. (15) and (17), the calculated values of α and β are 0.5941 and 0.0776, respectively. The sum of $\alpha + \beta$ = 0.6717 is thus in excellent agreement with the straight-line slope of 0.671 in Fig. 4. With but slight error, however, the validity of Eq. (24) extends far beyond the seeming validity of the special and restricted forms of $D(\theta)$ and $\tau(\theta)$ [Eqs. (11) and (12)] introduced in the similarity reduction.

Although the graphical results are not shown here, the time dependence of the soil-water content at the inlet boundary was also obtained from Fig. 2 and plotted on log-log scales, in a test of Eq. (20). Again, a straight line was found to describe the data very well up to T = 1000 min, the observed slope of 0.077 agreeing very well with the calculated β of 0.0776 already mentioned. For T above 1000 min, the water content at the inlet boundary increased more slowly than predicted by Eq. (20).

EXPERIMENTAL

Experiments were conducted on uniformly packed horizontal columns of soil, to which water was admitted at one end through fritted-glass porous plates used to simulate crusts. Measurements were made on four separate columns, using 0.4-cm-thick fritted-glass porous plates (crusts) of different hydraulic resistance. These were: an "extra-coarse" plate of practically negligible resistance of 0.2263 min, a "medium" plate of resistance 27.98 min, another "medium" plate of resistance 4595 min, and a "fine" plate of resistance 9567 min. The resistances of the first two plates increased appreciably during the course of the flow experiments, but these increases did not sensibly affect the results, as will be shown later. To suppress such flow-induced changes in resistance in the two higher-resistance plates, a large quantity of water was passed through them prior to starting the soil-column flow experiments. Consequently, during the ensuing 4 to 6 days of soil-column flow measurements, the increase in resistance of these two plates was no more than 5 to 7%, as

assessed by flow measurements on the plates alone before and after the soil-column flow measurements.

The soil used was a nonswelling Salkum silty clay loam from the State of Washington. The air-dry soil, which earlier had been wetted once with deionized water and then dried, was passed through a 0.5-mm sieve and then dry-mixed thoroughly in a twin-shell blender. The Plexiglas soil tube was 6.20 cm inside diameter and 40.0 cm long, with temporary extensions at each end. The soil was transferred through a filling tube placed inside the soil tube and its extensions. Final packing of the soil was accomplished by a small vibrating tool moved about over the outside surface of the soil tube. Bulk densities were measured by gamma-ray attenuation at 1-cm intervals along the length of the soil tube, the filling and packing process being repeated if uniformity was unsatisfactory. The mean bulk density of each packed column was essentially 1.09 g/cc, with practically all individual values within ± 2% of the mean. In no case was any individual value more than 3.5% different from the mean.

The water applicator consisted of a cylindrical Plexiglas chamber of the same outside diameter as the soil column, with the desired fritted-glass porous plate (disc 6.1 cm in diameter and 0.4 cm thick) secured across the end of the cylindrical chamber and made leak proof with a circular rubber O-ring. The chamber behind the porous plate was filled and supplied with water from a calibrated reservoir equipped with a constant-level Mariotte tube. The porous plate was wetted under vacuum prior to the filling of the chamber in the water applicator. The soil column and the cylindrical water applicator were aligned by placing them longitudinally on a V-shaped metal support. Water entry from the reservoir through the porous plate into the soil was initiated at time zero by moving the water applicator gently but firmly to bring the water-saturated porous disc against the soil. The water in the chamber behind the porous plate was maintained by the Mariotte tube at a level 1.0 cm below the bottom of the soil column. The cumulative volume of water absorbed and the distance of wet-front penetration within the soil were recorded periodically. The wet front was always within about ± 1 mm of a plane perpendicular to the axis of the soil column. The water temperature was maintained at 20 ± 0.5 °C.

Starting at 0.2 or 0.5 cm from the water-inlet end of the soil column, water contents at numerous positions were determined by gamma-ray attenuation. The gamma-ray beam sampled a column portion of about 0.1 cm in the direction of water movement. Gamma-ray intensities were determined from gamma counts occurring during preset time intervals ranging from 2.000 to 60.000 sec, depending on the rapidity of wetting. Gamma-ray intensities through a standard absorber were obtained every 1 to 2 hr to allow for any time-dependent changes in the counting apparatus if needed. The gamma-ray intensities were corrected for the dead time of the apparatus, and were then converted to water contents by the standard attenuation equation.

The resulting water-content data, considered as functions of time and position, were subjected to a computer analysis that is under preparation for separate publication. This provided direct evaluation of flux-gradient relationships and diffusivity functions for each soil column. For the numerous computations of slopes, functions, and integrals thus required, the least-squares curve-fitting techniques of parabolic splines and sliding parabolas (DuChateau et al., 1972) were employed.

RESULTS

From previous measurements it was known that the extra-coarse plate (r = 0.2263 min) constituted an essentially negligible crust resistance. Even in the presence of the more resistive medium plate (r = 27.98 min), the measured soil-water contents and cumulative water absorbed were indistinguishable from those found with the extra-coarse plate. The two plates of still higher resistance (r of 4595 and 9567 min), however, did slow down the flow drastically. For the highest crust resistance (r of 9567 min) the water contents are plotted in Fig. 5 against the Boltzmann variable $x/t^{1/2}$, for a number of positions x ranging from 1.0 to 29.0 cm from the water-inlet end of the soil column. This position parameter x that labels the curves in Fig. 5 differs, of course, from the time parameter used in the theoretical curves of Fig. 2. Nevertheless, the curves of Fig. 5 do move progressively outward, in qualitative agreement with Fig. 2, except that definite curve coalescence appears to have been attained for the three outermost curves (15.0 cm and beyond).

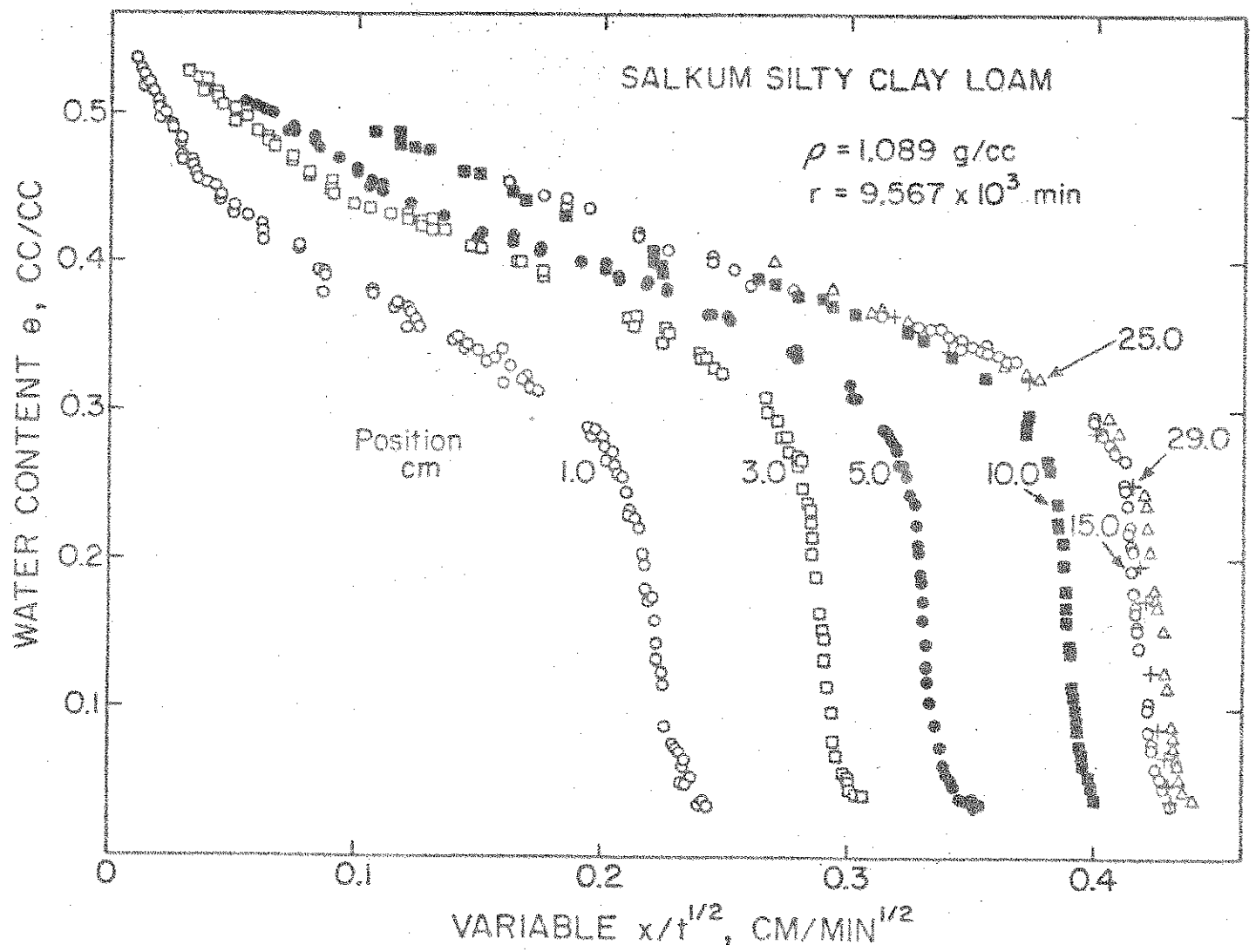

Figure 5 -- Experimental soil-water content θ versus $x/t^{1/2}$ at different fixed positions x during horizontal water entry into Salkum soil through a crust resistance of 9567 min; ρ is the mean soil bulk density.

For the two soil columns of effectively zero crust resistance (r of 0.2263 and 27.98 min), the computer analysis of flux-gradient and diffusivity-function relationships indicated deviations from the flux-gradient proportionality required by the Buckingham-Darcy equation, and upon which Eq. (1) is based. The deviations were of the same nature and about the same magnitude as those in the data of Rawlins and Gardner (1963) for Salkum silty clay loam, as treated in detail by Swartzendruber (1963). For the two soil columns with high crust resistance (r of 4595 and 9567 min), however, the computer analysis showed all flux-gradient data to fall within a relatively narrow range of gradients, so that any deviation from flux-gradient proportionality could not clearly be separated from the scatter in the data. Such an approximate validity of Eq. (1) thus provides justification for using these experimental results in a test of the diffusivity function of Eq. (11) used in the similarity-reduction analysis. A log-log plot of diffusivity versus $\theta - \theta_a$ is shown in Fig. 6 for the two soil columns of different but high-resistance crusts. For any given θ below about 0.25 ($\theta - \theta_a$ of 0.22), there is some trend of decrease in diffusivity with increase in position, which may still reflect some vestige of the nonproportional flux-gradient behavior as already discussed. Nevertheless, for given θ above 0.25, the diffusivities at different positions appear to coalesce within the error of determination, and there is good overall agreement between the two columns even though the crust resistances differ by two fold. Also, for $\theta - \theta_a \geq 0.15$ and within the scatter of the data, the diffusivities in Fig. 6 appear to be reasonably well represented by the straight line P'P. Furthermore, the slope of P'P is the $N = 5.10$ of Eq. (11) as calculated by Eqs. (15) and (17) from α and β determined in the manner now to be described.

The quantity $\alpha + \beta$ of Eq. (24) is the slope of a log-log plot of cumulative water absorption versus time, such as shown in Fig. 7 for the same two soil columns as in Fig. 6. For the same soil but different crust resistances, Eq. (24) specifies the log-log plots to consist of displaced straight lines but parallel to each other, since α and β depend only on the soil [from Eqs. (15), (17), (11), and (12)]. The experimental data in Fig. 7 do appear to exhibit displaced-parallel behavior over the time range from 15 to 1000 min. Why discrepancies occur for times smaller than 15 min is not known, but this would be

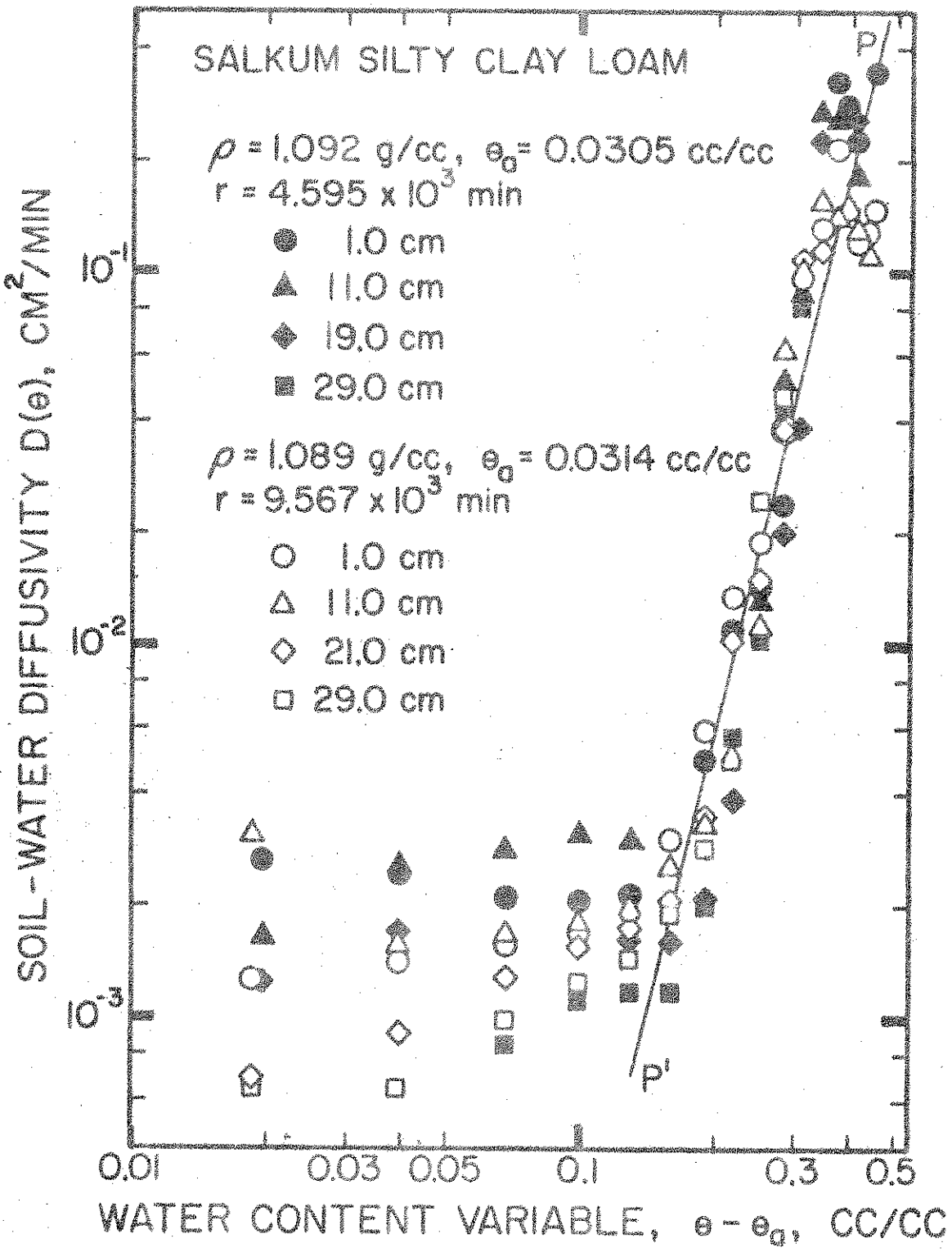

Figure 6 — Water diffusivity of Salkum soil for horizontal water entry through two different crust resistances, as obtained by direct analysis of water content versus time and postion; ρ is the mean soil bulk density. P'P is a straight line of slope 5.10.

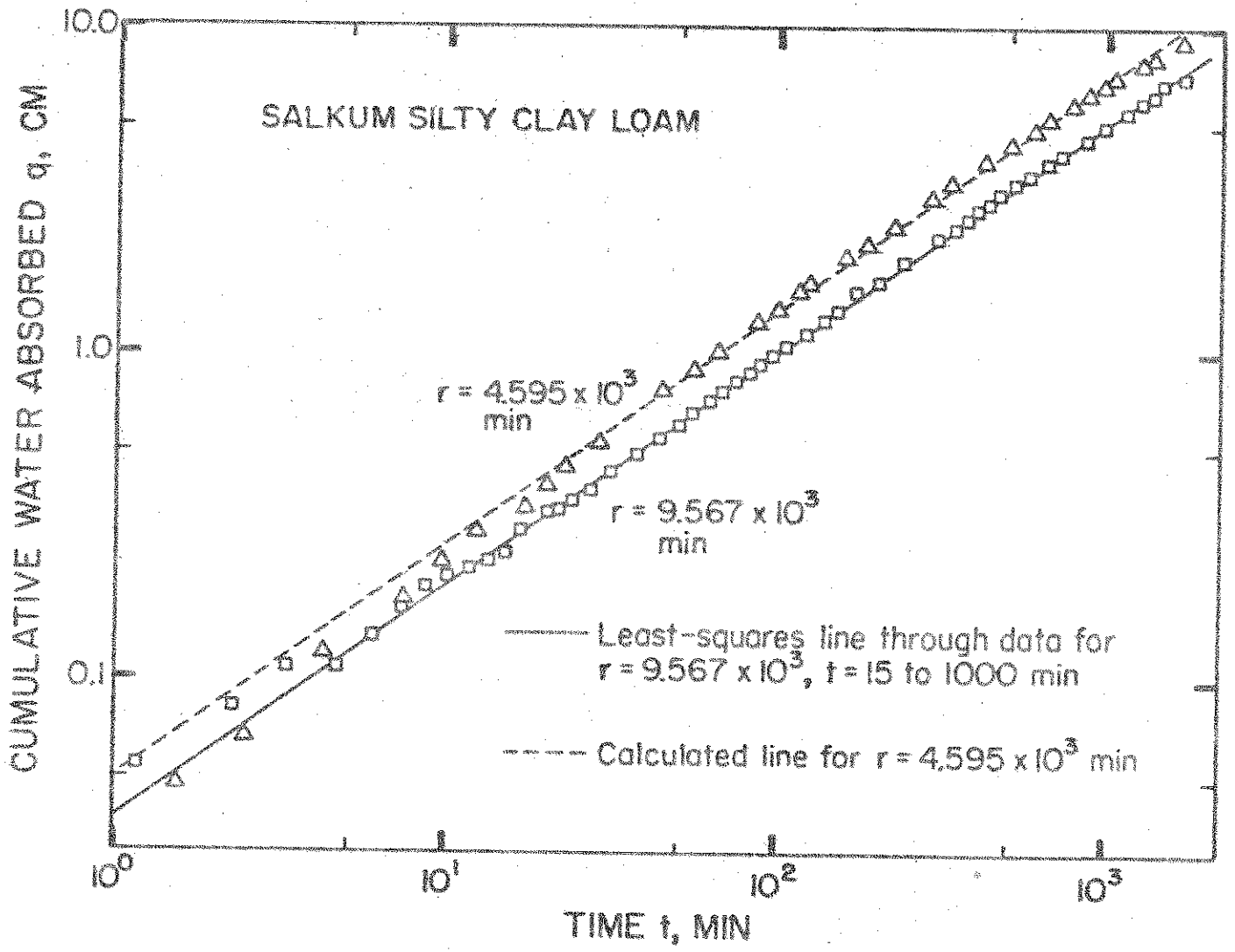

Figure 7 — Cumulative water absorbed horizontally by Salkum soil as a function of time, for two different crust resistances. The solid and broken straight lines indicate the applicability of Eq. (24) from similarity reduction.

the period for measurement errors and effects of possible contact resistance to be maximal. For the range 15 to 1000 min, $\alpha + \beta$ and S_R for the higher crust resistance (r of 9567 min) were evaluated by least squares, and this evaluation is depicted by the solid straight line in Fig. 7. Equation (27) was then used to derive a predicted S_R for the lower-resistance crust (r of 4595 min), as based upon S_R for the higher-resistance crust, the ratio of the two crust resistances, and the scaling transformations (4) and $Q = \gamma q$. Using this predicted S_R in Eq. (24), along with $\alpha + \beta = 0.713$, resulted in the dashed straight line of Fig. 7, which passes very well through the points for the lower-resistance crust over the time range 15 to 1000 min, and thus shows that $\alpha + \beta = 0.713$ is as valid for the lower-resistance crust as for the higher.

The value of β was then determined from data taken on the soil column with the higher crust resistance. Experimental water contents at 0.2 cm from the inlet end of the soil column were taken as the measured values of the boundary water content $\theta(0, T)$. Hence, $\theta(0, T) - \theta_a$ was plotted against time on log-log scales in accord with Eq. (20), which was found to be a good representation of the data over the time-range 15 to 1000 min. The least-squares value of β was found to be 0.060, which, when combined with $\alpha + \beta = 0.713$, yields $\alpha = 0.653$.

Possessing numerical values of α and β made it possible to investigate η and $f(\eta)$ from Eqs. (13) and (14), since gamma-ray measurements of water content versus time at various fixed positions were available. For a given crust resistance, and for times not exceeding the limit of 1000 min used in Eqs. (20) and (24) to evaluate β and α, a plot of $(\theta - \theta_a)T^{-0.060}$ versus $XT^{-0.653}$ should coalesce to a single curve independently of X and T, since $f(\eta)$ is a unique function. Such plots are shown in Fig. 8, where for each crust resistance the experimental values for six different positions do indeed coalesce reasonably well into a single curve identifiable as $f(\eta)$, except perhaps for the data at the 1.0-cm position in the column of lower curst resistance (r of 4595 min). Overall, the results in Fig. 8 are considered to be quite encouragingly in support of the validity of the similarity analysis.

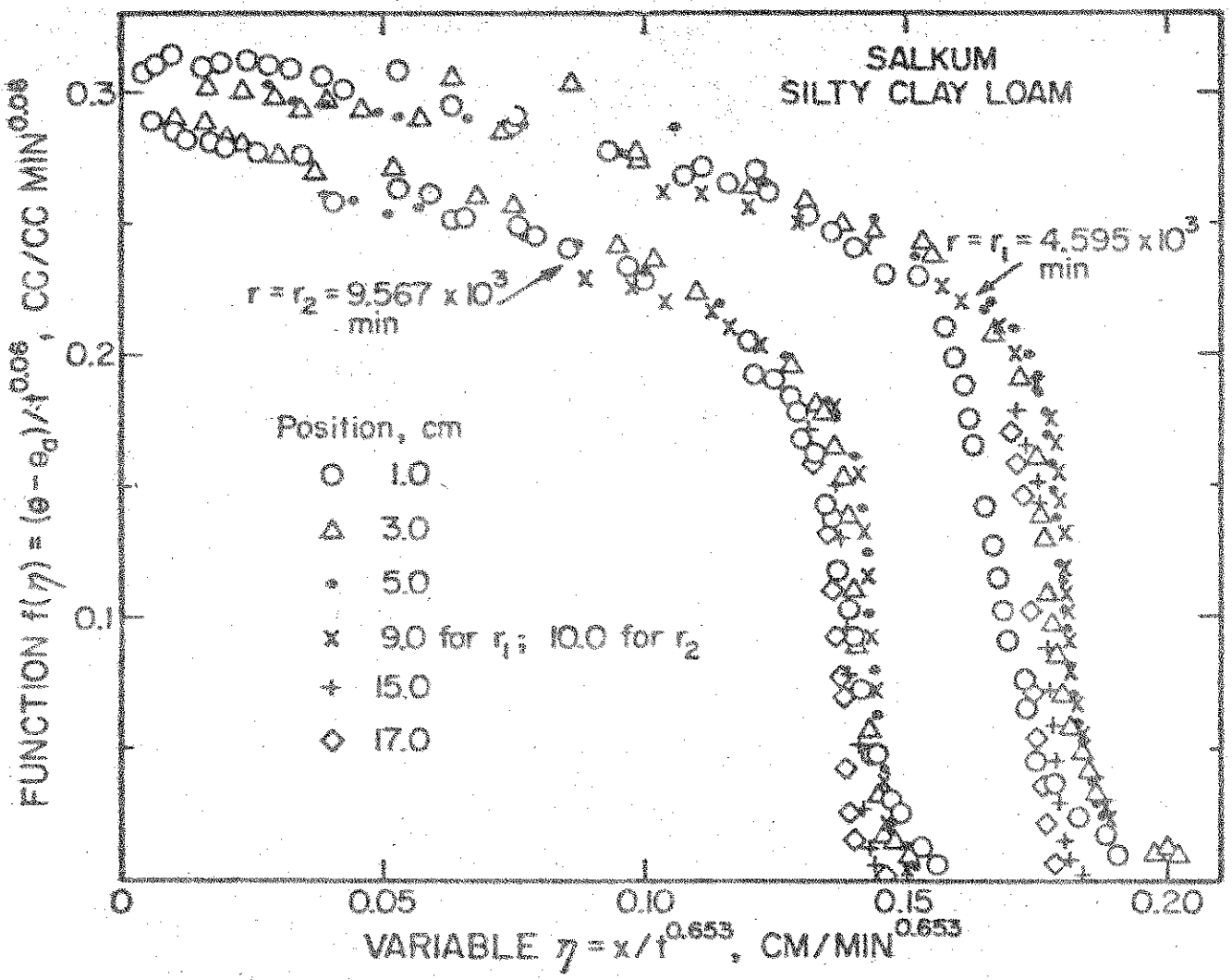

Figure 8 — Experimental values of $(\theta - \theta_a)t^{0.06}$ versus $x/t^{0.653}$ at different fixed positions x during horizontal water entry into Salkum soil through two different crust resistances.

DISCUSSION

The theoretical analyses given here provide descriptions of interest for several aspects of the entry of water into crusted soils, and the experimental validations indicate the theory to be applicable within reasonable limits. This is not to say, however, that the particular mathematical description considered here is without important limitations for various situations. The theory represented by Eqs. (1) and (3) may not always hold adequately, whether due to nonproportional flow, soil heterogeneity, temperature and salt effects, or other factors. Only one set of boundary and initial conditions has here been considered, and, of course, a constant crust resistance may not be realistic if a progressively more resistive crust is being formed during the course of the flow process. Nevertheless, the analysis presented here does provide a starting basis, and its extension to vertically downward infiltration would seem worthy of effort.

The transformations (4) are particularly useful in determining the effect of different resistances of crust from a solution (theoretical or experimental) of one particular case, and in then using this information to establish the resistance at which the flow will be sensibly affected. For example, in the Yolo soil 0.025 of the value of resistance used in calculating the data of Fig. 2 will result in a water content of nearly 0.485 on the boundary $X = 0$ in the first 6 min of flow, with a wet-front penetration of 0.75 cm. This resistance may thus be considered to have but a slight effect on the flow after a small time.

It is of interest that the similarity-reduction analysis involves, and gives rise to, time dependencies made up of powers of time that are different from 1/2; that is, Eqs. (13), (14), (20), and (24), wherein none of α, β nor $(\alpha + \beta)$ are equal to 1/2. The main limitations of this analysis are the requirements that the soil be adequately represented by the functional forms $D(\theta) = A(\theta - \theta_a)^N$ and $\tau(\theta) = B(\theta - \theta_a)^{-M}$ [Eqs. (11) and (12), respectively], and that the soil not become too wet beyond the crust. For water absorption into some types of naturally crusted air-dry soils, the above requirements may be closely or approximately met during early to intermediate stages, at

low and intermediate soil-water contents. In such cases, the similarity description of flow during early to intermediate stages can be combined with known flow behavior at large times. The point can be illustrated by the data for Salkum soil. The similarity equations hold reasonably well up to 1000 min in the two high-resistance sets of data (Figs. 7 and 8). That is about the time when the functions of θ versus $x/t^{1/2}$ begin to coalesce (Fig. 5).

CHAPTER 3.

SIMULTANEOUS MEASUREMENT OF TRANSIENT SOIL BULK DENSITY AND WATER CONTENT WITH DUAL-ENERGY GAMMA RAYS

In addition to changes in water content, some soil-water transport processes are accompanied by changes in the bulk density of the soil. Two important examples of this are the formation of a raindrop-induced soil crust during infiltration from rainfall (natural or simulated) by bare soil, and the entry of water into an initially air-dry swelling soil. Since the bulk density increases during crusting and decreases during swelling, the method of single-energy gamma-ray attenuation cannot be used because of the necessity for the bulk density to remain constant. Thus, experimental studies of both crusting and swelling have been hampered by the lack of a suitable means of measuring water content and bulk density simultaneously, independently, and nondestructively. In principle, such measurements can be made by observing the attenuation of gamma-rays of two distinct energies. This has been done for steady-state and slowly-changing soil-water systems (Soane, 1967; Gardenr and Calissendorff, 1967; Corey et al., 1971; and Gardner et al., 1972), but formidable difficulties have heretofore blocked the ready adaptation of the method to rapidly changing transient systems. It shall now be shown in this chapter how even these difficulties can be surmounted in a relatively simple and straightforward fashion.

METHODS AND MATERIALS[1]

Simultaneous Measurement of Water Content and Bulk Density by the Attenuation of Gamma Rays of Two Energies

Gamma-Ray Attenuation Theory

The intensity I of monoenergetic gamma radiation passing through a porous medium with a bulk density ρ and a water content θ is

---

[1] Some of the mathematical symbols hereinafter in this chapter are defined differently than in Chapter 2; hence, in this sense the two chapters should be viewed as separate and self contained.

$$I = I_e \exp(-X\mu_s\rho - X\mu_w\rho_w\theta) \tag{29}$$

where I_e is the gamma-ray intensity through the empty soil container, X is the thickness of the soil in the direction of the gamma-ray beam, ρ_w is the density of water, and μ_s and μ_w are the mass attenuation coefficients of soil and water, respectively. The mass attenuation coefficients for soil and water and the thickness of the soil in the direction of the beam are usually determined experimentally. The shape of the gamma-ray beam and the use of a cylindrical soil container make a precise evaluation of the thickness of soil difficult. In this case it is more convenient to evaluate the lumped calibration constants $U_s = X\mu_s$ and $U_w = X\mu_w\rho_w$ than to evaluate the individual quantities making up each calibration constant. Equation (29) rewritten in terms of the lumped calibration constants becomes

$$I = I_e \exp(-U_s\rho - U_w\theta) \tag{30}$$

The quantities I, I_e, and the mass attenuation coefficients, and hence the lumped calibration constants U_s and U_w, are dependent upon the gamma-ray energy. Cs-137 and Am-241 are the two gamma-ray sources most frequently used for measuring water content and bulk density by the double gamma-ray attenuation technique. Rearranging Eq. (30) and rewriting it for Am-241 and Cs-137, using subscripts to specify the gamma-ray sources, yields

$$\ln(I_e/I)_{Am} = U_{sAm}\rho + U_{wAm}\theta \tag{31}$$

$$\ln(I_e/I)_{Cs} = U_{sCs}\rho + U_{wCs}\theta \tag{32}$$

If the four lumped calibration constants in Eqs. (31) and (32) are known and the intensities I_e and I are measured for both Cs-137 and Am-241, Eqs. (31)

and (32) can be solved simultaneously for ρ and θ to yield

$$\rho = \frac{U_{wCs} \ln(I_e/I)_{Am} - U_{wAm} \ln(I_e/I)_{Cs}}{U_{sAm}U_{wCs} - U_{sCs}U_{wAm}} \tag{33}$$

$$\theta = \frac{U_{sCs} \ln(I_e/I)_{Am} - U_{sAm} \ln(I_e/I)_{Cs}}{U_{sCs}U_{wAm} - U_{sAm}U_{wCs}} \tag{34}$$

To minimize any errors in water content and bulk density measurements due to random decay processes, high intensities through the packed soil column are desirable. When high intensities are measured it is usually desirable to correct the measured intensities for the dead time of the electronic system. It may also be necessary to use an auxillary standard to reduce the intensities through the empty soil container to reasonable levels. Furthermore, measurements through a standard absorber are usually made at regular intervals, to correct for any electronic drift in the measuring instruments as well as intensity changes due to radioactive decay. In this work, measured intensities for Cs-137 and Am-241 were corrected for dead time, auxillary standards, and electronic drift and radioactive decay by methods described by Nofziger (1970) for single Cs-137 gamma-ray attenuation.

The Double Gamma-Ray Attenuation Apparatus

The applications of the double gamma-ray attenuation technique of determining the water content and bulk density of a porous medium by Soane (1967), Gardner and Calissendorff (1967), Corey et al. (1971), and Gardner et al. (1972) have been largely restricted to slowly changing systems, because of a low Am-241 intensity and/or because the Cs-137 and Am-241 intensities were measured separately and consecutively rather than simultaneously. Corey et al. (1971) suggested that both intensities can be measured simultaneously using a 4096-channel analyzer, but even so they only gave results for intensities measured consecutively with a 400-channel analyzer.

The double gamma-ray apparatus developed in this work has the capability of measuring the Cs-137 and Am-241 intensities simultaneously. To assemble the double gamma-ray apparatus, an Am-241 gamma-ray source, an amplifier-analyzer, and an electronic scaler were added to a gamma-ray system (Cs-137) already functional with a single-energy beam. The complete apparatus consisted of a 389-mc Am-241 gamma-ray source, a 280-mc Cs-137 gamma-ray source, a scintillation probe, a high-voltage power supply, two amplifier-analyzers (single channel), two scalers, and a teletypewriter.[2]

The Cs-137 source was contained within a lead shield 15 cm in diameter and 15 cm long, and was mounted behind the Am-241 source as shown in Fig. 9. The Am-241 source was sealed in a stainless steel source holder behind a thin aluminum window. The source was positioned to give an active area 1.4 mm high and 2.8 cm wide. The thickness of the source in the direction of the gamma-ray beam was only 0.9 mm, to minimize absorption of the Am-241 gamma-rays by the source material itself. The Am-241 source holder was mounted in a brass shield 5 cm long, 6.5 cm wide, and 12 cm high. A lead collimator 7.5 cm long in the direction of the beam containing a slit 1 mm high and 1.8 cm wide was mounted in the Cs-137 shield, between the two sources. A lead collimator 1 cm long in the direction of the beam with a slit 1 mm high and 2.8 cm wide was mounted in front of the Am-241 source. The Am-241 source was rotated to give the maximum intensity through its collimator, and the two collimators were then aligned. The scintillation probe, and a lead collimator 5.1 cm long in the direction of the beam with a slit 1 mm high and 4 cm wide, were mounted in another lead shield 15 cm in diameter and 15 cm long. Thus, as the composite, dual-energy gamma-ray beam emerged from the Am-241 collimator, it passed on through the collimator in front of the scintillation probe and fell on the sodium iodide crystal within the probe.

---

[2] The Cs-137 gamma-ray source, scintillation probe, and amplifier-analyzers were purchased from the Nuclear-Chicago Corporation, Box 367, Des Plaines, Illinois. The Am-241 gamma-ray source was purchased from Monsanto Research Corporation, 1515 Nicholas Road, Dayton, Ohio. The high-voltage power supply and scalers were purchased from Hewlett-Packard Company, 4002 Meadows Drive, Indianapolis, Indiana. The teletypewriter was purchased from Teletype Corporation, 5555 Touhy Avenue, Skokie, Illinois.

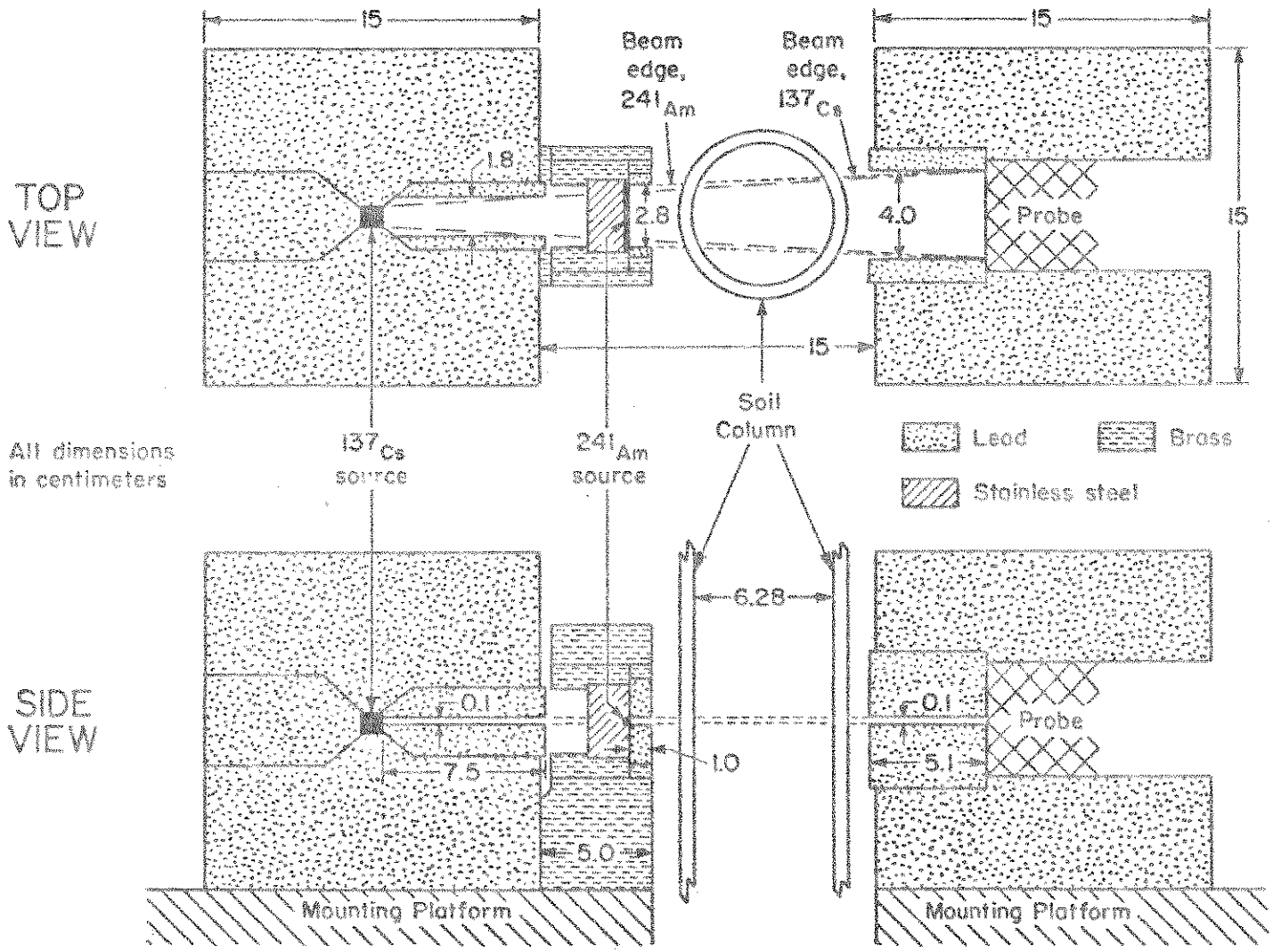

Figure 9 -- Schematic diagram of Am-241 and Cs-137 sources mounted to produce a dual-energy gamma-ray beam.

The Am-241 collimator and the detector collimator were mounted 9 cm apart on a heavy movable platform. The platform was supported by four long Saginaw screws which could be turned simultaneously to move the platform up or down smoothly and uniformly. By this means, the gamma-ray sources and detector could be located at any position of interest along a vertical soil column.

With the two gamma-ray sources mounted in this manner, gamma rays from both sources are detected in the single scintillation probe, and the gamma counts from the two sources must be separated electronically. To accomplish this, the scintillation probe, consisting of a thallium-activated sodium iodide crystal 5.1 cm long and 5.1 cm in diameter in series with a photomultiplier and preamplifier, was connected in parallel to two amplifier-analyzers. One amplifier-analyzer was adjusted to detect Cs-137 gamma rays and the other was adjusted for rays from Am-241. The amplifier-analyzer used to detect Cs-137 gamma-rays was operated in an integral mode, meaning that all pulses corresponding to photons having energies greater than 0.55 Mev were counted. The amplifier-analyzer used to detect the Am-241 gamma-rays was operated in a differential mode so that pulses corresponding to photons having energies within the energy band of 0.035 to 0.085 Mev were counted. The differential mode was needed to separate Am-241 photons from the higher energy Cs-137 photons. Even so, a wide energy band was used, to make the system relatively insensitive to small fluctuations in the electronic system.

The output pulses from each amplifier-analyzer were counted on a scaler. The two scalers were slaved together so that both units started and stopped simultaneously. The number of counts registered by each scaler during a chosen preset counting period could be recorded manually from the visual display, or automatically by means of a teletypewriter. The teletypewriter also punched the data on paper tape for computer processing. Since the teletypewriter was capable of recording only 10 characters per second, a buffer was built into the electronic interfacing unit between the scalers and the teletypewriter. At the end of a preset counting period, the outputs from the scalers were loaded very rapidly into the buffer. While the contents of the buffer were recorded on the teletypewriter, the scalers would reset and begin counting again.

The Effect of Cs-137 on Measured Intensities of Am-241

By mounting the Cs-137 gamma-ray source behind the Am-241 gamma-ray source and aligning the collimators, gamma rays from both sources concurrently pass through essentially the same portion of soil and are detected in one detector, and the intensities for both sources can be determined simultaneously. These characteristics are very desirable for measuring the bulk density and water content of rapidly changing soil systems. One problem does exist with this arrangement, in that the measured Am-241 intensity through a particular abosrber is larger if both Am-241 and Cs-137 sources are in place than if only the Am-241 source is present. Stated another way, a non-negligible intensity in the Am-241 energy band is measured when the Am-241 source is completely removed and only the Cs-137 source is present. As a result of this effect of Cs-137 on the measured intensity for Am-241, Eq. (31) no longer holds for the measured intensity in the Am-241 band. Some method of correcting the measured Am-241 intensity for the effect of Cs-137 must be found if the double gamma-ray attenuation theory is to be used with the apparatus as just described.

It has been suggested by Corey et al. (1971) that the effect of Cs-137 on the measured Am-241 intensity is somehow due to Compton scattering. The following considerations suggest the hypothesis that very few counts in the Am-241 band arise from Compton scattering in the absorbing medium between the Am-241 collimator and the scintillation crystal. From the equation for Compton scattering, one can calculate that a photon from Cs-137 having an energy of 0.66 Mev must be scattered 4 times at an angle of 180°, or even more times at smaller angles, to reduce its energy to 0.66 Mev, the energy of Am-241. The probability of a Cs-137 photon being thus scattered a sufficient number of times and reducing its energy to that of Am-241, and still remaining in the collimated gamma-ray beam, is very small. This suggests that most of the counts in the Am-241 band due to Cs-137 arise in the detector (possibly from Compton scattering there) rather than from Compton scattering in the absorbing medium between the collimators.

If the detector is the source of most of the counts in the Am-241 band due to Cs-137, the intensity in the Am-241 band due to Cs-137 may turn out to

be a function of the Cs-137 intensity only. If it can be shown that the intensity in the Am-241 band due to Cs-137 is a unique function of the Cs-137 intensity and is independent of the absorbing medium, and if the function can be evaluated, the measured Am-241 intensities can be corrected for the effect of Cs-137 in the Am-241 band.

The following set of experiments was performed to determine if the intensity in the Am-241 band due to Cs-137 was a unique function of the Cs-137 intensity. The Am-241 source was removed from its shield and was replaced by a brass absorber to reduce the Cs-137 intensity to the level obtained with the Am-241 source in place. The intensity in the Am-241 band due to Cs-137, along with the intensity in the Cs-137 band, were simultaneously measured for the useful range of Cs-137 intensities and for different absorbing materials. The sequence and kind of absorbers used are given in Table 1. Measurements through glass, brass, and water were repeated three times to determine the reproducibility of the functional relationship for a particular material. In each of the 15 experiments, between 80 and 90 intensity measurements were made. The preset counting period at each intensity was adjusted to obtain approximately 10^6 counts for Cs-137. This resulted in approximately 10^5 counts in the Am-241 band. The water and porous materials were placed in a V-shaped container made of Plexiglas. This container provided a convenient method of changing the thickness of the absorber, and hence the Cs-137 intensity. Intensity measurements through a standard absorber were made approximately every 40 min. To allow correction for any small changes that might have occurred in the electronic system, each measured Cs-137 intensity was multiplied by the ratio of the mean Cs-137 intensity through the standard absorber for the entire set of experiments and the Cs-137 intensity through the standard at the time of interest. A similar correction scheme was used for the Am-241 intensity.

A weighted non-linear regression analysis was performed on the data from each experiment and on the data as pooled together. A cubic polynomial was chosen as the regression model. Several other mathematical models were tried but were considered unsatisfactory. The standard deviation of the intensity in the Am-241 band was not constant for the entire range of intensities but increased with intensity. (The data were obtained in a manner such that the

Table 1. Percent relative difference between the predicted intensity in the Am-241 band due to Cs-137 for a cubic polynomial fitted to the data for one absorber and that fitted to the pooled data for all absorbers (x = Cs-137 intensity, $\hat{y}_p$ = predicted Am-241 intensity due to Cs-137 for pooled regression equation).

Order of Experiment	Absorbing Medium	Percent Relative Difference		
		x = 4000.0 cps $\hat{y}_p$ = 413.71 cps	x = 8000.0 cps $\hat{y}_p$ = 810.74 cps	x = 12000.0 cps $\hat{y}_p$ = 1194.00 cps
1	Glass	-0.26	-0.14	-0.15
5	Class	-0.66	-0.27	-0.18
11	Glass	0.07	-0.08	0.16
2	Brass	-0.32	-0.44	-0.22
9	Brass	-0.36	-0.26	0.10
13	Brass	-0.41	-0.18	0.17
3	Water	-0.25	0.00	0.02
7	Water	-0.07	0.12	-0.18
15	Water	0.03	0.08	0.09
4	[Salkum silty clay loam] air dry	0.23	0.07	-0.20
6	[Salkum silty clay loam] wet	0.16	0.28	-0.01
8	[75% banding sand, 25% silt] air dry	0.64	0.18	-0.07
10	[75% banding sand, 25% silt] wet	0.63	0.33	0.34
12	Russell silt loam, air dry	0.24	0.24	0.15
14	Russell silt loam, wet	0.15	0.23	0.15

standard deviation in counts for all of the data points was nearly constant, but because of different preset counting periods, the standard deviation in intensity was not constant.) Principles of statistics indicate that if the standard deviation is not constant for all of the data points, each data point used in a regression analysis should be weighted by a weighting factor which is inversely proportional to the square of its standard deviation (Pennington, 1970). The standard deviation in counts in the Am-241 band due to Cs-137 was found experimentally to agree quite well with that of a Poisson distribution, meaning that the standard deviation in counts σ is given by $\sigma = N^{1/2}$, where N is the total number of counts measured in the Am-241 band. The corresponding standard deviation in intensity is given by $\sigma_I = \sigma/T$ where T is the preset counting period during which N counts were observed. Since the weighting factor used for each point should be inversely proportional to the square of its standard deviation, the weighting factors used in this investigation were inversely proportional to N/T^2 (directly proportional to T^2/N).

The intensity in the Am-241 band due to Cs-137, considered as a function of the intensity of Cs-137 through an absorber of wet Salkum silty clay loam, is shown in Fig. 10. The curve shown is the cubic polynomial fitted to the pooled data for all of the absorbers. The curve is given by $\hat{y}_p = a + bx + cx^2 + dx^3$, where $a = 1.1343 \times 10^{1}$, $b = 1.0056 \times 10^{-1}$, $c = 9.5979 \times 10^{-8}$, $d = -2.1916 \times 10^{-11}$, $\hat{y}_p$ is the intensity in the Am-241 band due to Cs-137, and x is the intensity in the Cs-137 band. Although the curve is nearly a straight line, it does bend downward significantly, and this curvature must be taken into account to obtain a precise correction.

The percent relative difference between the predicted Am-241 intensity due to Cs-137 for a particular material and that for the pooled data are shown for three Cs-137 intensities in Table 1. All of the predicted values fall within ± 0.7% of the pooled value. Predicted intensities in the Am-241 band from three repeated experiments for glass, brass, and water differ by as little as 0.1% to as much as 0.7%. The maximum and minimum percent relative differences between measured Am-241 intensities due to Cs-137 and predicted intensities from the pooled regression equation evaluated at the measured Cs-137 intensities are shown in Table 2. For each of the absorbers, data points lie on both sides

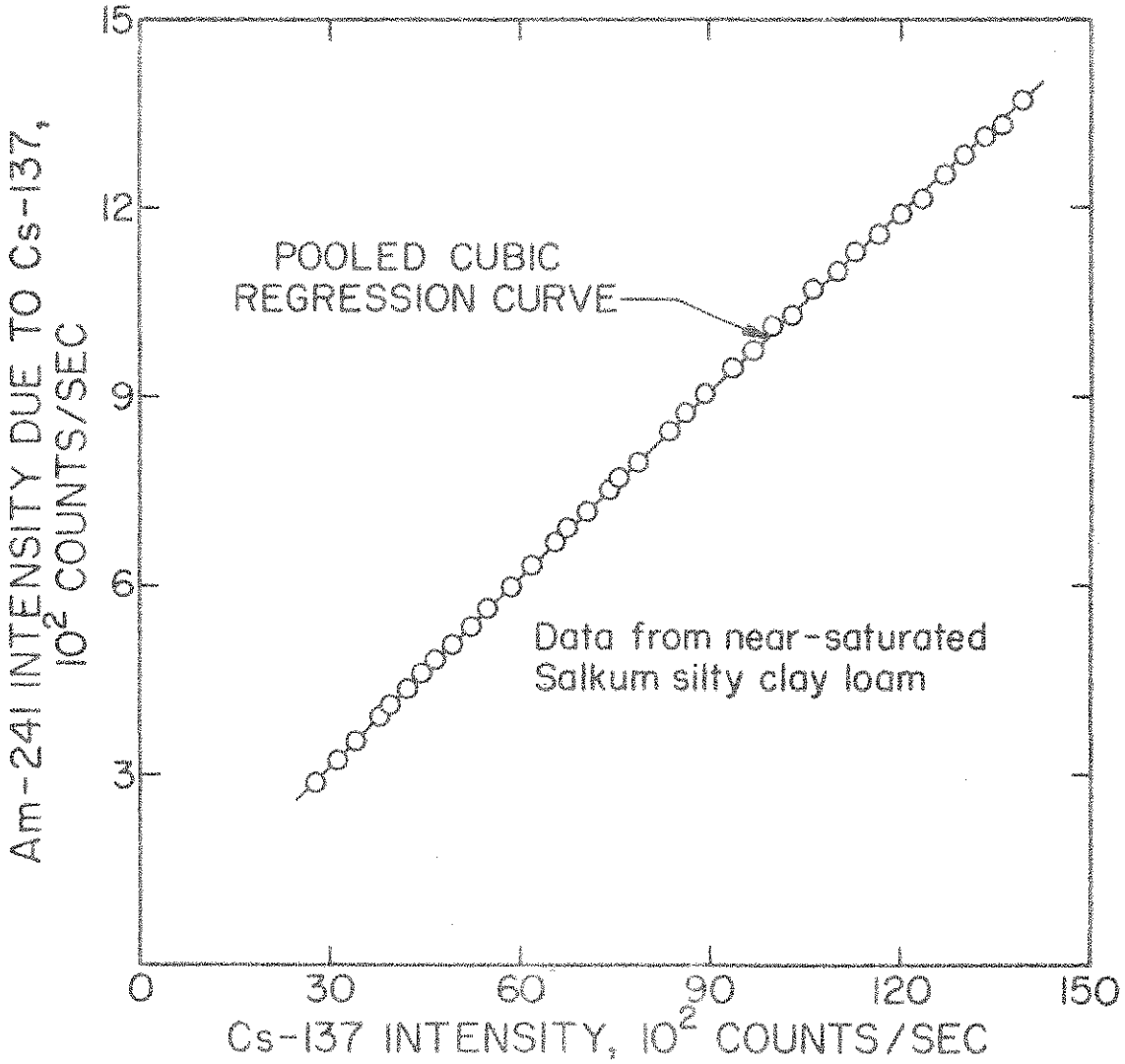

Figure 10 -- Intensity in the Am-241 band due to Cs-137, versus Cs-137 intensity.

Table 2. Maximum and minimum percent relative differences between measured intensity in Am-241 band due to Cs-137 and the corresponding predicted intensity from the pooled regression equation (x_j = measured Cs-137 intensity, y_j = measured intensity in Am-241 band due to Cs-137, $\hat{y}_p(x_j)$ = predicted intensity in Am-241 band due to Cs-137 for pooled regression equation).

Order of Experiment	Absorbing Medium	Percent Relative Difference $\frac{y_j - \hat{y}_p(x_j)}{\hat{y}_p(x_j)} \times 100$	
		Maximum	Minimum
1	Glass	0.64	-1.30
5	Glass	0.60	-1.17
11	Glass	0.91	-1.44
2	Brass	0.84	-1.20
9	Brass	0.92	-1.88
13	Brass	1.06	-1.71
3	Water	1.11	-1.16
7	Water	1.07	-1.35
15	Water	0.90	-1.03
4	[Salkum silty clay loam] air dry	1.30	-1.28
6	wet	1.52	-0.95
8	[75% banding sand, 25% silt] air dry	1.48	-0.85
10	wet	1.40	-0.75
12	Russell silt loam, air dry	1.29	-0.86
14	Russell silt loam, wet	1.08	-0.56

of the pooled curve. These overall results are taken as evidence that the intensity in the Am-241 band due to Cs-137 is essentially independent of the absorbing medium.

The significance of a relative difference of ± 0.7% in the predicted intensity in the Am-241 band due to Cs-137 depends upon the intensity due to the Am-241 source alone. For soil columns used in this study, the Am-241 source intensities are at least 9 times as large as the intensity in the Am-241 band due to Cs-137. The maximum relative difference in the Am-241 intensity that would result from using the regression equation for any of the 15 experiments instead of the equation for the pooled data is thus only ± 0.08%. On the basis of these results, it was concluded that the intensity in the Am-241 band due to Cs-137 can be considered a unique function of the Cs-137 intensity, and can be taken into account and evaluated in the manner here indicated.

In the remainder of this work, each measured Am-241 intensity was corrected for the effect of Cs-137 by subtracting from the Am-241 intensity the intensity predicted by the pooled regression equation from the measured Cs-137 intensity. For all measurements to be reported in this work, the value of the Cs-137 intensity always fell somewhere between the limits of the range (2770 to 13900 counts per sec) shown in Fig. 10, so that no extrapolation of the regression equation beyond its fitted range was ever involved. This correction for the effect of Cs-137 on the measured intensity in the Am-241 band is good only for the physical and electronic systems used in this investigation, although the same correction scheme with an appropriate regression equation would be expected to hold for other physical and/or electronic systems.

Dead-Time Determination

Following the detection of a photon by a scintillation detector, there is a short period of time called "dead time" during which the detector is insensitive to additional photons. Therefore, if two photons enter the detector separated in time by less than the dead time, only one of the photons will be detected and the resulting measurement will be in error. As a result of this kind of error, the theoretical gamma-ray attenuation equations may no longer hold precisely for measured intensities that are very large. If the dead time

of the detector is known, the measured intensity can be corrected for this error using the equation

$$I = I_m/(1 - \delta I_m) \tag{35}$$

where I and I_m are the corrected and measured intensities, respectively, and δ is the dead time. The method of obtaining the dead time for each gamma-ray system used in this research is as follows.

Single gamma-ray attenuation theory predicts the intensity of radiation I passing through an absorber of thickness x to be given by

$$I = I_0 \exp(-\mu\rho x) \tag{36}$$

where I_0 is the intensity in the absence of any absorber, ρ is the density of the absorber, and μ is the mass attenuation coefficient of the absorber. Written another way, Eq. (36) becomes

$$\ln I = \ln I_0 - \mu\rho x \tag{37}$$

The agreement between the theoretical equations [Eqs. (36) and (37)] and the corrected data points is dependent upon the dead time used. Fritton (1969) described a method in which the dead time of the system was taken to be that value of δ for which the agreement between the corrected experimental data and Eq. (37) was best as measured by a weighted sum of squares of the deviations from Eq. (37). Weighting was used to account for the change in standard deviation with intensity. The method used in the present work differs from that of Fritton only in that the dead time was taken to be that value for which the agreement between the corrected experimental data and Eq. (36) was best, rather than using Eq. (37). That is, the weighted sum of squares of deviations in intensities was minimized instead of the weighted sum of squares of deviations of ln I. The computational technique used in this connection is described by Pennington (1970).

Experimentally, the Am-241 and Cs-137 intensities were measured through various thicknesses of glass. The preset counting period at each thickness was adjusted so approximately one million counts were recorded in the Cs-137 band at each thickness. The corresponding number of counts in the Am-241 band ranged from 0.3 to 5.8 million. The dead times, determined to within ± 0.1 μsec, were found to be 3.2 and 6.2 μsec for Cs-137 and Am-241, respectively. These values agree quite well with values reported by Fritton (1969), and with those of Nofziger (1970) as obtained by a two-source method.

Experimental Verification of Gamma-Ray Attenuation Theory

Single-source Am-241 and Cs-137 systems. As a preliminary step in testing the double gamma-ray attenuation apparatus, it was of interest to see if both Am-241 and Cs-137 as separate gamma-ray systems obeyed the theoretical attenuation equations. With the Am-241 source removed from the apparatus, intensities of Cs-137 gamma-rays passing through known thicknesses of glass were measured. After this was completed the Cs-137 source was removed. The Am-241 source was mounted in front of the detector, and similar intensity measurements were made for Am-241. The measured Cs-137 and Am-241 intensities were corrected for dead-time effects using dead times of 3.2 and 6.2 μsec, respectively.

The ln I as a function of the thickness of glass is shown in Fig. 11 for Cs-137 and in Fig. 12 for Am-241. The lines shown are weighted least-squares lines fitted to Eq. (36). The theoretical linear relationship between ln I and thickness of absorber appears to hold very well for both sources.

Dual-source Am-241 and Cs-137 system. Having verified the theoretical attenuation equations for the separate, individual sources, a similar study was conducted for the combined sources wherein both intensities were measured simultaneously. With both sources in place and producing a dual-energy beam, the gamma-ray intensities were measured simultaneously for various thicknesses of glass. The measured Am-241 intensity was corrected for the effect of Cs-137 in the Am-241 band using the pooled regression equation as already described. The measured Cs-137 intensity and the corrected Am-241 intensity were then corrected for dead-time effects, using the dead times of 3.2 and 6.2 μsec, respectively, as before.

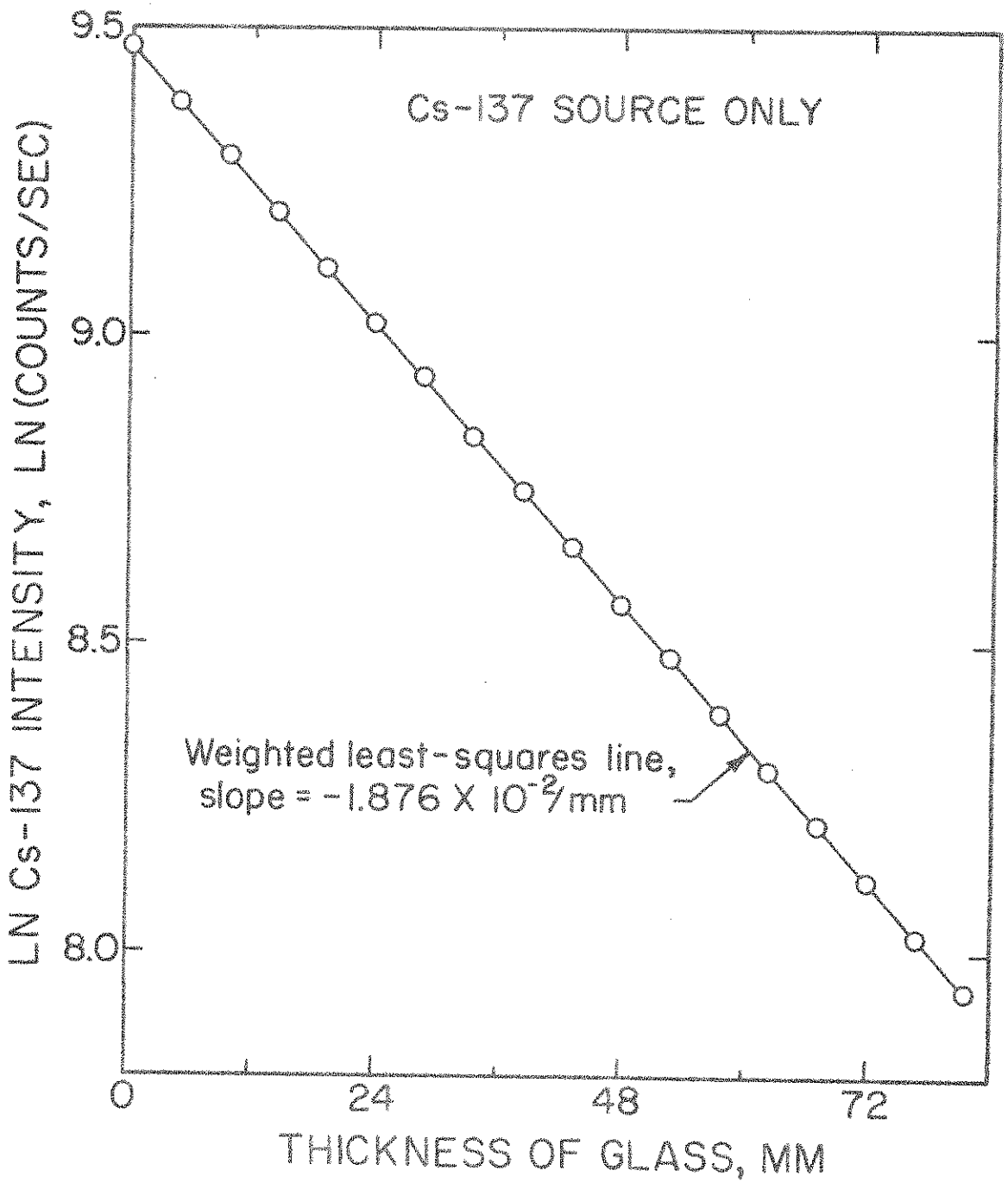

Figure 11 — Experimental verification of gamma-ray attenuation equation for single Cs-137 source.

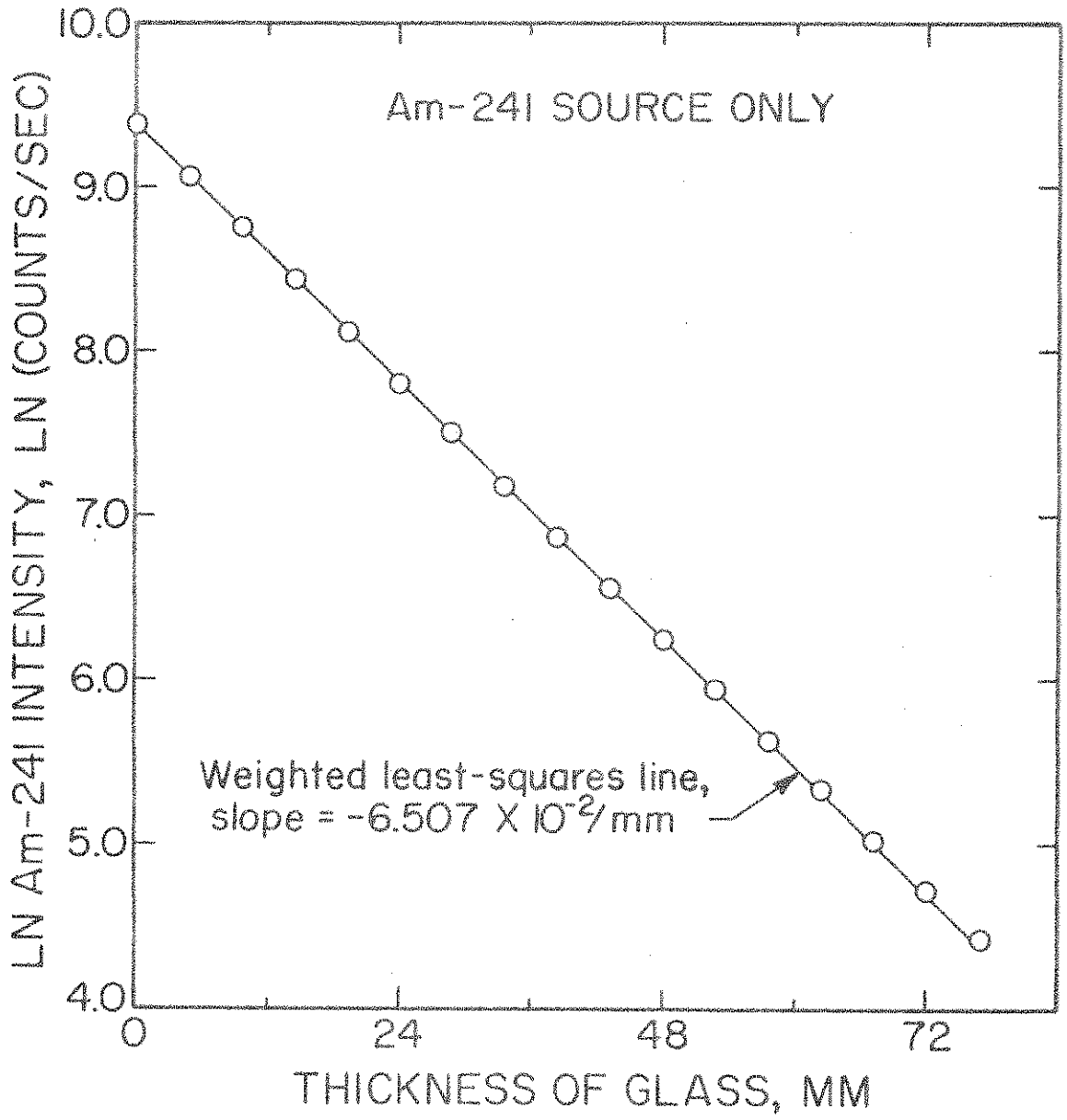

Figure 12 -- Experimental verification of gamma-ray attenuation equation for single Am-241 source.

The ln I as a function of the thickness of glass is shown in Fig. 13 for Cs-137 and in Fig. 14 for Am-241. The lines shown are weighted least-squares lines fitted to Eq. (36). Figure 14 also shows the non-linear relationship between ln I and the thickness of glass for Am-241 when no correction is made for the effect of Cs-137 in the Am-241 band. The Cs-137 and the corrected Am-241 intensities appear to follow the attenuation theory very well. The validity of the overall operation of the combined-source system is attested by the good agreement between the slopes of the fitted lines in Figs. 11 and 13 for Cs-137 and Figs. 12 and 14 for Am-241. The slopes for the combined-source system differ from the slopes for the separate-source systems by only 0.1% for Cs-137 and 1% for Am-241.

Water-content and bulk-density measurements with the dual-energy beam. Before Eqs. (33) and (34) can be used to determine water contents and bulk densities, the four calibration constants, U_{wCs}, U_{wAm}, U_{sCs}, and U_{sAm} must be evaluated. The method used in this research to evaluate these constants has been described by Swartzendruber et al. (1968) and by Nofziger (1970), and is summarized here. Equation (31), for example, relates $\ln(I_e/I)_{Am}$ at a particular position along a soil column to the bulk density and water content at that position. This equation cannot be used to determine the coefficients because, in most cases, only the average bulk density $\bar{\rho}$ and the average water content $\bar{\theta}$ are known precisely for the whole column, rather than ρ and θ at individual positions. If the intensities, I_e and I, are both measured at a sufficiently large number of positions uniformly distributed along the soil column, and if U_{wAm} and U_{sAm} are the same for all of the positions, then Eq. (31) implies

$$\overline{\ln(I_e/I)_{Am}} = U_{sAm}\,\bar{\rho} + U_{wAm}\,\bar{\theta} \qquad (38)$$

where $\overline{\ln(I_e/I)_{Am}}$ is the average of the $\ln(I_e/I)_{Am}$ values for each position. The average bulk density $\bar{\rho}$ can be evaluated by dividing the mass of oven-dry soil in the soil column by the volume of the column, and the average volumetric water content $\bar{\theta}$ can be determined by dividing the total volume of water in the soil column by the volume of the column. With $\bar{\rho}$, $\bar{\theta}$, and $\overline{\ln(I_e/I)_{Am}}$ known, only U_{sAm} and U_{wAm} in Eq. (38) are unknown. Hence, Eq. (38) can serve as one of two

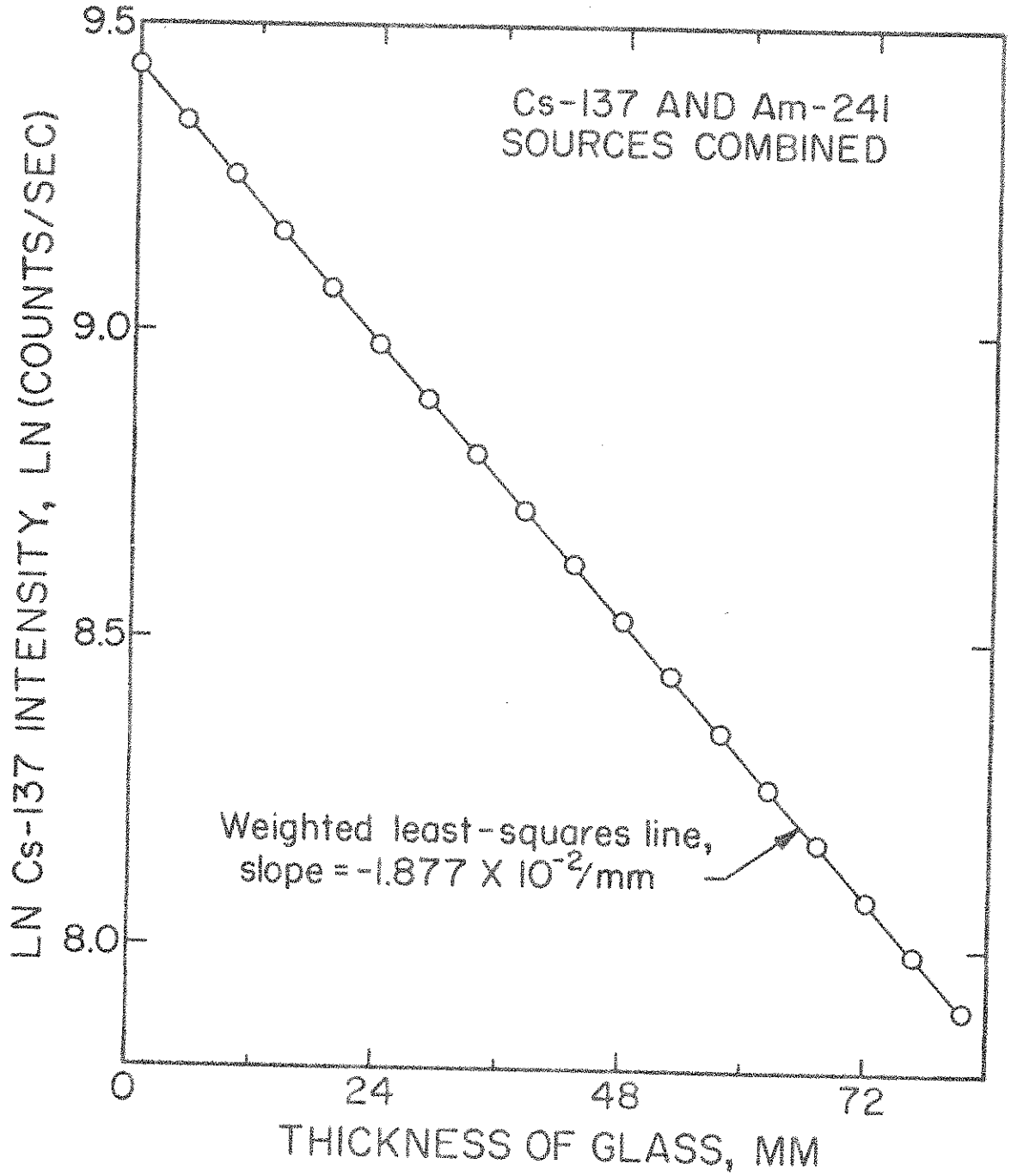

Figure 13 -- Experimental verification of gamma-ray attenuation equation for Cs-137 for combined sources.

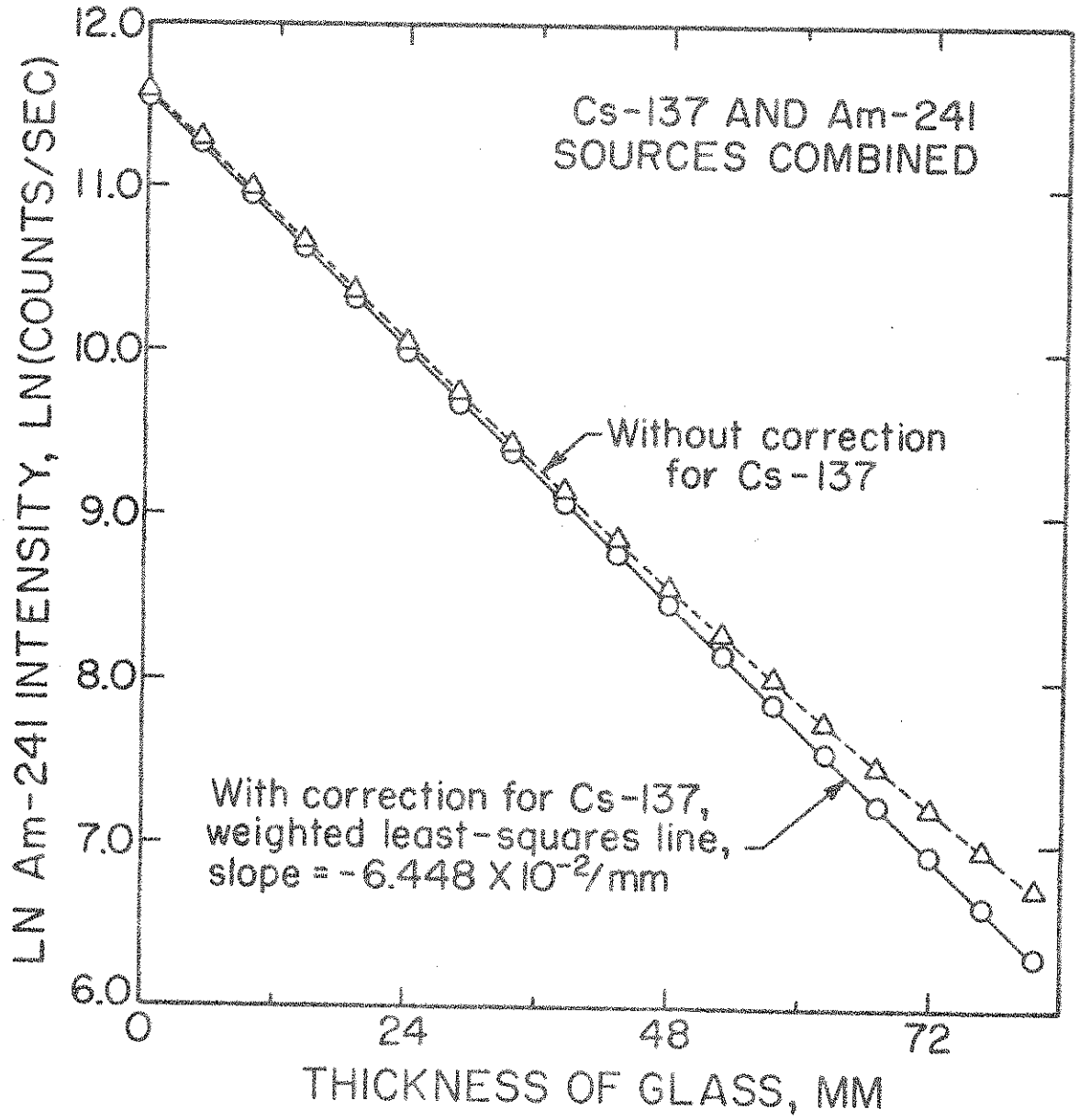

Figure 14 -- Experimental verification of gamma-ray attenuation equation for Am-241 for combined sources.

necessary equations to determine U_{sAm} and U_{wAm}. A second equation can be obtained by applying Eq. (31) to the soil column filled with pure water (ρ = 0.0, θ = 1.0). If the intensity through the water-filled column is represented by I_w and if measurements of I_e and I_w are made at a number of positions along the column, then

$$\overline{\ln(I_e/I_w)_{Am}} = U_{wAm} \tag{39}$$

Hence, Eqs. (38) and (39) can be used to evaluate U_{sAm} and U_{wAm}. If the method used to obtain Eqs. (38) and (39) from Eq. (31) is applied to Eq. (32), the equations

$$\overline{\ln(I_e/I)_{Cs}} = U_{sCs}\bar{\rho} + U_{wCs}\,\bar{\theta} \tag{40}$$

$$\overline{\ln(I_e/I_w)_{Cs}} = U_{wCs} \tag{41}$$

can be obtained, from which U_{sCs} and U_{wCs} can be evaluated. For calibration purposes, the most convenient soil condition to work with in Eqs. (38) and (40) is that of air dryness. The air-dry $\bar{\theta}$ was taken as $\bar{\rho}$ times the air-dry gravimetric water content, divided by the density of water.

An experiment was conducted to test the capability of the double gamma-ray apparatus for determining bulk densities and water contents. To obtain a range of bulk densities and water contents, double gamma-ray measurements were obtained for ten different mixtures of water and Salkum silty clay loam, each mixture being packed into a Plexiglas cell 3.0 cm long and of 6.28 cm inside diameter. The Cs-137 and Am-241 intensities through the empty cell and through each filled cell were measured at 30 positions along the cell. As a result, the entire length of the cell was scanned. The gravimetric water content and bulk density were obtained for each cell. From measurements through two water-filled cells, two calculated values of each of the constants U_{wAm} and U_{wCs} were obtained from Eqs. (39) and (41), respectively. Each calibration constant was taken to be the average of its two respective calculated values. In a similar manner, each of the constants U_{sAm} and U_{sCs} was taken as the average of two

calculated values from Eqs. (38) and (40), respectively, obtained on two air-dry soil columns.

With the calibration constants thus evaluated, water contents and bulk densities for every position along each cellwere calculated from Eqs. (34) and (33), respectively. The mean water content and the mean bulk density were determined from their individual values at each position in each cell, and were compared with the gravimetric values. The mean double-gamma water content, and the difference between the mean double-gamma water content and the gravimetric water content, are shown as functions of the gravimetric water content in Fig. 15. The double-gamma water contents differ from the gravimetric water contents by less than 0.008 cc/cc. The mean double-gamma bulk density, and the difference between the mean double-gamma bulk density and the gravimetric bulk density, are shwon as functions of the gravimetric bulk density in Fig. 16. The double-gamma and gravimetric bulk densities differ by less than 0.021 g/cc. The double-gamma water contents and bulk densities are considered to be in satisfactory agreement with the gravimetric values. Any residual errors are believed to reflect the overall accuracy of the calibration process and the gravimetric measurements.

Soil Preparation and Packing

Two natural soils and two artificial mixtures were used as porous media in this investigation. One soil, Salkum silty clay loam, is a moderately fine-textured soil which exhibits no noticeable one-dimensional swelling when wetted in an unconfined system. Water movement into this soil was previously studied by Rawlins and Gardner (1963) and by Nofziger (1970). The soil was crushed to pass through a 0.5-mm sieve. The other soil, Raub silt loam, is moderately fine textured and exhibits a slight one-dimensional swelling when wetted in an unconfined system. This soil was crushed to pass through a 1-mm sieve. The artificial mixtures were composed of various proportions of untreated banding sand,[3] ground silica[3] (silt), and bentonite.[4] One mixture consisted of 75%

---

[3] Banding sand and ground silica No. 290, Ottawa Silica Company, Ottawa, Illinois.

[4] Volclay No. 200, American Colloid Company, Skokie, Illinois.

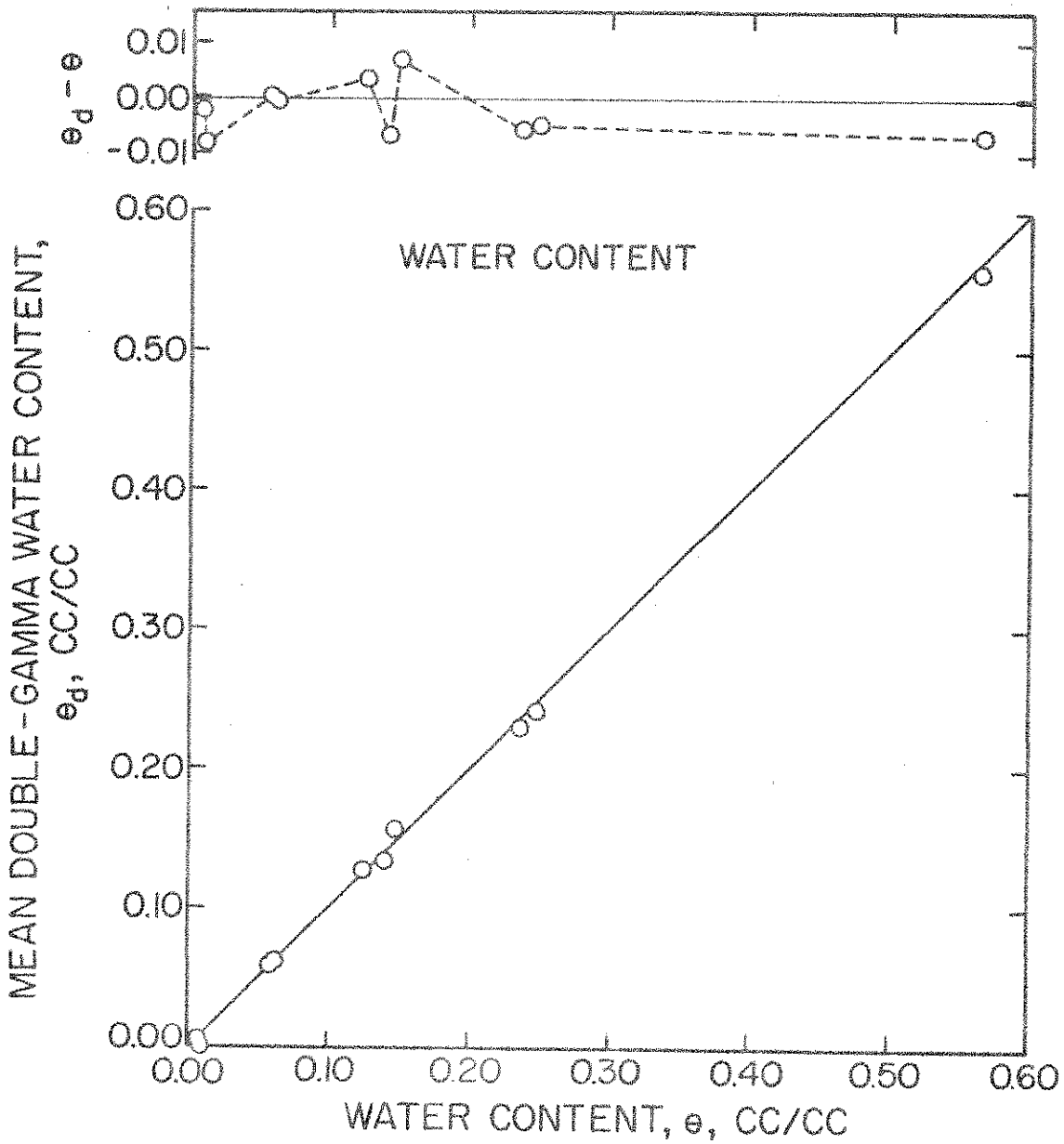

Figure 15 -- Experimental verification of the dual-energy gamma-ray attenuation technique for measuring water content. The straight line is the 1:1 relationship.

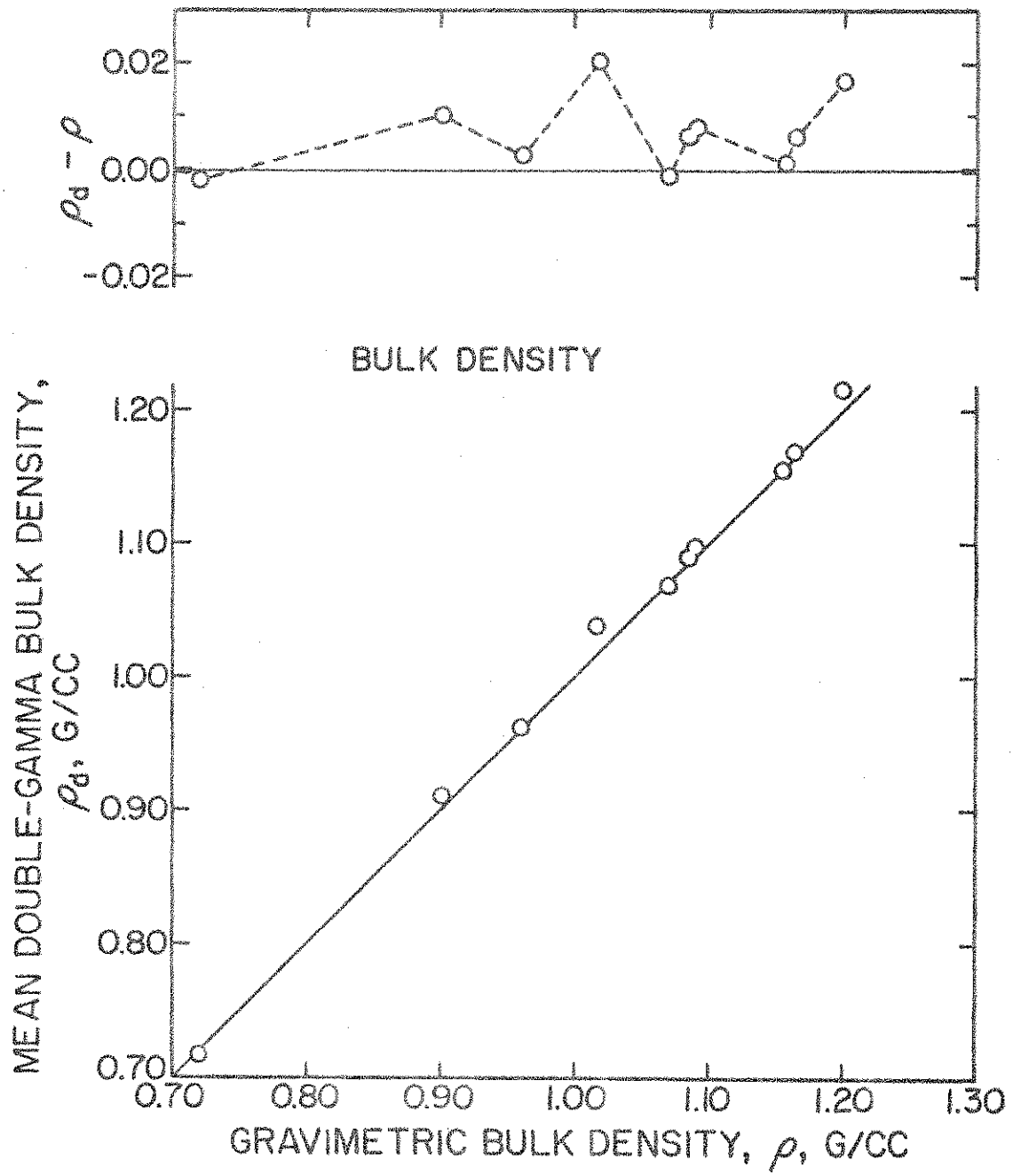

Figure 16 -- Experimental verification of the dual-energy gamma-ray attenuation for measuring bulk density. The straight line is the 1:1 relationship.

banding sand, 20% silt, and 5% bentonite. This mixture also exhibits slight one-dimensional swelling when wetted in an unconfined system. Horizontal water aborption by this artificial mixture has been studied by single gamma-ray attenuation (Cs-137) by Tsuji (1971). The second artificial mixture consisted of 50% silt and 50% bentonite. This mixture was selected because of its very marked one-dimensional swelling when wetted in an unconfined column.

Each porous medium was thoroughly mixed in a twin-shell dry blender and then packed into a soil column. The natural soils were packed into a Plexiglas cylinder 67 cm long, with an inside diameter of 6.28 cm and a wall thickness of 0.65 cm. The artificial mixtures were packed into a Plexiglas cylinder 24.1 cm long having the same inside diameter and wall thickness as the longer cylinder. The outlet ends of the cylinders were covered with a perforated Plexiglas plate and a thin film of glass wool. An extension cylinder 25 cm long, having the same inside and outside diameters as the soil columns, was attached to the inlet end of the columns during packing. The extended soil columns were mounted vertically for filling and packing. The porous media were placed in the columns through a funnel and a glass filling tube 3.1 cm in diameter and 100 cm in length. After filling the column and a portion of the extension, a weighted disc was placed on the soil and the column was vibrated up and down along four sides with a small vibrator consisting of a vibrating-type engraving tool,[5] in which the regular sharp-tipped cutting bit was replaced by a short, blunt brass rod. After the extended soil column reached the desired average bulk density, the extension was removed and a solid Plexiglas cover was attached.

Each packed soil column was weighed to determine the average bulk density. The uniformity of bulk density was determined by the use of the double gamma-ray attenuation apparatus, and, if unsatisfactory, the soil was removed and the packing process was repeated. The overall process was repeated until acceptable uniformity was achieved.

---

[5] Burgess Vibro-graver, Model V-73, purchased from E. H. Sargent and Company, Chicago, Illinois.

The Water Applicator

The water applicator used for all of the infiltration experiments was similar to that used by Nofziger (1970). A short cylinder of Plexiglas, of the same diameter as the outer diameter of the soil columns, and containing a short cylindrical cavity at one end, was closed over with an extra-coarse fritted-glass porous plate 6.1 cm in diameter. The porous plate thus served as one side of the short cylindrical water chamber of the water applicator, the chamber in turn being connected to a calibrated water supply. The plane of the fritted-glass plate was mounted perpendicular to the central axis of the applicator and the soil column. The glass plate extended 1 mm from the remainder of the water applicator to insure complete contact with the soil in the column. For infiltration into natural soils in the long columns, the water applicator was connected by tygon tubing to a calibrated water supply consisting of a 500-ml cylinder combined in parallel with a 250-ml burette. For infiltration into the artificial mixtures, the water applicator was connected to a small reservoir consisting of a 250-ml burette combined in parallel with a 100-ml burette. The large and small reservoirs were calibrated gravimetrically against the water levels in the 250- and 100-ml burettes, respectively. Water was applied to the inlet top end of the soil columns at a suction of 1 cm of water, maintained by the use of a Mariotte bubbling tube.

Making an Infiltration Run

In preparation for the infiltration part of these experiments, the water applicator was saturated with water under vacuum, was connected to the water-supply reservoir, and was mounted on the double-gamma apparatus several centimeters above the inlet end of the packed column. Boiled deionized water was used for all of the porous media except the artificial mixture of 5% bentonite in sand and silica flour, in which the permeating liquid was 0.0001 N NaCl in boiled deionized water, as used by Tsuji (1971). After allowing time for the temperatures of the water, soil, and air to reach equilibrium, the solid Plexiglas cover was removed from the end of the soil column, and the double-gamma sources and detector were set at the first position of interest.

Infiltration was initiated by moving the water applicator against the end of the soil column, at which time the scalers and cumulative timer were simultaneously engaged. For positions near the soil-column inlet, where very rapid changes in water content occurred, the preset counting periods were as small as 5 sec. For positions where the changes in water content were much slower, preset counting periods as large as 90 sec were used. After the wet front passed the first position of interest, the double-gamma sources and detector were moved to a deeper position of interest. As time permitted, repeated measurements were made both behind and ahead of the wet front. Intensity checks through the standard absorber were made approximately every two hours.

During the wetting process, the gamma-ray intensities ranged from approximately 360,000 to 270,000 counts per min for Cs-137, and from approximately 540,000 to 320,000 counts per min for Am-241, for the three columns with mean bulk-densities near 1.2 g/cc. For the column having a mean bulk-density of 1.814 g/cc, the gamma-ray intensities varied from 265,000 to 210,000 counts per min for Cs-137, and from 290,000 to 190,000 counts per min for Am-241.

In addition to the gamma-ray measurements, the position and shape of the visual wet front, the air temperature, and the cumulative water inflow were recorded with time. Air temperatures in the laboratory during all of these experiments ranged from 20.6° C to 25.3° C. The temperature fluctuations within a particular infiltration experiment ranged from 0.4° C to 3.6° C. The position of the wet front for all of the artificial mixtures and for the column of Raub soil varied by less than ± 1 mm from the mean position. The position of the wet front for the Salkum soil varied up to ± 2 mm. For no position around the circumference of any column was any portion of the wet front consistently ahead or behind the mean position of the wet front.

Calibration and Data Analysis

The calibration constants, U_{wAm}, U_{wCs}, U_{sAm}, U_{sCs}, were determined using Eqs. (38), (39), (40), and (41) for the 24.1-cm and 67-cm soil columns, from gamma-ray intensity measurements through water filled columns and through the initially air-dry soil columns used for transient measurements. Intensity

measurements through the empty column and the water- and soil-filled columns were made every 5 mm in the 24.1-cm column and every 1 cm in the 67-cm column. Intensity measurements were based on counting periods of 600 sec for the empty and water-filled columns, and 300 sec for the soil-filled columns. Values of the calibration constants as determined and used for each soil column are shown in Table 3.

Table 3. Calibration constants for determining the water content and bulk density of four porous media by double gamma-ray attenuation.

Porous Medium	Calibration Constants			
	U_{sAm} cc/g	U_{wAm}	U_{sCs} cc/g	U_{wCs}
50% Bentonite 50% Silt	1.5709	1.1824	0.4642	0.5182
5% Bentonite 20% Silt 75% Banding sand	1.5096	1.1824	0.4643	0.5182
Salkum silty clay loam	1.8275	1.1875	0.4673	0.5175
Raub silt loam	1.7025	1.1875	0.4669	0.5175

The calculation of water contents and bulk densities from gamma-ray measurements was performed on Purdue University's CDC 6500 computer. The gamma-ray measurements during the transient parts of the experiments were automatically recorded on paper tape, and the paper tape was used to enter the data into the computer. This data handling capability was very helpful since large quantities of data were analyzed.

One problem which occurs in gamma-ray attenuation measurements is that of making water content and bulk density measurements frequently enough to describe transient changes in the system and, at the same time, basing each measurement on as large a counting period as possible to obtain maximal

accuracy. The problem is especially real in measurements near the wet front, since gamma-ray measurements at a particular position should preferably begin prior to wet-front arrival while the soil is still air dry, and should then continue during the rapid increase in water content that occurs as the wet front passes. To obtain sufficient data for the rapidly changing system, relatively small preset counting periods are used for all the measurements. As a result, there is a tendency to persist too long with short preset counting periods into stages wherein the system is no longer changing rapidly. Hence, the computer program devised to determine water contents and bulk densities was provided with a testing scheme to determine if consecutive gamma-ray measurements should be used to calculate several water-content and bulk-density values or if they could be combined to provide a single, more accurate evaluation of water content and bulk density.

The testing scheme[6] was set up to provide approximately two calculated water contents for every change of 0.01 cc/cc in water content. The range in water content for a given series of consecutive gamma-ray measurements at a particular position was determined from the first and last gamma-ray measurements in the series. From this, an estimate of the number of water content and bulk density calculations needed to describe the portion of data was determined. Consecutive pairs of Cs-137 intensities were then compared, and if they differed by less than 3 times the standard deviation of the measured intensity, the two intensity valves were averaged together and associated with the average time of the two measurements; if the intensities differed by more than 3 standard deviations, the individual values were retained and no averaging was done. Any averaging done for the Cs-137 intensities was also carried out on the corresponding Am-241 intensities. Following the testing of the first two intensities, the next two intensities were compared in a similar manner. The process was continued for all of the data pairs. If necessary, the process was repeated several more times to further reduce the number of intensity values and hence the number of water contents and bulk densities.

---

6 The devising of this scheme was a cooperative effort between the author and Dr. L. R. Ahuja, Postdoctoral Research Associate, Department of Agronomy.

As a result of this testing scheme, approximately 5000 measured intensities for a typical infiltration experiment were combined in a manner such that only approximately 1000 water contents and bulk densities were calculated. This corresponds to approximately 45 water contents and bulk density values for each position along the column. Experience has shown that this testing scheme is conservative, in that less averaging is performed than would be possible without distorting the transient curves.

RESULTS AND DISCUSSION

Swelling Porous Media

Water Content and Bulk Density Changes During Infiltration

The movement of water into a confined air-dry mixture of 50% bentonite and 50% silt, along with the associated changes in bulk density of the porous medium, were determined with the double gamma-ray attenuation apparatus. The double-gamma water content and bulk density as functions of time from the initiation of infiltration at given positions are shown in Fig. 17. Because the times had a large relative range, they have been plotted on a logarithmic scale. At each position a definite decrease in bulk density occurs simultaneously with an increase in water content. The decrease in bulk density and increase in water content are largest for the position nearest the water inlet, and become smaller for more distant positions. At very large times, a minimum in bulk density, followed by a slight increase, appears for the position 0.6 cm from the inlet end. The same behavior occurred for positions 0.2 and 0.4 cm from the inlet end, which are not plotted in the figure.

Bulk-density distributions are shown in Fig. 18 for several times throughout the transient experiment. The plotted points were obtained over a period of approximately four hours and thus are not instantaneous distributions, although the water contents and bulk densities were changing very slowly at these times. From this figure, one again can see that the bulk density for positions near the inlet did decrease very substantially when wetting occurred, as a consequence of swelling of the clay. The swelling at small times appears to have compressed the dry soil immediately ahead of the wet front, an effect which persists in a lesser degree to the end of the soil column. At later times, the swelling appears to continue to compress the dry soil, as well as to compress some of the previously expanded wet soil nearer the inlet.

Since the column of porous material was confined at the ends, its average bulk density had to remain unchanged with time. This condition provides a useful check on the operation of the double-gamma system. The average double-

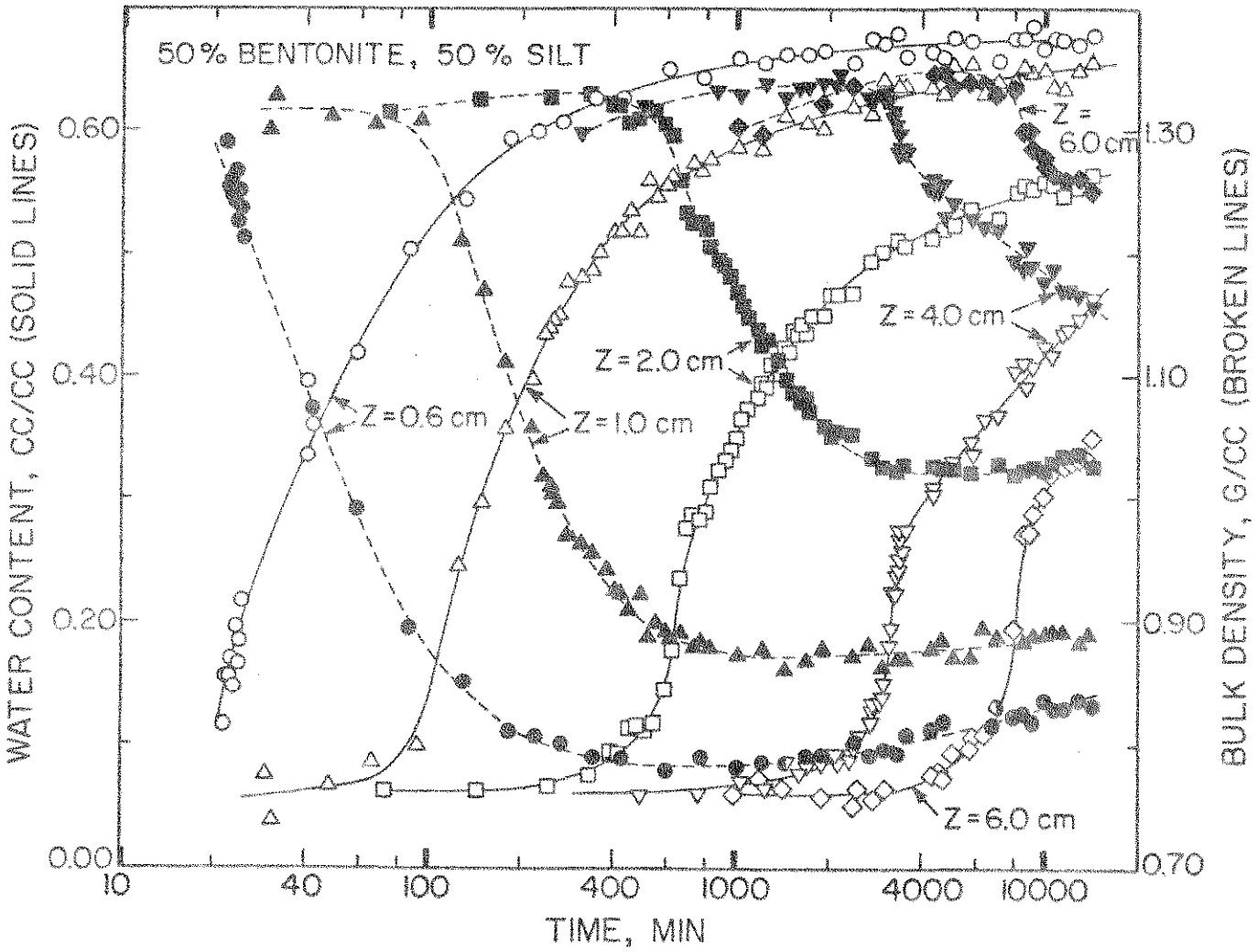

Figure 17 -- Water content and bulk density transients for several positions along the column of 50% bentonite and 50% silt.

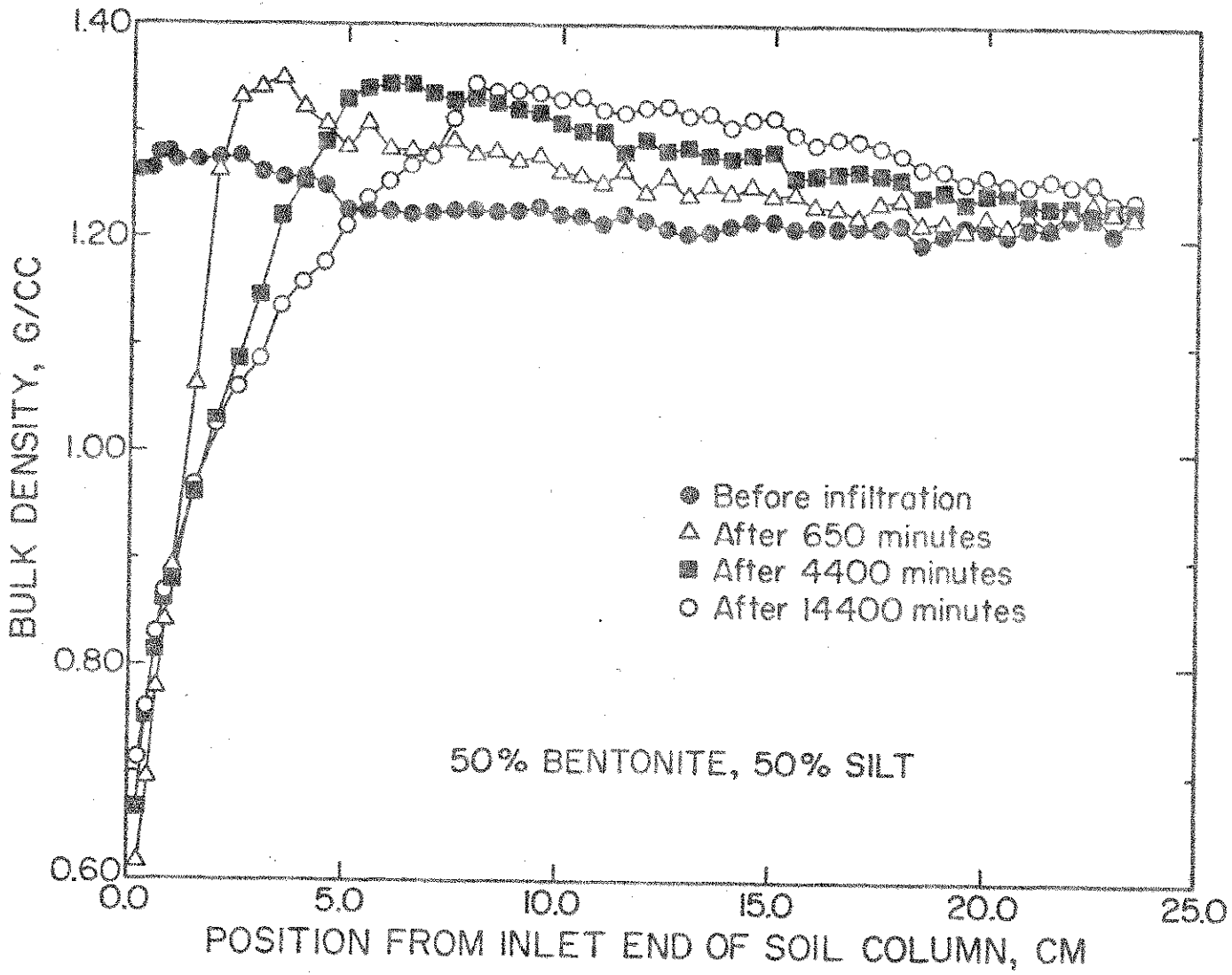

Figure 18 -- Bulk density distributions at several times during the wetting of the mixture of 50% bentonite and 50% silt.

gamma bulk density ρ_{ave} can be determined from the relation

$$\rho_{ave} = \frac{1}{L} \int_0^L \rho(Z) dZ \qquad (42)$$

where L is the length of the column, and $\rho(Z)$ is the double-gamma bulk density at a distance Z from the inlet end of the soil column. Values of ρ_{ave} were determined for each of the bulk-density distributions shown in Fig. 18. The gravimetric bulk density and the average double-gamma bulk density before infiltration were 1.224 g/cc. The average double-gamma bulk densities after 650, 4400, and 14450 min exceeded the gravimetric bulk density by 0.001, 0.008, and 0.008 g/cc, respectively. This reproducibility of the average bulk density is considered quite acceptable, in view of the large local changes in bulk density.

Water Infiltration

At present, no theoretical models exist for the movement of water into a confined swelling soil. Although one would not really expect rigid-media theory to hold for these confined but swelling mixtures, it is of interest to observe the nature of the deviations which might be encountered. Consider one-dimensional water entry into a rigid porous medium that is uniform in bulk density and of constant initial water content less than saturation, and to which a constant higher water content is applied and maintained at the inlet end $Z = 0$ from time $t = 0$ onward. The series solution of Philip (1957) may be expressed in the form (Swartzendruber, 1969)

$$Z = \phi(\theta) t^{1/2} + \sum_{i=2}^{\infty} f_i(\theta) t^{i/2} \qquad (43)$$

where $Z = Z(\theta, t)$ is the vertical position coordinate positive downward, and $f_i(\theta)$ are particular functions of the volumetric water content θ, and $\phi(\theta)$ is the solution to the one-dimensional horizontal water entry problem (Klute, 1952), in the sense that

$$x/t^{1/2} = \phi(\theta) \tag{44}$$

where x is the horizontal position coordinate (distance from the water-inlet end of the soil column), and $\phi = x/t^{1/2}$ is also known as the Boltzmann variable.

For the range of data represented in Figs. 17 and 18, Z is small enough (wet-front depth < 8.5 cm) so that gravity effects can be neglected; this in turn means that the summation in Eq. (43) can be neglected, so that the solution simplifies to

$$Z/t^{1/2} = \phi(\theta) \tag{45}$$

which is identical to the horizontal solution [Eq. (44)]. Hence, on the basis of Eq. (45), rigid-media theory implies that plots of volumetric water content versus Boltzmann variable $Z/t^{1/2}$ should coalesce for all values of Z and t. The volumetric water content as a function of the Boltzmann variable for several positions along the column is shown in Fig. 19. Not only do the experimental curves fail to coalesce, but the deviations are systematic, in that the curves shift progressively in the general direction of the origin of coordinates.

The use of the material coordinate in describing water movement in swelling soils is suggested by the results of Raats and Klute (1969), Philip and Smiles (1969), and Philip (1969). The material coordinate m = m(Z, t) is expressed as

$$m(Z, t) = \frac{1}{\rho_p} \int_0^Z \rho(w, t)\,dw \tag{46}$$

where ρ_p is the particle density of the porous medium and $\rho(w, t)$ is the bulk density of the porous medium at position w and time t. It seems worthwhile to determine whether such a variable would be of use even if the ends of the column are fixed, as in the present experiments. Values of m(Z, t) for all positions Z and all experimental values of time t were obtained from Eq. (46) for a particle density of 2.72 g/cc, by use of the trapezoidal approximation to the integral. (A particle density of 2.72 g/cc was determined to be the equivalent particle density for a mixture composed of 50% bentonite with a particle density

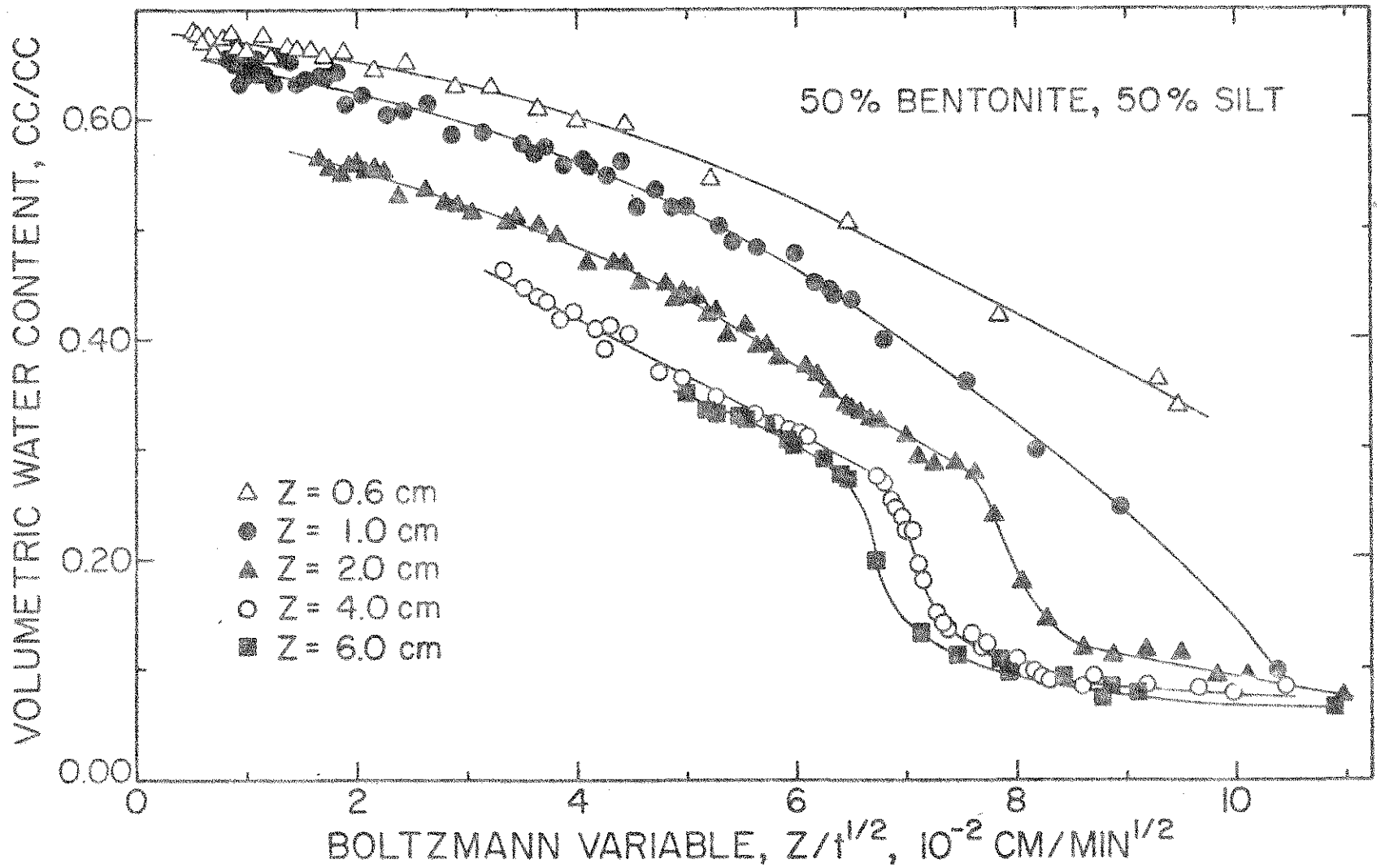

Figure 19 -- Volumetric water content versus Boltzmann variable for several positions along the column of 50% bentonite and 50% silt.

of 2.80 g/cc and 50% silica flour with a particle density of 2.65 g/cc.) Values of $\rho(w, t)$ for variable w at a given t were obtained by linear interpolation. From the resulting values of $m = m(Z, t)$, the quantity $m/t^{1/2} = \phi_m(Z, t)$ was calculated, where ϕ_m has been called the reduced material coordinate by Philip and Smiles (1969). Values of $\phi_m = m/t^{1/2}$ were determined for various positions, and for all of the experimental values of time at each position. The volumetric water content as a function of the reduced material coordinate is shown in Fig. 20 for several positions along the column. Curve coalescence is greatly improved in comparison with Fig. 19 but is still not complete, particularly at high water contents and at the position nearer than 1 cm to the water inlet.

Since the upper limit of the water content is the saturated value θ_s, given by θ_s = total porosity = $(\rho_p - \rho)/\rho_p$ where ρ_p is the particle density and ρ is the bulk density, it is clear that θ_s will change throughout the wetted portion of the column by virtue of the change in bulk density ρ. This suggests that coalescence at the higher water contents might be improved if the saturation $S = \theta/\theta_s$ were taken as the water-content variable, rather than θ alone. Plots of S versus $m/t^{1/2}$ are shown in Fig. 21, where it is evident that coalescence is appreciably improved when compared with Fig. 20. Particularly is this true for the higher saturations (or water contents). The only points not brought into acceptable coalescence are those at low water contents for the position nearer than 1 cm to the water inlet. At present, no theoretical reason can be given for the generally good coalescence exhibited by the curves in Fig. 21, but it is an encouraging feature that would seem to deserve further theoretical considerations.

Double gamma-ray measurements, as shown in Figs. 17, 18, 19, 20, and 21, were also obtained on two other separate columns, one at a bulk density of 1.250 g/cc and the other at 1.318 g/cc. Results for the 1.250-g/cc column were in close agreement with those shown in the above figures, and were considered to represent excellent confirmation. Results for the 1.318-g/cc column were qualitatively similar also, the main difference being that bulk densities were generally higher than in the columns of 1.224 and 1.250 g/cc, quite in keeping with the fact that the mean bulk density was higher from the beginning.

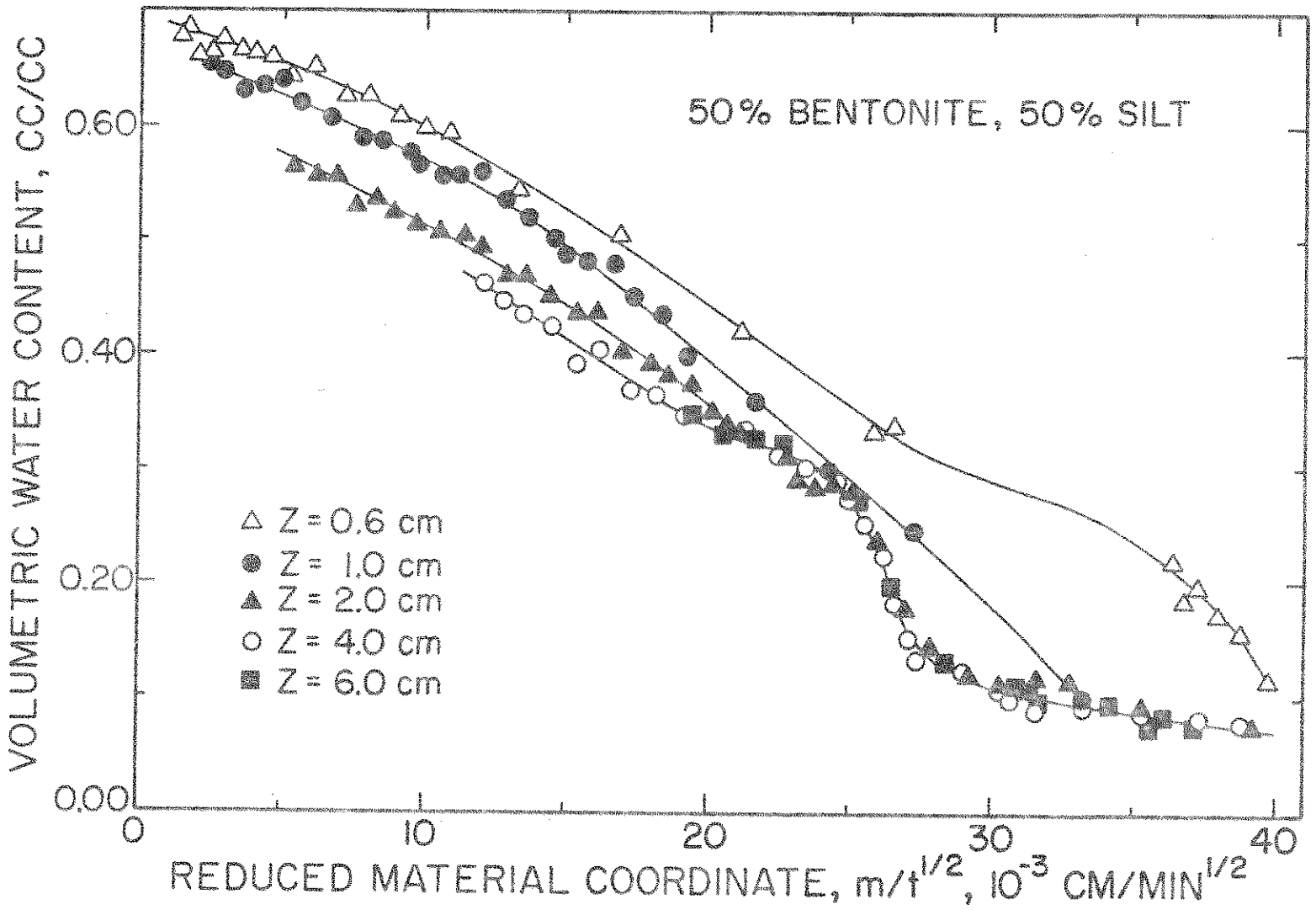

Figure 20 -- Volumetric water content versus the reduced material coordinate for several positions along the column of 50% bentonite and 50% silt.

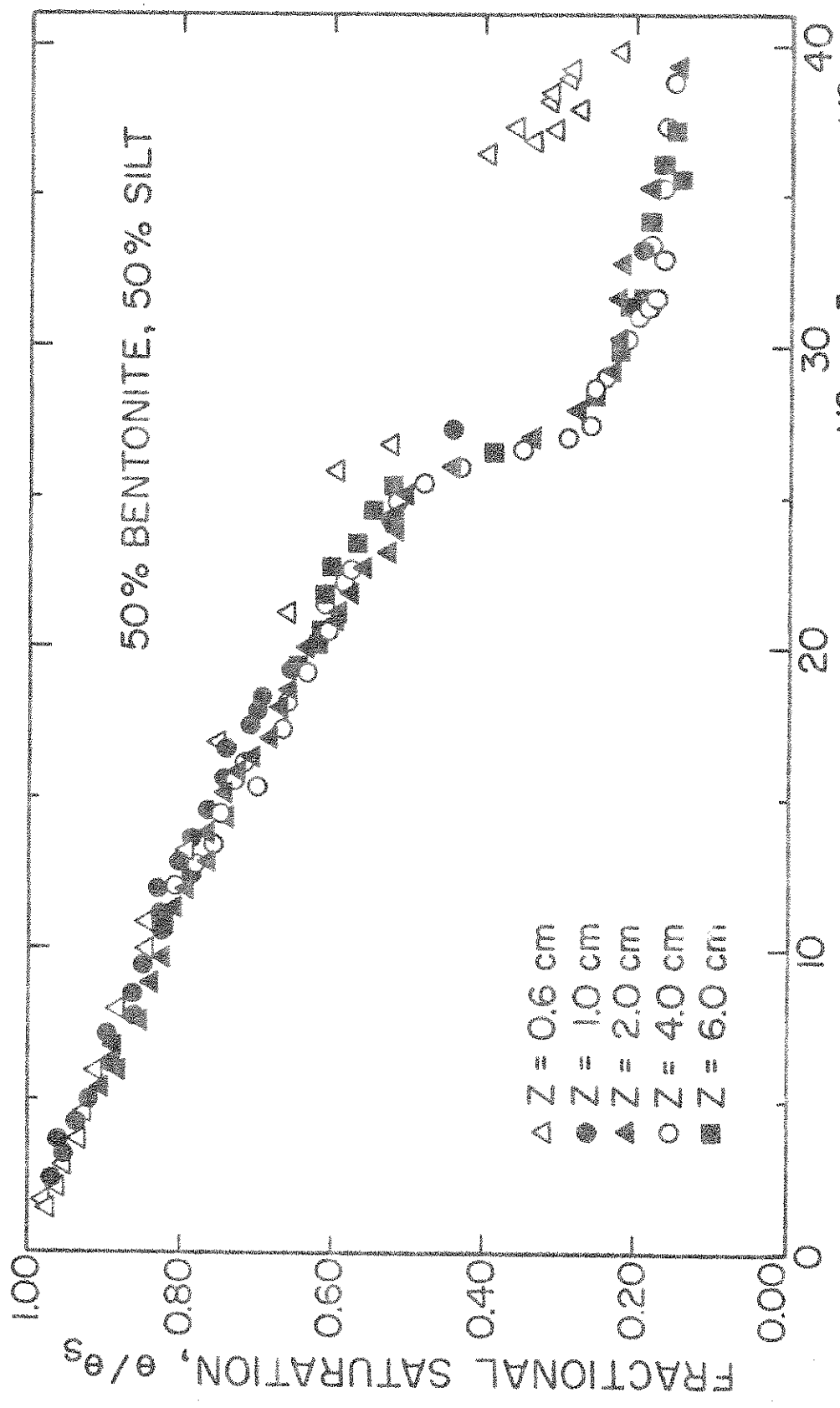

Figure 21 -- Fractional saturation versus the reduced material coordinate for several positions along the column of 50% bentonite and 50% silt.

From Figs. 17 and 18, it is clear that the equal-part mixture of bentonite and silt did swell very profoundly during the wetting process. Although this is the very purpose for which double-gamma measurements are primarily envisioned, it is of some interest to inquire as to the results if only single-gamma measurements had been obtained. Single-gamma water contents were calculated for the position 1 cm from the water inlet, for Cs-137 alone and Am-241 alone, and are plotted against the double-gamma water content in Fig. 22. In view of the very substantial deviations of the data points from the unity line, it is quite clear that the use of the single gamma-ray principle in a profoundly swelling material does indeed produce water-content estimates that are enormously in error.

Nonswelling Porous Media

Initial Bulk-Density Distributions

The infiltration of water and the associated changes in bulk density were studied using the double gamma-ray attenuation apparatus for Salkum Silty clay loam, Raub silt loam, and a mixture of 5% bentonite, 75% banding sand, and 20% silt. Initial bulk density distributions for the three porous media are shown in Fig. 23. The average bulk density for the Salkum soil was 1.209 g/cc, with all of the individual bulk-density values within a maximum range of 2.6% of the average value but with the maximum range not necessarily centered on the average value. The Raub soil had a bulk density of 1.194 g/cc, with all of the individual bulk densities within a maximum range of 5.2%. The 5% bentonite mixture was packed to an average bulk density of 1.814 g/cc, with all the individual values within a maximum range of 4.4% of the average value.

Bulk Density Changes Resulting From Wetting

Just before terminating each transient experiment, double-gamma measurements were made for positions along each soil column, for comparison with the initial bulk-density distribution taken prior to the application of water. The difference between the final and initial bulk densities as a function of position along the soil column is shown in Fig. 24 for the three materials. The final bulk densities in the air-dry portions of the columns tend to

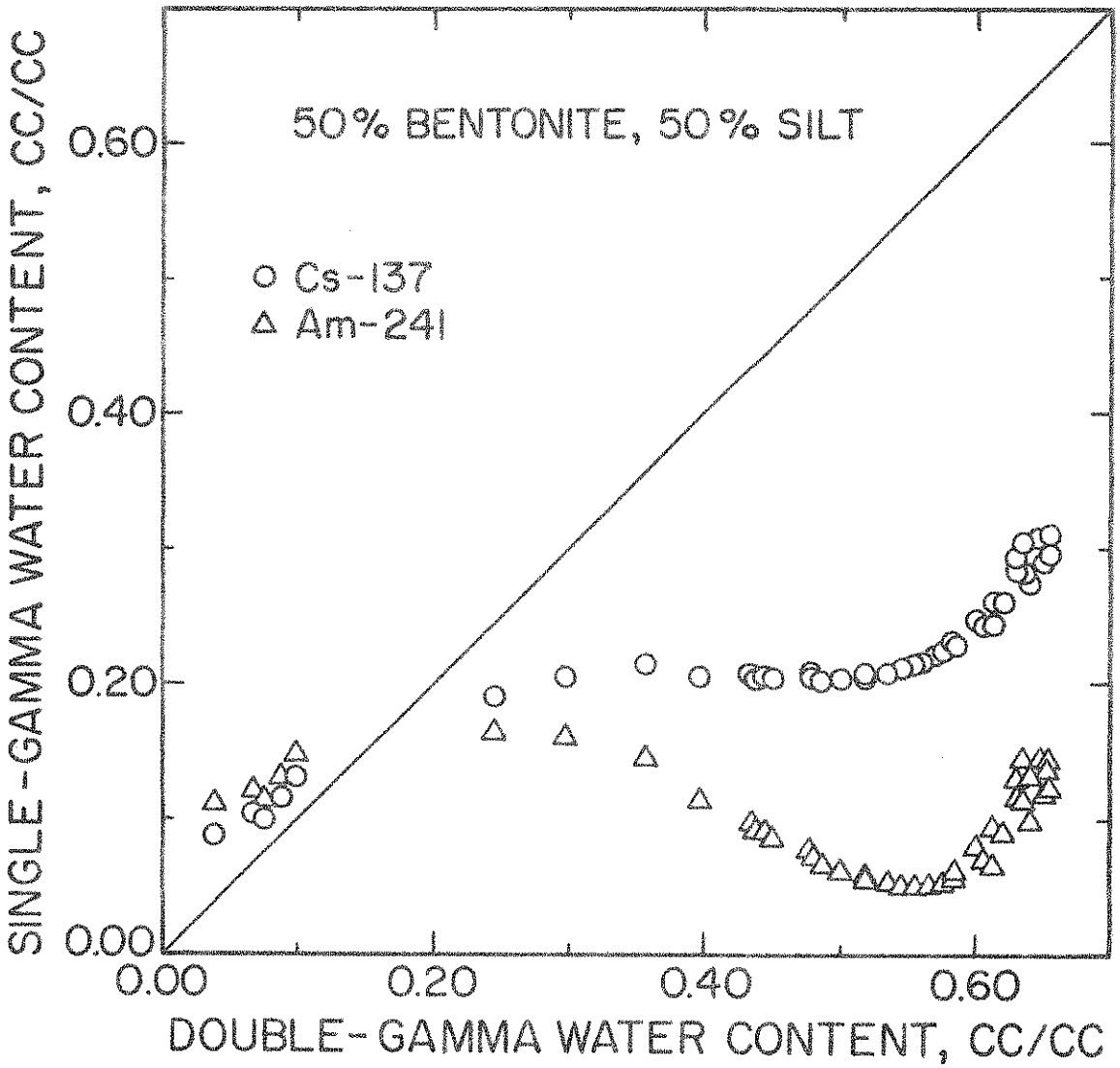

Figure 22 -- Single-gamma water content versus double-gamma water content for mixture of 50% bentonite and 50% silt. The straight line is the 1:1 relationship.

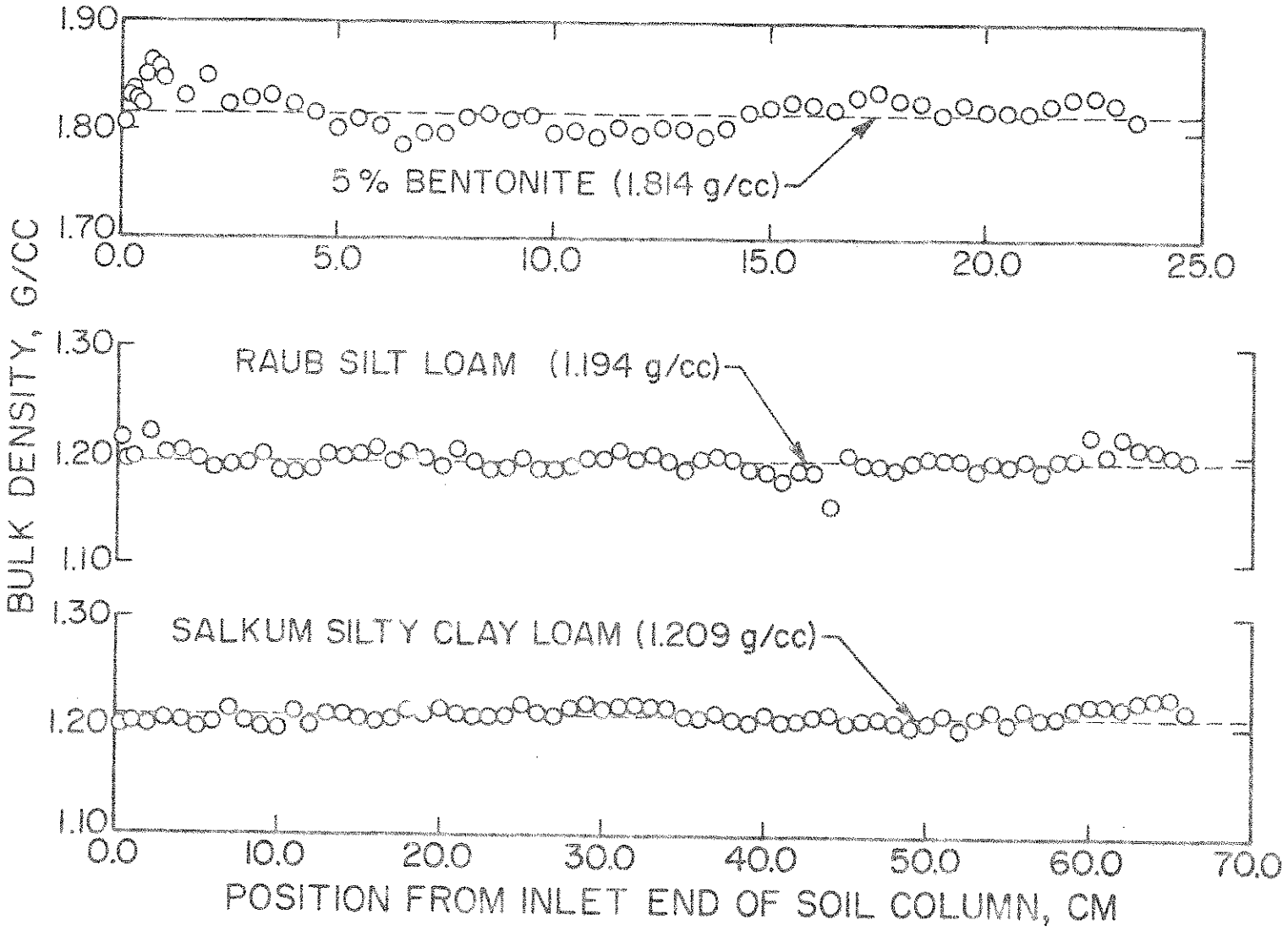

Figure 23 -- Initial bulk density distributions for Salkum silty clay loam, Raub silt loam, and the 5% bentonite mixture.

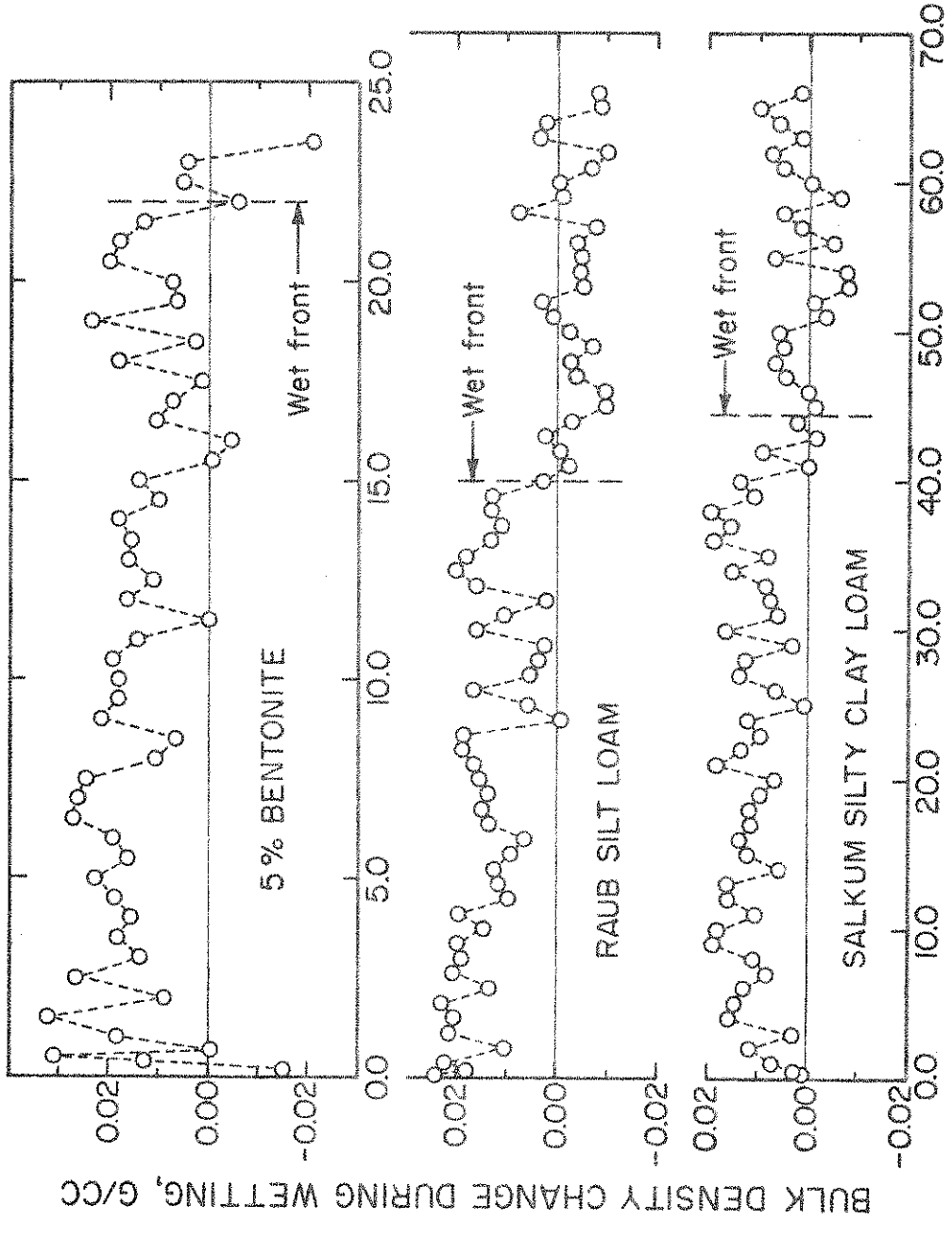

Figure 24 — The change in bulk density during wetting for various positions along columns of Salkum silty clay loam, Raub silt loam, and the 5% bentonite mixture.

fluctuate about their original values by approximately ± 0.01 g/cc, while those in the wet portions of the columns tend to fluctuate approximately ± 0.013 g/cc about values 0.01 to 0.015 g/cc above their original values.

Since the amount of soil in each column remains unchanged during wetting, the mean bulk density of the wetted column must be equal to that of the initially air-dry column. The mean double-gamma bulk density for the air-dry and wetted columns was determined using the trapezoidal approximation to Eq. (42) in the same way as for the highly swelling 50% bentonite described earlier. The mean double-gamma bulk density for each wetted column exceeded that when air dry by 0.008 g/cc for Salkum, by 0.007 g/cc for Raub, and by 0.013 g/cc for the 5% bentonite mixture. These results suggest a small error in the double-gamma bulk densities of the order of 0.01 to 0.015 g/cc. It is in terms of such an overall accuracy that the bulk-density changes shown in Fig. 24 must be viewed.

The change in the double-gamma bulk density of Salkum silty clay loam during infiltration is shown for positions 5 cm and 1 cm from the inlet in Figs. 25 and 26, respectively. The 5-cm position was selected because the scatter in the double-gamma bulk density was greater for that position than any other in the Salkum soil. The 1-cm position was selected to illustrate results obtained for very small preset counting periods and very small cumulative times. Preset counting periods for the 5-cm position ranged from 10 sec to 300 sec, and for the 1-cm position from 5 sec to 300 sec. The broken lines in Figs. 25 and 26 indicate the error in bulk density arising from the random nature of radioactive decay. The lines mark the error limit in bulk density arising from an error in the Am-241 intensity of plus or minus two standard deviations, and a simultaneous error in the Cs-137 intensity of minus or plus two standard deviations. The change in preset counting period and the decrease in intensity due to wetting were taken into account in determining the standard deviations in intensity. With error limits assigned and calculated in this manner, approximately 99% of the observed values should fall within these limits.

The observed changes in bulk density for the 5-cm position tended to be somewhat greater than could be expected from radioactive decay, except prior to 60 min where only a few points fell outside the calculated limit. All of

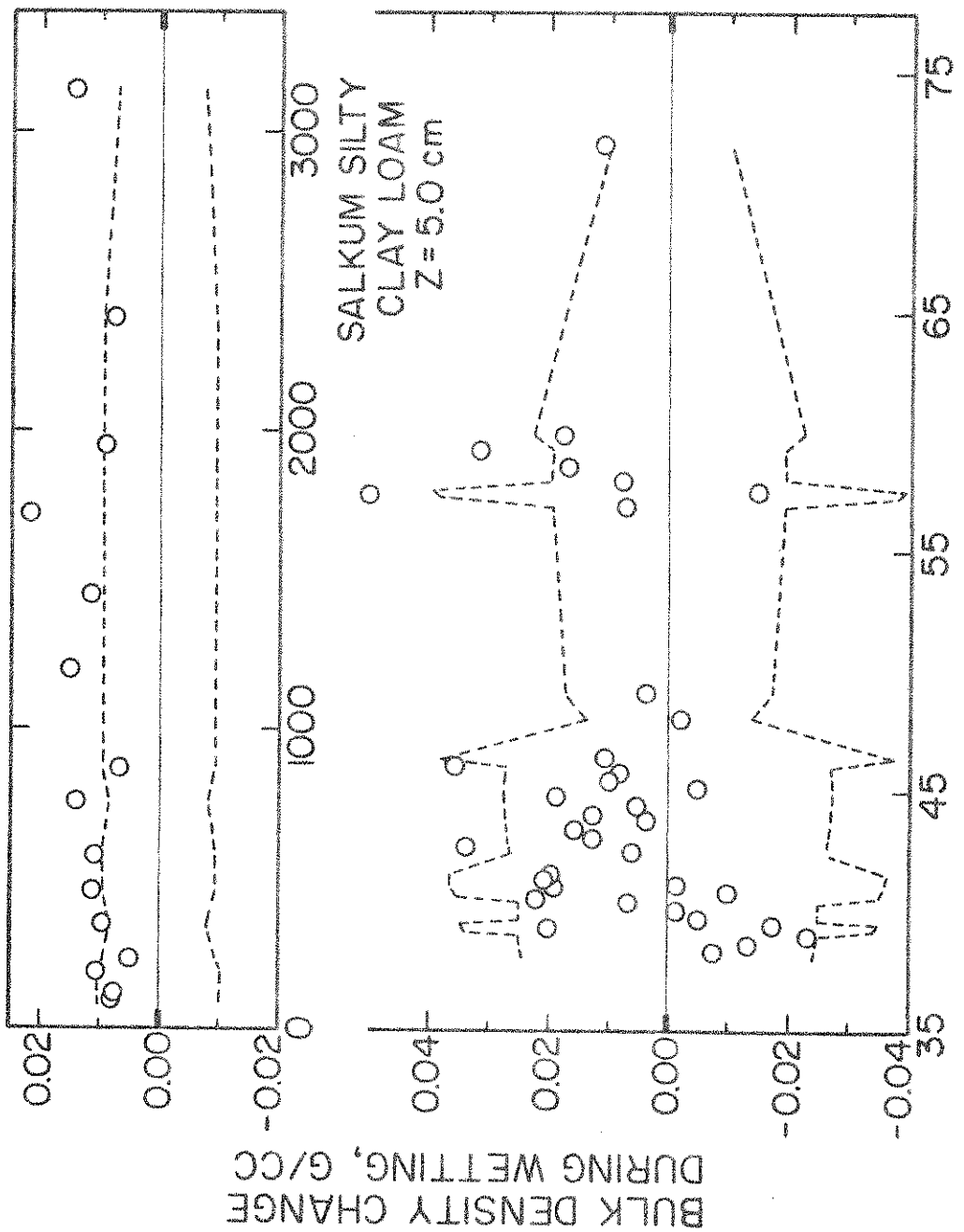

Figure 25 -- The change in bulk density as a function of time for the 5-cm position in Salkum silty clay loam. The broken lines represent the bulk density error limits due to random radioactive decay.

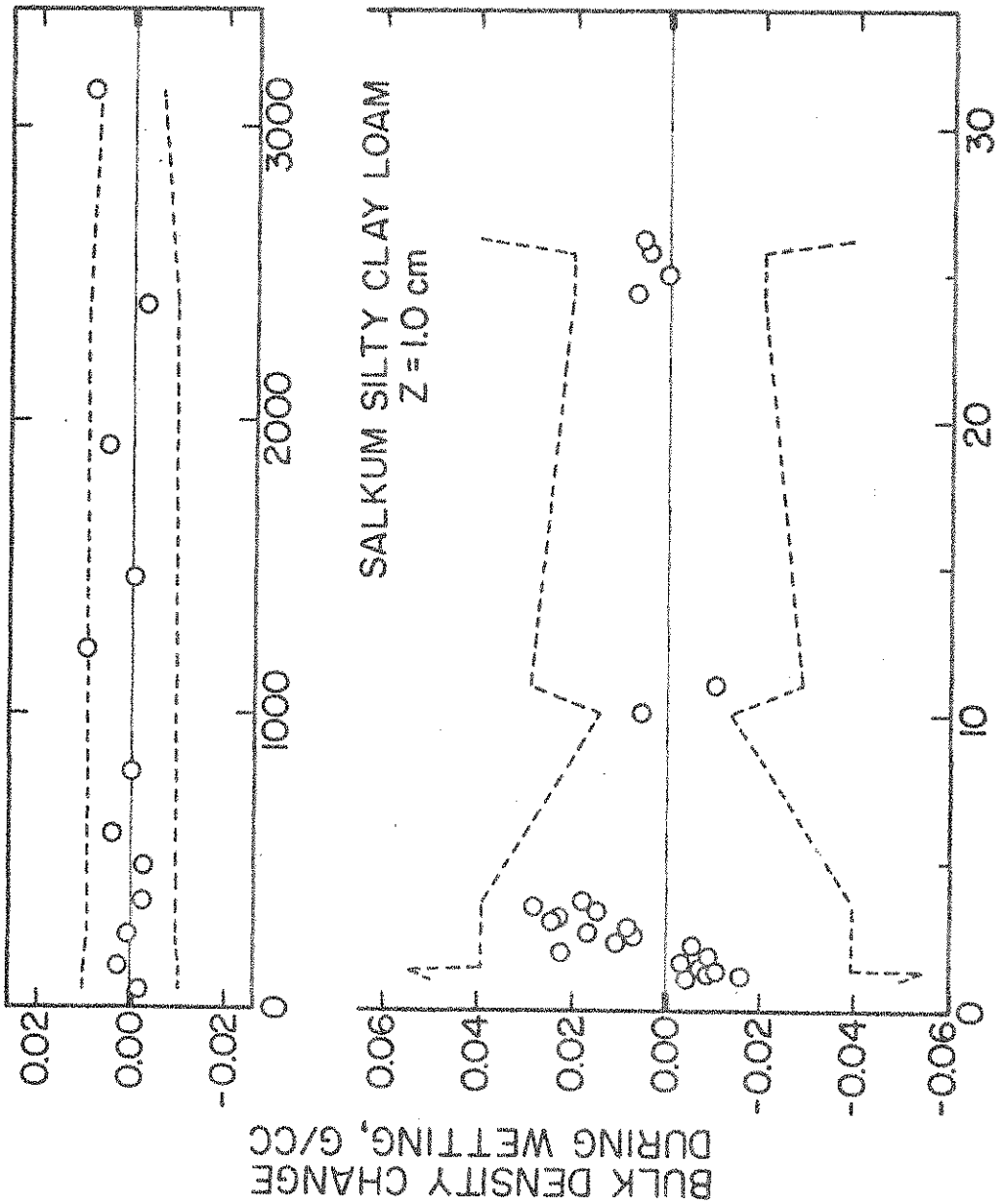

Figure 26 -- The change in bulk density as a function of time for the 1-cm position in Salkum silty clay loam. The broken lines represent the bulk density error limits due to random radioactive decay.

the observed values for the 1-cm position fell within the error limits, except for the final data point. The tendency shown for the 5-cm position was present in many positions. A swelling tendency, which would be manifested as a decrease in bulk density, did not exist for either of the positions graphed, nor for any other of the positions inspected. Since the mean double-gamma bulk densities for all of the wetted columns exceeded the mean bulk densities for the air-dry columns, the small increase in bulk density observed for the 5-cm position and many other positions is thought to represent a bias in the double-gamma bulk density determination, rather than a real increase in bulk density.

Water Infiltration

Since no measurable swelling effect (reduction in bulk density) was found, it would be expected that water contents measured by single-energy gamma-ray attenuation should agree with water contents as measured by the double-gamma-ray method. Such comparisons are shown in Fig. 27 for Salkum silty clay loam, at a position 5.0 cm from the water-inlet end of the soil column. In marked contrast with Fig. 22, the results now fall very close to the unity line, particularly for the single-gamma-ray beam from Cs-137. The same type of data are shown for the 5% bentonite (in 20% silt and 75% banding sand) in Fig. 28, with results generally in accord with those for Salkum but with more scatter in the data points. Some of the additional scatter is attributable to the generally lower water contents and the markedly higher bulk density in the 5% bentonite, when compared with the Salkum. These results indicate that earlier single-gamma measurements on Salkum (Rawlins and Gardner, 1963; Nofziger, 1970) and the 5% bentonite (Tsuji, 1971) can now be confidently accepted as valid. Furthermore, these earlier measurements had indicated appreciable deviations from soil-water diffusivity theory for rigid media.

Nevertheless, it is still deemed of interest here to examine the extent to which the double-gamma measurements of water content do or do not conform to rigid-media flow theory. To do this, it must be remembered that the earlier studies of Nofziger (1970) and Tsuji (1971) were for horizontal flow, while the present ones are for vertical flow. To provide a framework in which to evaluate the vertical-flow results, we return to Philip's (1957) rigid-flow solution,

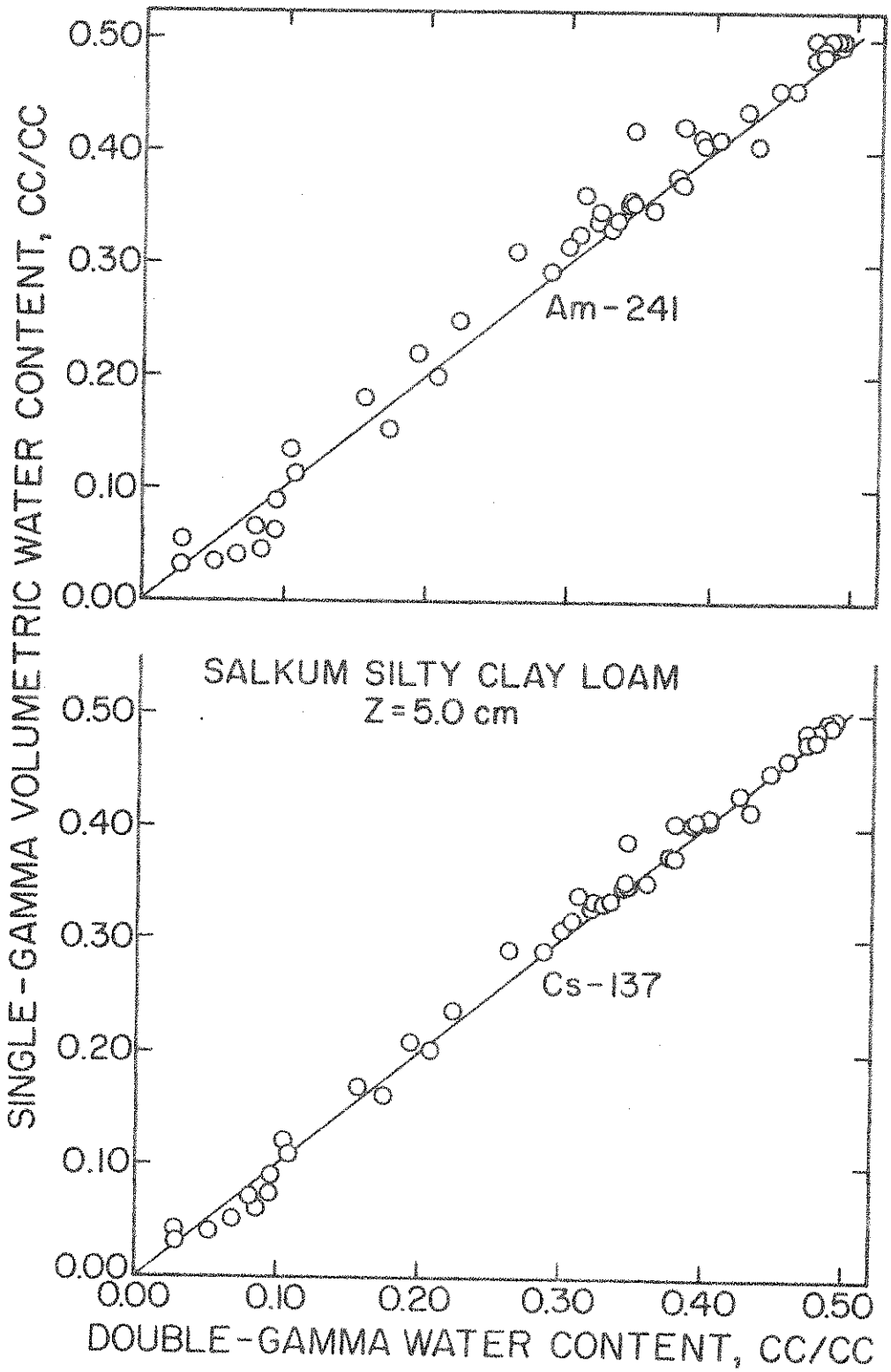

Figure 27 -- Single-gamma water content versus double-gamma water content for Salkum silty clay loam. The straight lines represent the 1:1 relationships.

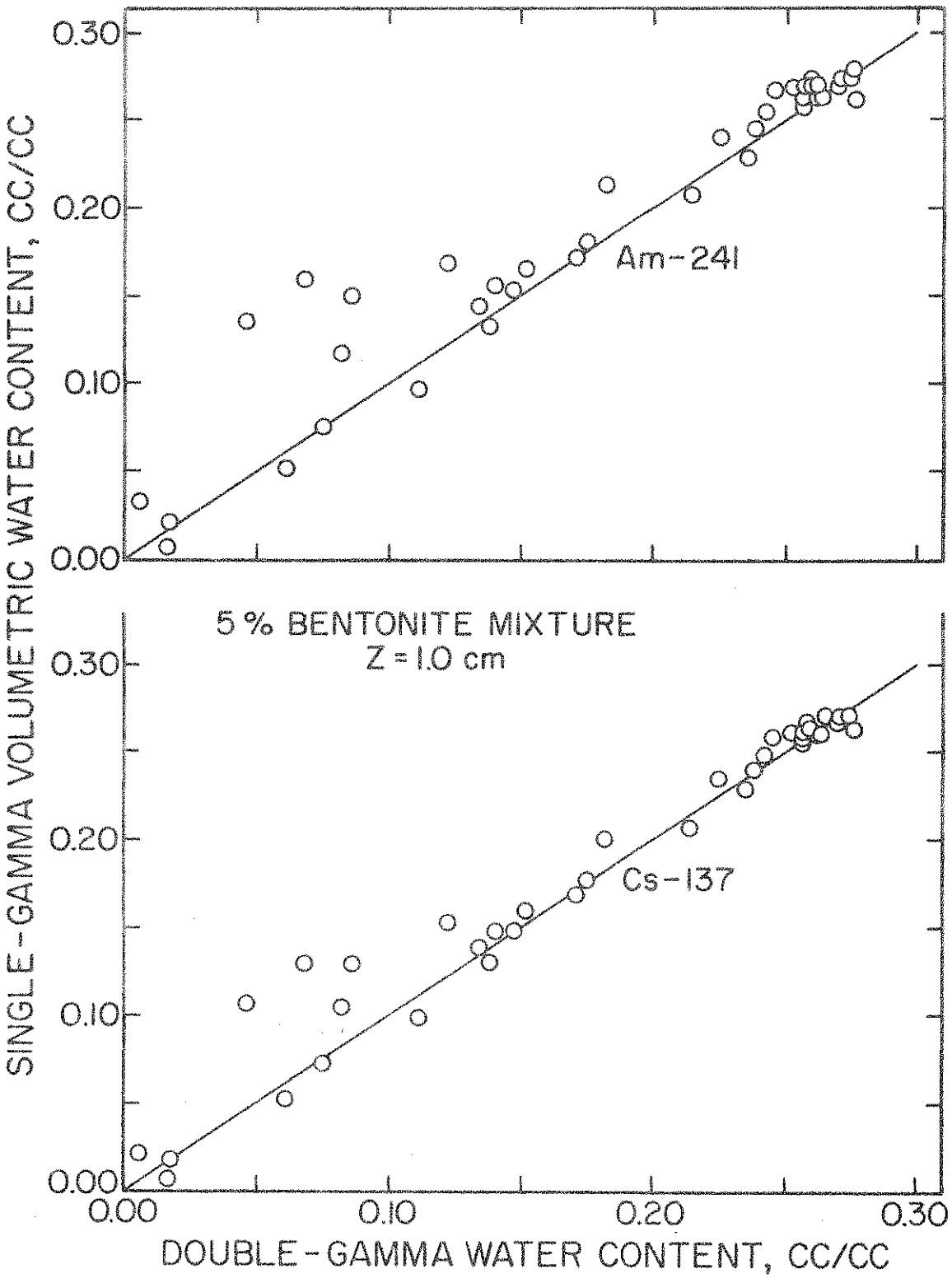

Figure 28 -- Single-gamma water contents versus double-gamma water contents for the 5% bentonite mixture. The straight lines represent the 1:1 relationships.

Eq. (43), and note that the infinite series converges rapidly, so that usually only three or four terms are needed for small to intermediate times. Rearranging Eq. (43) and writing it in truncated form for a particular water content θ_c yields

$$Z_c/t^{1/2} = \phi(\theta_c) + f_2(\theta_c)t^{1/2} + f_3(\theta_c)t + f_4(\theta_c)t^{3/2} \qquad (47)$$

where Z_c is the vertical position of the particular water content θ_c. The functions f_2, f_3, and f_4 decrease rapidly in magnitude; f_2 and f_3 are generally positive although f_4 can be positive or negative (Philip, 1957; Nielsen et al., 1961). As a result, $Z_c/t^{1/2}$ is an increasing function of $t^{1/2}$ for small to intermediate times. A similar approach can also be applied for the case of horizontal flow, in which instance Eq. (44) is utilized by writing it for θ_c, namely

$$x_c/t^{1/2} = \phi(\theta_c) \qquad (48)$$

where x_c is the horizontal position of the particular water content θ_c. Equation (48) implies that $x_c/t^{1/2}$ is a constant for all values of time and any particular water content.

The means of assessing the vertical-flow results is to determine for a fixed water content θ_c the specific Boltzmann variable $Z_c/t^{1/2}$, and to plot $Z_c/t^{1/2}$ against $t^{1/2}$ in a test of Eq. (47). Now the time (and hence $t^{1/2}$) that a given θ_c arrived at a given position Z_c is the same as the time that the given position reached the given water content. For the curves of water content versus time at given positions, hereinafter referred to as water-content transients, a parabolic spline function was fitted to each transient by least squares, based upon the technique of DuChateau et al. (1972). The advantage of this technique is that the investigator is not required to choose a single mathematical equation for the curve to be fitted to the entire range of the data. Instead, parabolas are fitted by least squares to small segments of the data, under the conditions that the entire curve be continuous and have a continuous first derivative. Illustrations of such parabolic-spline curves

fitted to the actual data are given in Figs. 29 and 30 for several positions in Salkum silty clay loam, where it is clear that the fitted curves pass very acceptably through the data. From a family of such fitted curves, it is thus a straightforward matter to determine the times at which θ_c reaches the various depths Z_c, and hence to calculate $Z_c/t^{1/2}$ for each $t^{1/2}$.

Plots of $Z_c/t^{1/2}$ versus $t^{1/2}$ for several fixed water contents in the Salkum soil are shown in Fig. 31. For all five water contents, the curves at first decrease very rapidly with $t^{1/2}$ and then became nearly constant, in marked contrast with the theoretical requirement of Eq. (47) that $Z_c/t^{1/2}$ shall increase with $t^{1/2}$ for small to moderate times. To provide a basis of comparison with the earlier horizontal studies, $x_c/t^{1/2}$ for the Salkum data of Nofziger (1970) are plotted against $t^{1/2}$ in Fig. 32. Once again, the curves at first decrease very rapidly with $t^{1/2}$, but then change somewhat abruptly to a gentle but sustained negative slope, in contrast with the theoretical requirement of Eq. (48) that $x_c/t^{1/2}$ shall be constant and hence independent of $t^{1/2}$.

For the 5% bentonite mixture, plots of $Z_c/t^{1/2}$ versus $t^{1/2}$ are shown in Fig. 33 for five fixed water contents. As before, the curves at first decrease very rapidly, but, in contrast with Fig. 31, they continue to decrease appreciably rather than to flatten out. Corresponding curves of $x_c/t^{1/2}$ versus $t^{1/2}$ for the horizontal data of Tsuji (1971) are shown in Fig. 34, where sustained reductions occur at the first two water contents of 0.04 and 0.08 cc/cc. For the three higher water contents, however, a still different type of behavior emerges, in that the curves increase with $t^{1/2}$ in the beginning, reach a maximum, and then decrease to varying extents thereafter. In neither of Figs. 33 or 34, however, does the soil-water diffusivity theory for rigid media describe the data with precision.

For the Raub soil, plots of $Z_c/t^{1/2}$ versus $t^{1/2}$ are shown in Fig. 35 for six fixed water contents. For all of the water contents the curves decrease initially, then increase slightly, and finally decrease slightly once more. In general, the relative changes in $Z_c/t^{1/2}$ for a given water content tend to be less for the Raub than for the 5% bentonite or the Salkum. Results for a separate duplicate vertical column of Raub were generally in good agreement with those in Fig. 35. No data were obtained for horizontal columns of Raub soil.

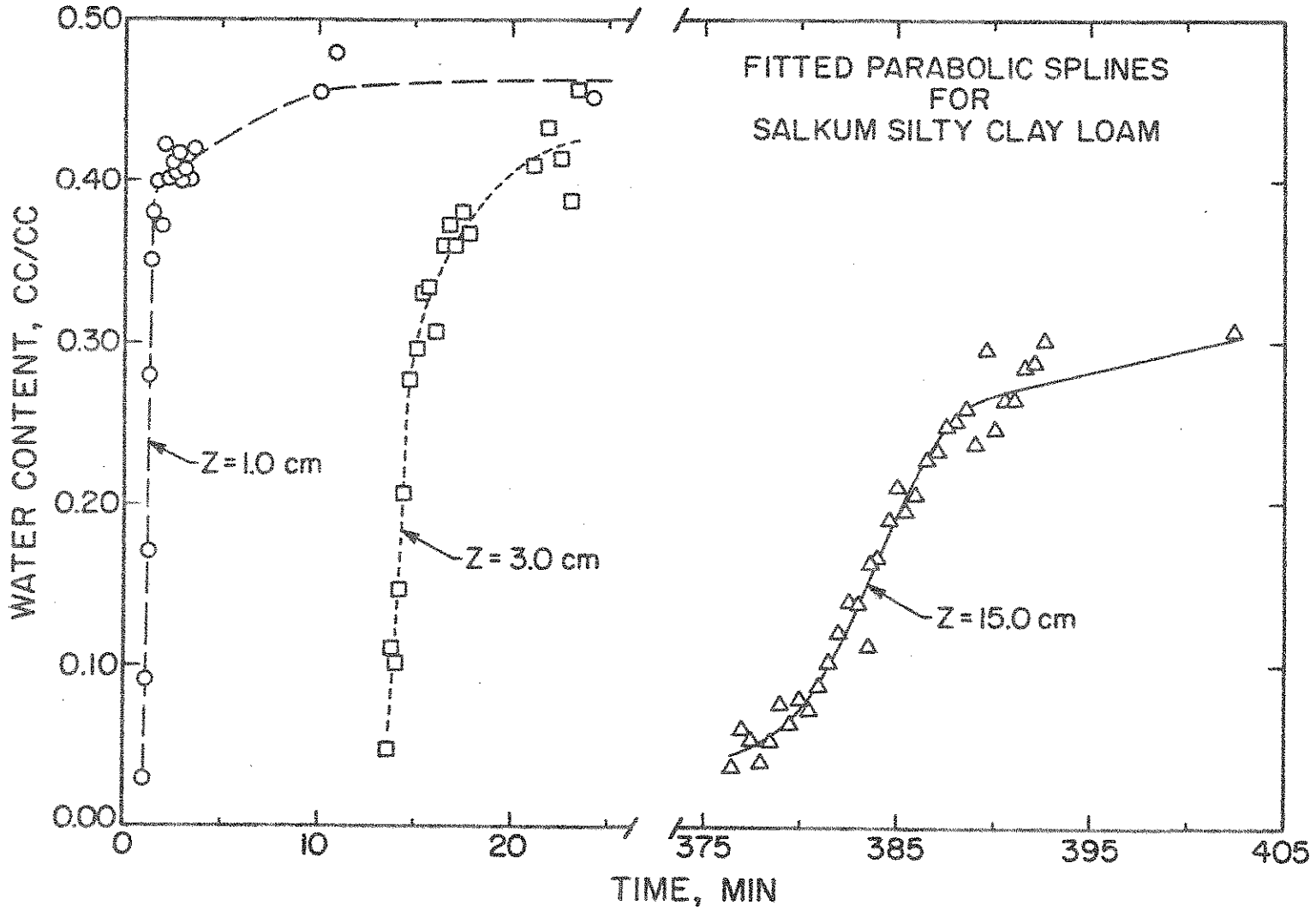

Figure 29 -- Examples of fitted parabolic splines for the early portions of three water-content transients in Salkum silty clay loam.

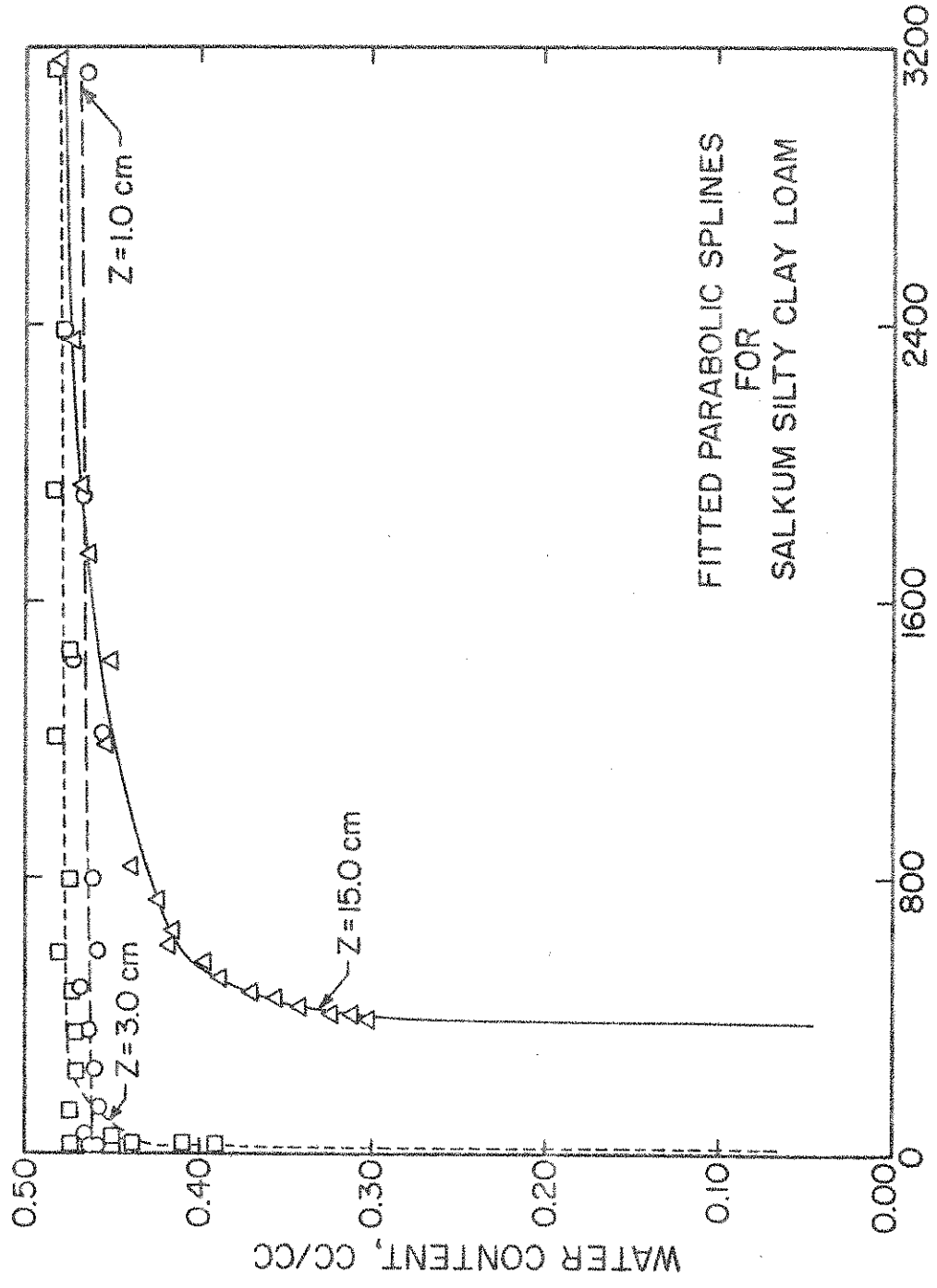

Figure 30 -- Examples of fitted parabolic splines for final portions of three water-content transients in Salkum silty clay loam.

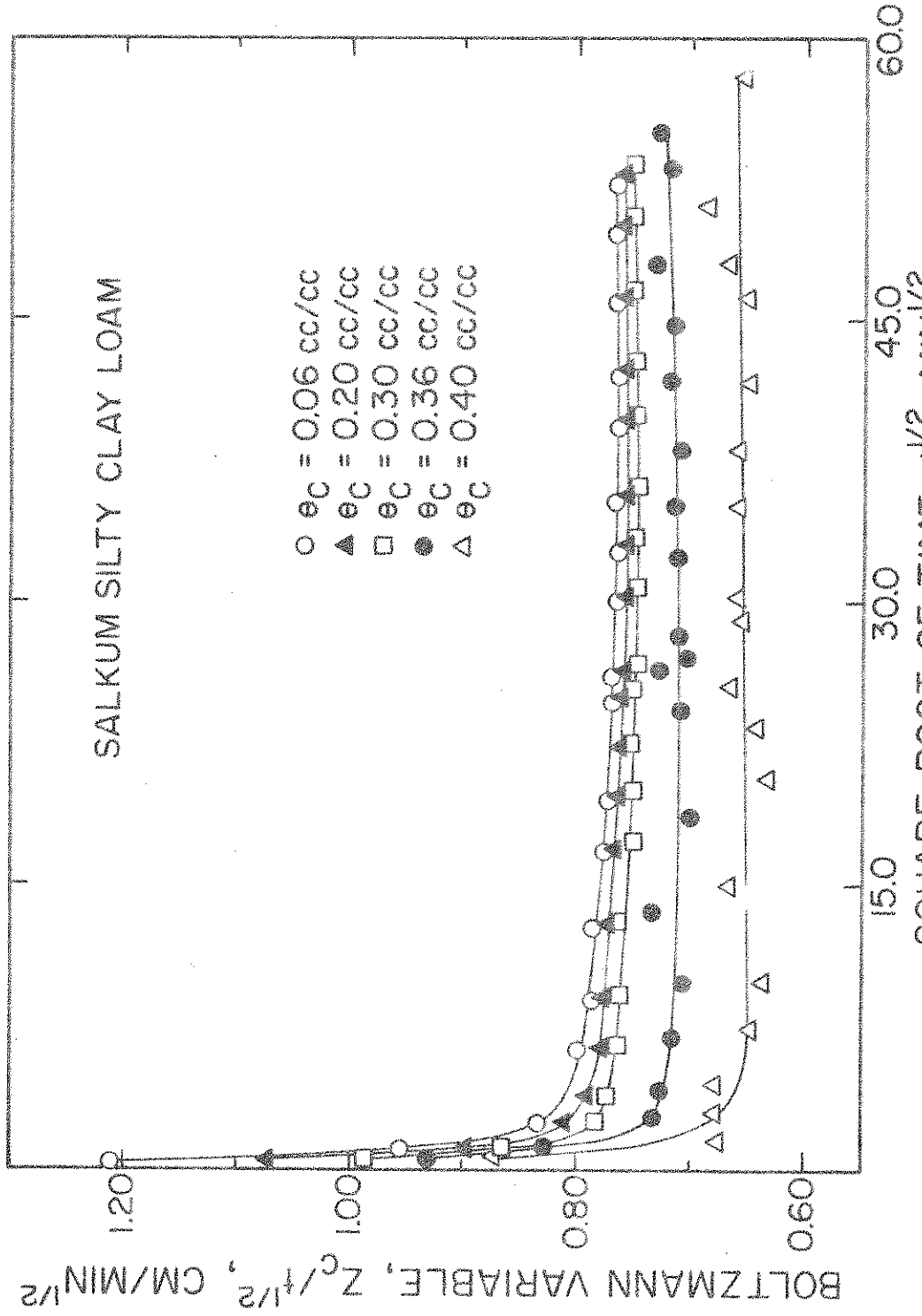

Figure 31 -- Boltzmann variable versus square root of time for several water contents for vertical infiltration in Salkum silty clay loam.

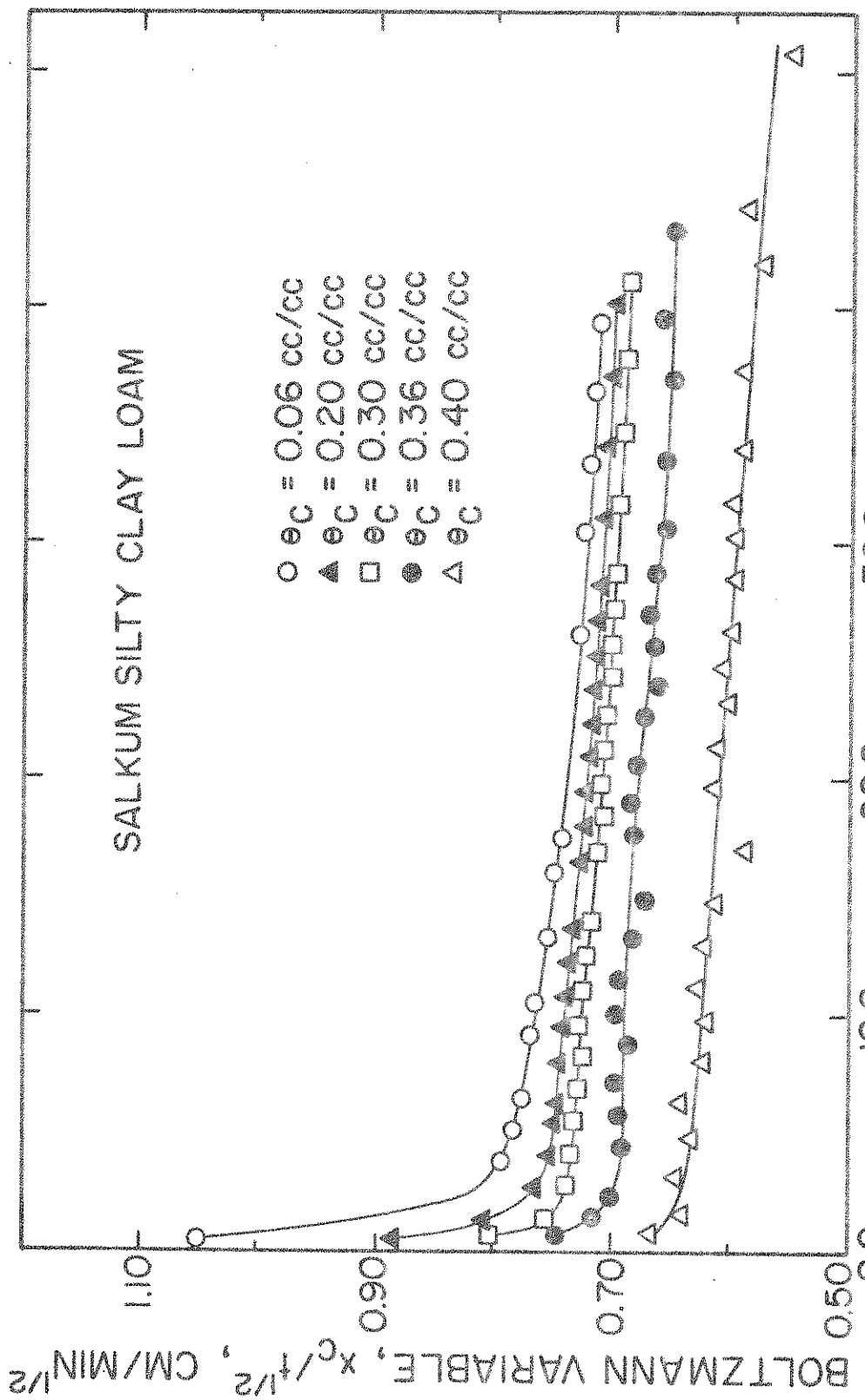

Figure 32 -- Boltzmann variable versus square root of time for several water contents for horizontal water absorption by Salkum silty clay loam (Nofziger, 1970).

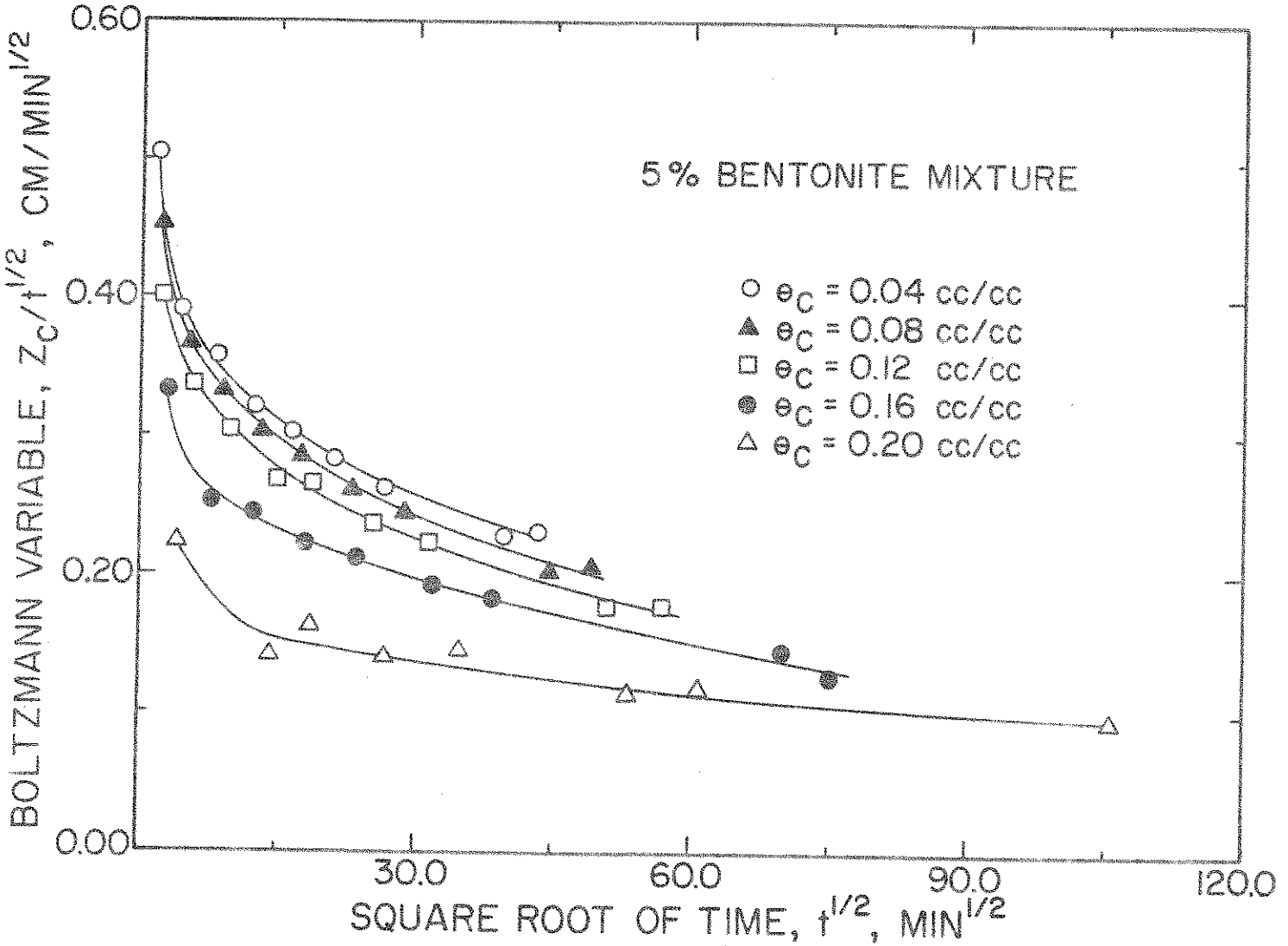

Figure 33 -- Boltzmann variable versus square root of time for several water contents for vertical infiltration in the 5% bentonite mixture.

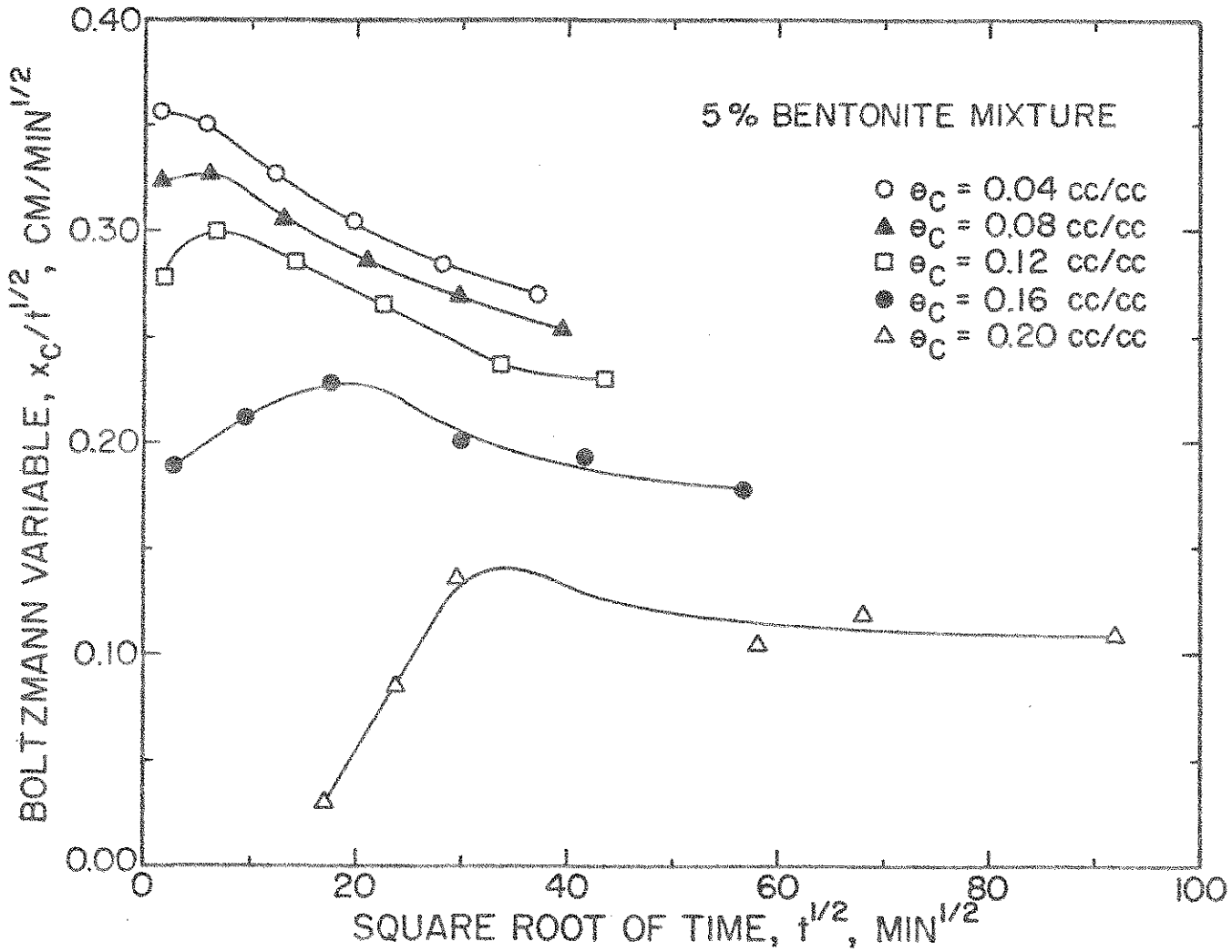

Figure 34 -- Boltzmann variable versus square root of time for several water contents for horizontal water absorption by the 5% bentonite mixture (Tsuji, 1971).

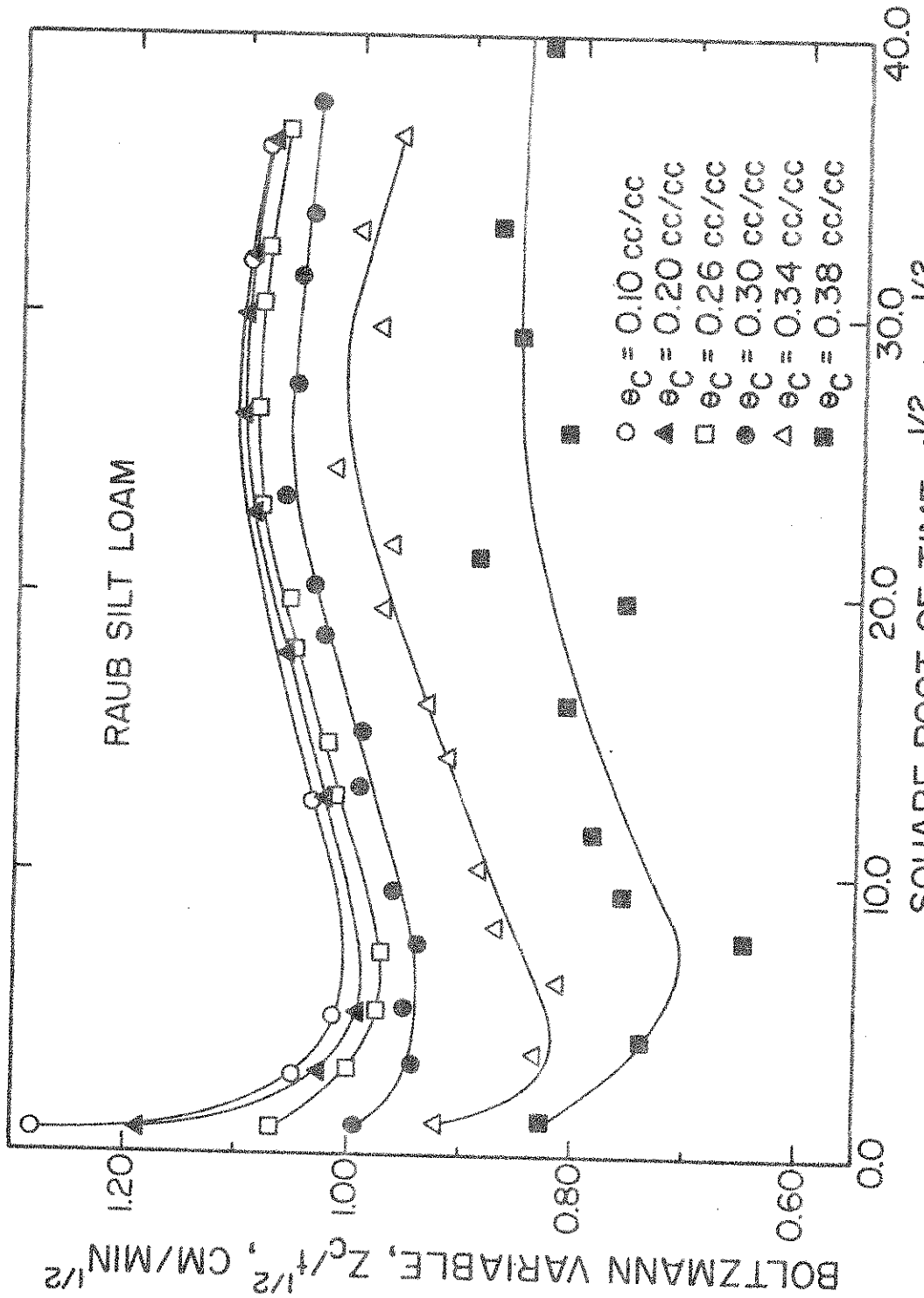

Figure 35 — Boltzmann variable versus square root of time for vertical infiltration into Raub silt loam.

The results indicate that soil-water diffusivity theory fails to describe precisely the movement of water into these three soils. Since no measurable change in bulk density was observed for any of the soils, the deviations observed here, as well as those observed in horizontal flow for Salkum silty clay loam (Rawlins and Gardner, 1963; Nofziger, 1970) and for the 5% bentonite mixture (Tsuji, 1971), do not appear to be due to macroscopic swelling.

BIBLIOGRAPHY

Ahuja, L. R., and D. Swartzendruber. 1972. An improved form of soil-water diffusivity function. Soil Sci. Soc. Amer. Proc. 36:9-14.

Ames, W. F. 1965. Similarity for the nonlinear diffusion equation. Ind. Eng. Chem. Fundamentals 4:72-76.

Brooks, R. H., and A. T. Corey. 1964. Hydraulic properties of porous media. Hydrology Paper No. 3, Colorado State Univ., Fort Collins, Colo.

Carslaw, H. W., and J. C. Jaeger. 1959. Conduction of Heat in Solids, pp. 321-323. Oxford University Press, London.

Corey, J. C., S. F. Peterson, and M. A. Wakat. 1971. Measurement of attenuation of ^{137}Cs and ^{241}Am gamma rays for soil density and water content determinations. Soil Sci. Soc. Amer. Proc. 35:215-219.

Crank, J. 1956. The Mathematics of Diffusion, pp. 39-41, 186-218. Oxford University Press, London.

Crank, J., and P. Nicolson. 1947. A practical method for numerical evaluation of solutions of partial differential equations of the heat-conduction type. Proc. Cambridge Phil. Soc. 43:50-67.

DuChateau, P. C., D. L. Nofziger, L. R. Ahuja, and D. Swartzendruber. 1972. Experimental curves and rates of change from piecewise parabolic fits. Agron. J. 64:538-542.

Duley, F. L. 1939. Surface factors affecting the rate of intake of water by soils. Soil Sci. Soc. Amer. Proc. 4:60-64.

Eddy, R. P. 1952. A method for the numerical solution of a heat conduction problem. NAVORD Report 2725, pp. 1-6.

Edwards, W. M., and W. E. Larson. 1969. Infiltration of water into soils as influenced by surface seal development. Trans. Amer. Soc. Agr. Eng. 12:463-465, 470.

Ellison, W. D. 1947. Soil erosion studies -- Part III, Some effects of soil erosion on infiltration and surface runoff. Agr. Eng. 28:245-248.

Forsythe, G. E., and W. R. Wasow. 1960. Finite-Difference Methods for Partial Differential Equations, pp. 143-145. John Wiley and Sons, New York.

Fritton, D. D. 1969. Resolving time, mass absorption coefficient and water content with gamma-ray attenuation. Soil Sci. Soc. Amer. Proc. 33:651-655.

Gardner, W. H., and C. Calissendorff. 1967. Gamma-ray and neutron attenuation in measurement of soil bulk density and water content. Proc. Symp. Isotope Radiation Techniques Soil Physics Irrig. Studies, Istanbul, pp. 101-113. Internat. Atomic Energy Agency, Vienna.

Gardner, W. H., G. S. Campbell, and C. Calissendorff. 1972. Systematic and random errors in dual gamma energy soil bulk density and water content measurements. Soil Sci. Soc. Amer. Proc. 36:393-398.

Green, W. H., and G. A. Ampt. 1911. Studies on soil physics: I. Flow of air and water through soils. J. Agr. Sci. 4:1-24.

Hanks, R. J., and S. A. Bowers. 1962. Numerical solution of the moisture flow equation for infiltration into layered soils. Soil Sci. Soc. Amer. Proc. 26:530-534.

Hillel, D., and W. R. Gardner. 1970. Transient infiltration into crust-topped profiles. Soil Sci. 109:69-76.

Horton, R. E. 1940. An approach toward a physical interpretation of infiltration-capacity. Soil Sci. Soc. Amer. Proc. 5:399-417.

Klute, A. 1952. A numerical method for solving the flow equation for water in unsaturated soils. Soil Sci. 73:105-116.

Mannering, J. V., and D. Wiersma. 1970. The effect of rainfall energy on water infiltration into soils. Proc. Indiana Acad. Sci. 79:407-412.

McIntyre, D. S. 1958. Permeability measurements of soil crusts formed by raindrop impact. Soil Sci. 85:185-189.

Moore, R. E. 1939. Water conduction from shallow water tables. Hilgardia 12:383-401.

Nielsen, D. R., D. Kirkham, and W. R. van Wijk. 1961. Diffusion equation calculations of field soil water infiltration profiles. Soil Sci. Soc. Amer. Proc. 25:165-168.

Nofziger, D. L. 1970. The validity of soil-water diffusivity theory for horizontal water absorption. Unpublished M.S. Thesis, Purdue University, Lafayette, Indiana.

Pennington, R. H. 1970. Introductory Computer Methods and Numerical Analysis, pp. 415-421. Macmillan Company, London.

Philip, J. R. 1957. The theory of infiltration: 1. The infiltration equation and its solution. Soil Sci. 83:345-357.

Philip, J. R. 1969. Hydrostatics and hydrodynamics in swelling soils. Water Resources Res. 5:1070-1077.

Philip, J. R., and D. E. Smiles. 1969. Kinetics of sorption and volume change in three component systems. Austral. J. Soil Res. 7:1-19.

Raats, P. A. C., and A. Klute. 1969. One-dimensional, simultaneous motion of the aqueous phase and the solid phase of saturated and partially saturated porous media. Soil Sci. 107:329-333.

Rawlins, S. L., and W. H. Gardner. 1963. A test of the validity of the diffusion theory for unsaturated flow of soil water. Soil Sci. Soc. Amer. Proc. 27:501-511.

Richards, L. A. 1931. Capillary conduction of liquids through porous mediums. Physics 1:318-333.

Richtmeyer, R. D., and K. W. Morton. 1967. Difference Methods for Initial Value Problems, pp. 185-205. Interscience Publishers, New York.

Rubin, J., and R. Steinhardt. 1963. Soil water relations during rain infiltration: 1. Theory. Soil Sci. Soc. Amer. Proc. 27:246-251.

Soane, B. D. 1967. Dual energy gamma-ray transmission for coincident measurement of water content and dry bulk density of soil. Nature 214:1273-1274.

Sor, K., and A. R. Bertrand. 1962. Effect of rainfall energy on the permeability of soils. Soil Sci. Soc. Amer. Proc. 26:293-297.

Swartzendruber, D. 1960. Water flow through a soil profile as affected by the least permeable layer. J. Geophys. Res. 65:4037-4042.

Swartzendruber, D. 1963. Non-Darcy behavior and the flow of water in unsaturated soils. Soil Sci. Soc. Amer. Proc. 27:491-495.

Swartzendruber, D. 1969. The flow of water in unsaturated soils, pp. 215-292, in R. J. M. DeWiest (ed.), Flow Through Porous Media. Academic Press, New York.

Swartzendruber, D., R. W. Skaggs, and D. Wiersma. 1968. Characterization of the rate of water infiltration into soil. Purdue University Water Resources Research Center, Technical Report 5, pp. 17-25.

Tackett, J. L., and R. W. Pearson. 1965. Some characteristics of soil crusts formed by simulated rainfall. Soil Sci. 99:407-413.

Tsuji, G. Y. 1971. Factors influencing water transport properties of particulate mixtures containing swelling clays. Unpublished Ph.D. thesis, Purdue University, Lafayette, Indiana.

van Duin, R. H. A. 1955. Tillage in relation to rainfall intensity and infiltration capacity of soils. Neth. J. Agr. Sci. 3:182-191.

PROJECT PUBLICATIONS

PAPERS PUBLISHED

Ahuja, L. R., and D. Swartzendruber. 1972. An improved form of soil-water diffusivity function. Soil Sci. Soc. Amer. Proc. 36:9-14.

DuChateau, P. C., D. L. Nofziger, L. R. Ahuja, and D. Swartzendruber. 1972. Experimental curves and rates of change from piecewise parabolic fits. Agron. J. 64:538-542.

MANUSCRIPTS ACCEPTED

Ahuja, L. R., and D. Swartzendruber. Horizontal soil-water intake through a thin zone of reduced permeability. Accepted by Journal of Hydrology, September 22, 1972.

THESES

Nofziger, D. L. 1972. Water and soil behavior under transiently wetting conditions. Ph.D. Thesis, Purdue University, West Lafayette, Indiana.

MANUSCRIPTS IN PREPARATION

Nofziger, D. L., L. R. Ahuja, and D. Swartzendruber. Flux-gradient and soil-water diffusivity relationships from curves of water content versus time. To be submitted to Soil Sci. Soc. Amer. Proc.

PAPERS PRESENTED

(Annual Meeting, American Society of Agronomy and Soil Science Society of America, Miami Beach, Florida, Oct. 29-Nov. 2, 1972.)

Nofziger, D. L., and D. Swartzendruber. 1972. Simultaneous measurement of water content and bulk density of soil with dual-energy gamma rays. Agron. Abstr. 64th Annual Meeting, p. 76.

Swartzendruber, D., and D. L. Nofziger. 1972. Transient water content and bulk density during confined wetting of swelling and nonswelling soils. Agron. Abstr. 64th Annual Meeting, p. 77.